50772-101

REPORT DOCUMENTATION PAGE	1. REPORT NO. NSF/RA-800212	2.	3. Recipient's Accession No. PB81 132698

4. Title and Subtitle
Coupled Walls in Earthquake-Resistant Buildings, Modeling Techniques and Dynamic Analysis

5. Report Date
June 1980

6.

7. Author(s)
M. Saatcioglu, A. T. Derecho, W. G. Corley

8. Performing Organization Rept. No
PCA R/D Ser. 1628

9. Performing Organization Name and Address
Construction Technology Laboratories
5420 Old Orchard Road
Skokie, IL 60077

10. Project/Task/Work Unit No
CR 4314-4325

11. Contract(C) or Grant(G) No.
(C)

(G) ENV7715333

12. Sponsoring Organization Name and Address
Engineering and Applied Science (EAS)
National Science Foundation
1800 G Street, N.W.
Washington, D.C. 20550

13. Type of Report & Period Covered

14.

15. Supplementary Notes
Construction Technology Laboratories is a division of Portland Cement Association.

16. Abstract (Limit: 200 words)

This investigation is part of a combined analytical and experimental program to develop design information for earthquake-resistant reinforced concrete structural wall systems. Modeling techniques developed and used for dynamic analysis of coupled wall structures are presented. Particular attention is placed on simulation of inelastic action and detailed aspects of hysteretic moment-rotation relationships. The study includes the following: selection and design of a 20-story coupled wall structure for dynamic analysis; determination of modeling requirements and development of modeling techniques for computer analysis; modification of the computer program to incorporate improved modeling capabilities; and dynamic analysis to test the analytical model and investigate the effects of selected model features on inelastic response of coupled walls.

17. Document Analysis   a. Descriptors

Concrete structures
Earthquake resistant structures
Dynamic structural analysis
Buildings

Walls
Computer programs
Mathematical models

b. Identifiers/Open-Ended Terms

Earthquake Hazards Mitigation

c. COSATI Field/Group

18. Availability Statement	19. Security Class (This Report)	21. No. of Pages
NTIS	20. Security Class (This Page)	22. Price

(See ANSI-Z39.18)   See Instructions on Reverse

OPTIONAL FORM 272 (4-77)
(Formerly NTIS-35)
Department of Commerce

NSF/RA 800212

PCA R/D Ser. 1628

Report to

NATIONAL SCIENCE FOUNDATION
Washington, D.C.

Grant No. ENV77-15333

COUPLED WALLS IN EARTHQUAKE-RESISTANT BUILDINGS

Modeling Techniques and Dynamic Analysis

by

Murat Saatcioglu
Arnaldo T. Derecho
and
W. Gene Corley

June 1980

TABLE OF CONTENTS

TABLE OF CONTENTS

(Cont'd)

COUPLED WALLS IN EARTHQUAKE-RESISTANT BUILDINGS

Modeling Techniques and Dynamic Analysis

by

M. Saatcioglu[1], A. T. Derecho[2], and W. G. Corley[3]

INTRODUCTION

Performance of multistory reinforced concrete structures subjected to recent earthquakes has demonstrated that superior damage control and human life safety can be achieved if buildings are stiffened by properly designed structural walls. For functional reasons, reinforced concrete walls are usually pierced or connected to other walls by beams. The resulting structural system is referred to as a "coupled wall system."

The coupling of two or more walls by beams of moderate stiffness at the floor levels produces a substantial increase in stiffness of the resulting system as compared to uncoupled walls. The coupling action results in tensile and compressive axial forces in walls that lead to a reduction in bending moment in the individual walls.

Superiority of a coupled wall system in aseismic design can be explained by its capacity to dissipate energy while maintaining substantial lateral stiffness. Under dynamic forces, most of the energy can be dissipated by significant yielding in beams while the walls continue providing overall stiffness and stability to the structure.

---

(1)Structural Engineer, (2)Manager, Structural Analytical Section, and (3) Divisional Director, Engineering Development Division, Construction Technology Laboratories, Portland Cement Association, Skokie, Illinois.

To examine behavior of coupled walls under earthquake load-
ing, an analytical investigation is being carried out at the
Construction Technology Laboratories of the Portland Cement
Association. This investigation is part of a combined
analytical and experimental program to develop design
information for earthquake-resistant reinforced concrete
structural wall systems.

Modeling techniques developed and used for dynamic analysis
of coupled wall structures are presented in this report.
Particular attention is placed on simulation of inelastic
action and detailed aspects of hysteretic moment-rotation
relationship. Results of dynamic analyses are presented to
clarify potential problems that arise in modeling for dynamic
inelastic analysis of coupled walls. These results also
suggest modeling techniques to analysts interested in dynamic
inelastic analysis for design purposes.

OBJECTIVE AND SCOPE

The main objective of the overall project is to develop
design information for earthquake resistant structural wall sys-
tems. In fulfilling this objective it is essential to examine
effects of selected structural and ground motion parameters on
dynamic inelastic response. This part of the project is con-
cerned with coupled wall systems.

The objective of the first phase of the investigation, which
is reported here, is to examine the analytical tools, determine

modeling procedures for dynamic analysis, and verify the valid-
ity of these procedures through dynamic analysis. The following
major items are covered in this report:

1. Selection and design of a 20-story coupled wall
    structure for use in dynamic analysis.

2. Determination of modeling requirements and develop-
    ment of modeling techniques for computer analysis.

3. Modification of the computer program used for dyna-
    mic analysis to incorporate improved modeling
    capabilities.

4. Dynamic analyses to test analytical model and
    investigate the effects of selected model features
    on inelastic response of coupled walls.

SELECTION OF PROTOTYPE STRUCTURE

A 20-story coupled wall structure was selected for dynamic
analysis. This height of structure was considered reasonably
representative of the majority of multistory structures. The
following section gives a brief review of architectural and
structural considerations involved in selecting the prototype
structure.

Architectural Considerations

Structural layout of buildings is influenced considerably
by aesthetic and functional requirements. Although required
lateral stiffness is a structural consideration, in most cases,
the locations of structural walls are dictated by architectural

-3-

requirements. The following classification of structures, based on occupancy, illustrates different uses of coupled walls.

Office Buildings

Office buildings generally require open office space with minimum interruption by vertical members. Therefore, central core exterior column or exterior wall-interior column layouts have been generally favored. Structural walls in the form of elevator and stairway shafts can be effectively used to provide lateral stiffness to a multistory building. Some cases require construction of isolated walls that may interact with frames.

For tall structures where more than one elevator shaft is used, it becomes necessary to provide corridor openings in walls. This leads to coupled walls. Similarly, in the case of exterior walls, window openings may be necessary. Therefore, structural walls are usually pierced to form coupled walls. Figure 1(a) illustrates common use of coupled walls in office buildings.

Residential Buildings

Use of coupled walls is more common in residential buildings where walls can act as permanent partitions. Structural walls used in apartment, hotel, and other residential buildings provide acoustical privacy and fire separation. A more common use of coupled walls has them combined with gravity-load carrying
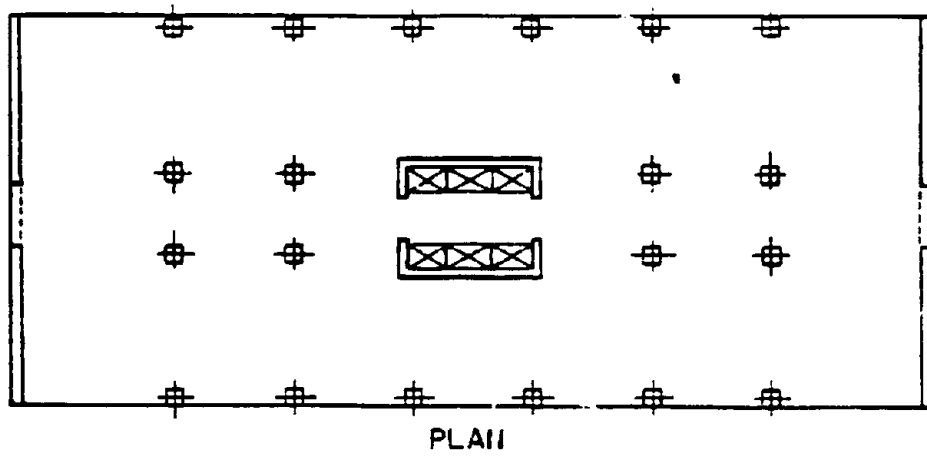
PLAN

Fig. 1a Common Use of Coupled Walls in Office Buildings
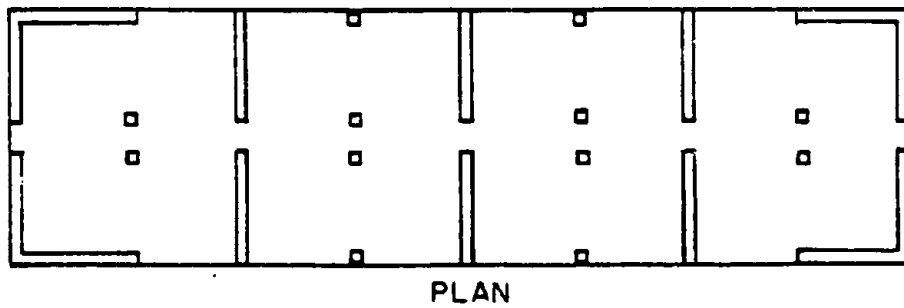

PLAN

Fig. 1b Common Use of Coupled Walls in Residential
Buildings

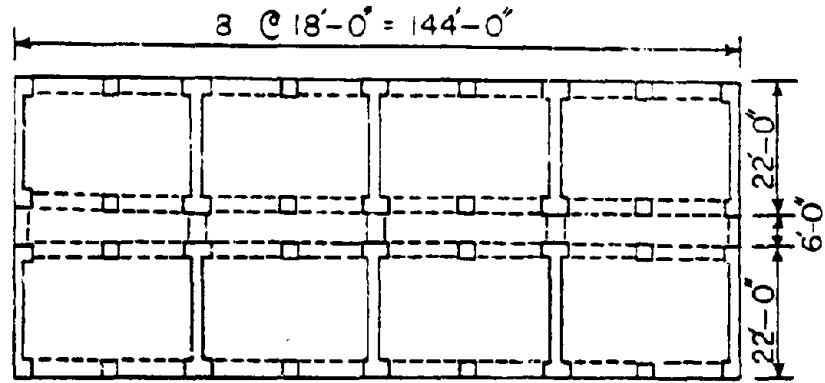frames. Figure 1(b) shows common use of coupled walls in apartment buildings.

Based on the preceding brief discussion of general architectural use of coupled walls, two types of coupled wall structures appear to be common. One is representative of an office building interior core with relatively narrow walls, the other is typical of residential buildings with relatively wide walls. This information provides a basis for establishing practical ranges of selected parameters characterizing coupled wall structures.

For this investigation, the architectural layout shown in Fig. 2 is used in dynamic analysis.

Structural Considerations

With the architectural layout assumed as shown in Fig. 2, the next step was to determine structural properties of the 20-story structure. The structure floor plan was chosen to be symmetric in both directions. This is generally desirable to minimize torsional effects which are beyond the scope of this investigation. Floor slabs are considered sufficiently stiff to cause all points on the same floor level to deflect by equal amounts horizontally.

Different combinations of wall and beam sizes were considered. Member sizes are required to determine effective stiffnesses that can be used in computing fundamental period. As a result of many trials, a structure with fundamental period of 1.0 second was used for this part of the investigation.

-6-

3 @ 18'-0" = 144'-0"

22'-0"
6'-0"
22'-0"

1' = 0.305 m.
1" = 25.4 mm

PLAN

19 @ 9'-0" = 171'-0"

12'-0"

9 @ 18'-0" = 162'-0"

21'-0"

ELEVATION

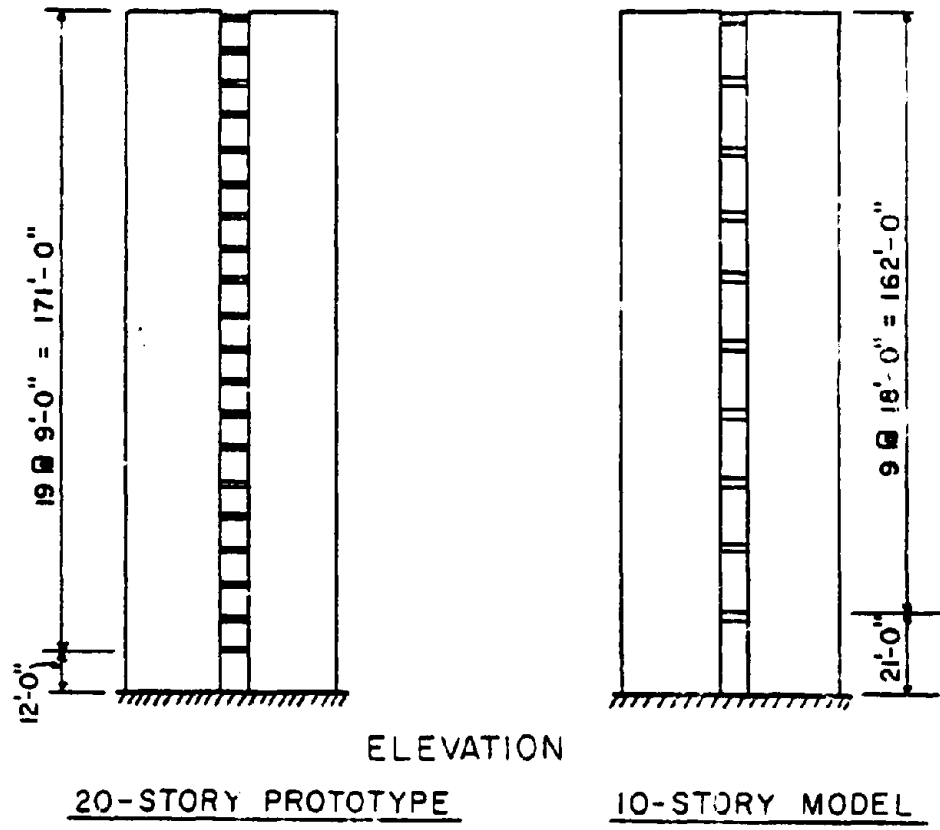20-STORY PROTOTYPE   10-STORY MODEL

Fig. 2 Coupled Wall Structure Selected for Investigation

-7-

The tributory mass associated with seismic response is such that the walls resist seismic forces acting on two bays. This implies that columns which appear at every other bay are assumed to carry only vertical loads and have no resistance to lateral forces.

Design Under Static Loading

Having determined size and hence stiffness of members, the next step is to determine the required strength of members. This is done by using UBC-76[1] requirements. The structure is analyzed under the so-called equivalent lateral forces specified in UBC-76 for Seismic Zone 4. Results of the analysis showed a top displacement of 2.1 inches. This corresponds to a drift ratio of 1/1000. Yield moments for both beams and walls as well as other structural properties are listed in Table 1.

It is usual practice to provide stiffness and strength taper along the height of a tall structure. For this reason, wall thickness is varied twice along the structure height. This is expressed in terms of relative stiffness values of 100%, 80%, and 65% for the structure base, mid-height, and top portion respectively. Percentage reinforcement is also varied at three locations along the wall height. This is specified in terms of relative flexural strengths equal to 100%, 75%, and 50%. The significance of strength and stiffness taper on dynamic response is investigated and discussed later in this report.

TABLE 1 - PROPERTIES OF THE SELECTED STRUCTURE

Properties	Prototype	Model
Fundamental Period	1.0 sec.	1.0 sec.
Number of Stories	20	10
Height	183 ft	183 ft
Wall Stiffness Parameters EI GA EA	8.28×10^{10} k-in.^{2} 6.09×10^6 kips 1.42×10^8 kips	8.28×10^{10} k-in.^{2} 6.09×10^6 kips 1.42×10^8 kips
Stiffness Taper+	1.0EI at base 0.8EI at 6th floor 0.65EI at 12th floor	1.0EI at base 0.8EI at 3nd floor 0.65EI at 6th floor
Beam Stiffness Parameters EI GA EA	2.275×10^7 k-in.^{2} 3.94×10^5 kips 9.215×10^5 kips	4.55×10^7 k-in.^{2} 7.87×10^5 kips 1.84×10^6 kips
Wall Yield Moment, M_y	400,000 k-in.	400,000 k-in.
Strength Taper*	1.00M_y at base 0.75 M_y at 6th floor 0.50 M_y at 12th floor	1.00 M_y at base 0.75 M_y at 3nd floor 0.50 M_y at 6th floor
Beam Yield Moment, M_y	3,000 k-in.	6,000 k-in.
Damping	5% of critical	5% of critical
Post-Yield Stiffness on Primary Curve	5% of elastic for walls 6% of elastic for beams	5% of elastic for walls 6% of elastic for beams
Weight	1,880 k/wall	1,880 k/wall
Weight for Inertia Forces	3,270 k/wall	3,150 k/wall
Base Fixity Condition	fully fixed	fully fixed
Ground Motion	Pacoima Dam 1971, S16E	Pacoima Dam 1971, S16E
Intensity of Ground Motion**	1.5 El Centro 1940, N-S	1.5 El Centro 1940, N-S

*Yield moments are also adjusted at every floor based on the weight of the structure.
**Based on spectrum intensity.
+The same taper also applies for "GA" and "EA."

1 ft = 0.305 m   1 k = 4.448 kN
1 k-in. = 0.113 kN m   1 k-in.^{2} = 0.00287

Reduced (Lumped) Model

Because of the large number of cases covered in this project, it was considered essential to lump the 20-story structure vertically to reduce the number of members and hence the computer time required for analysis. The principal requirement in lumping is that the 20-story prototype and the reduced model yield essentially the same analysis results. To achieve this objective, the following criteria is followed:

a. Overall structure geometry must be maintained, i.e., the height of the structure as well as coupling arm must be preserved.

b. Fundamental periods of the prototype and the model must be the same.

c. Displacements of the prototype and the model must be in close agreement.

d. Shear force, bending moment, and ductility envelopes for the prototype and the model must be in close agreement.

Reduction of 20 stories into 10 stories through lumping means a reduction in the number of coupling beams. The simple omission of every other beam without changing properties of the remaining beams results in a structure with essentially same beam stiffness, lesser wall stiffness (due to increased height between supporting beams), and lesser overall stiffness. The contribution of wall stiffness to overall structural stiffness is more significant than the contribution of beam stiffness.

Because of this, it is not possible to base the lumping procedure on the requirement of preserving relative stiffnesses of beams and walls meeting at a joint as in the case of frames. If walls are sufficiently stiff as compared to beams, overall structural stiffness is dominated by the walls. This means that beams can be lumped at every other floor without changing overall structural stiffness. As wall stiffness approaches beam stiffness, there is a change from wall dominance to frame behavior. The structure considered in this report has a high wall-to-beam stiffness ratio. Therefore, lumping two beams at every other floor produces a 10-story model having essentially the same fundamental period and response as the prototype structure.

Static and dynamic analyses were conducted to compare responses of the 20-story prototype and the 10-story model. Comparison of bending moments under static loading is shown in Fig. 3. Comparison for dynamic loading is discussed under "Dynamic Analyses."

Other means of lumping were also tried. Both wall and beam stiffnesses were varied to obtain a lumped model with fundamental period same as the prototype. Although it was possible to match the period, structural response of the model did not always agree with response of the prototype. Table 2 summarizes the cases covered in this trial procedure.

COMPUTER PROGRAM FOR DYNAMIC ANALYSIS

Dynamic response analysis was carried out using program DRAIN-2D[2] developed at the University of California at

20

20 - Story Prototype

10 - Story Model

STORY LEVEL

15

10

5

1 k - in. = 0.113 kN-m

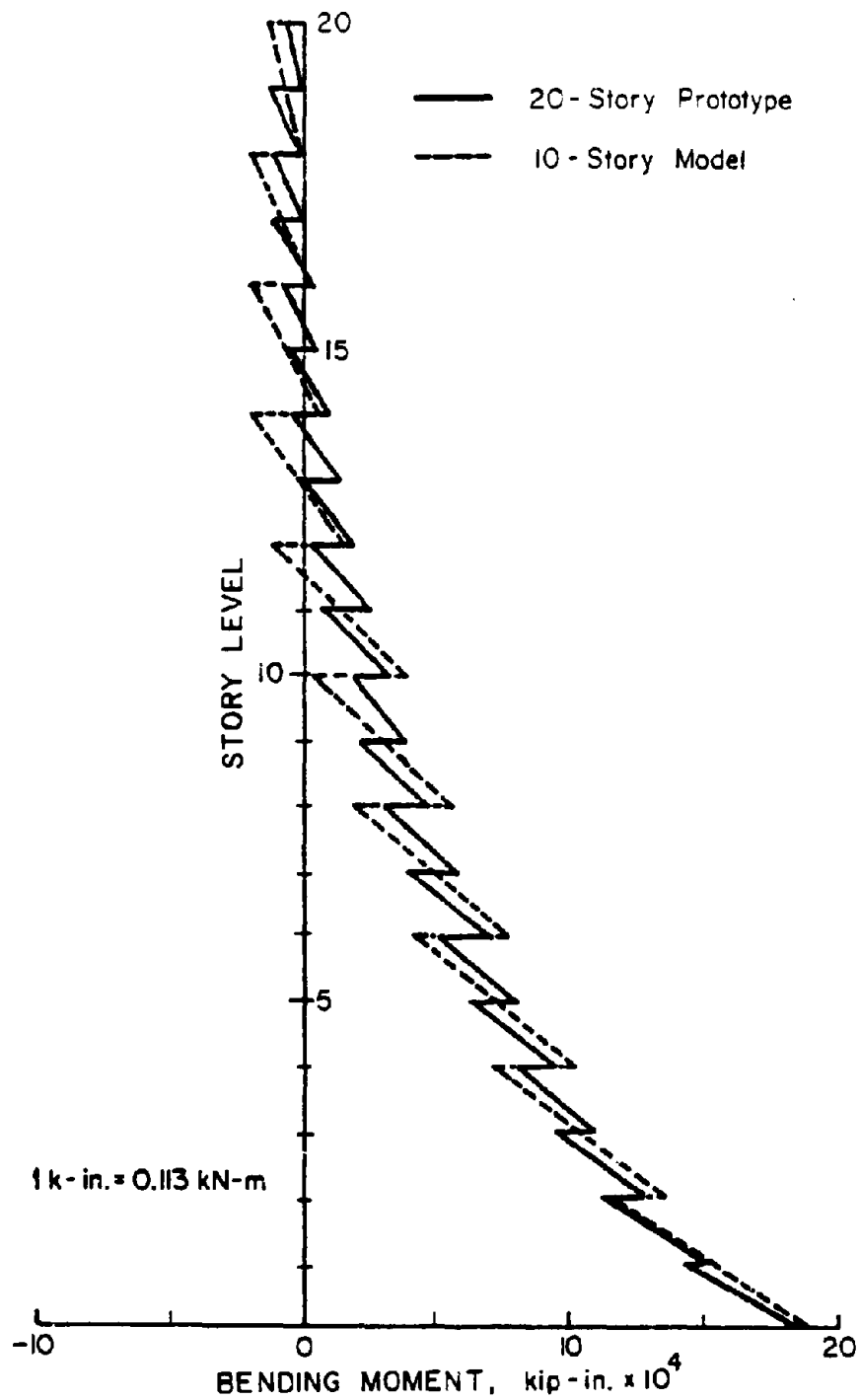-10   0   10   20

BENDING MOMENT, kip-in. $\times 10^4$

Fig. 3 Comparison of 20-Story Prototype and 10-Story
(Reduced) Model Under Equivalent Static
Forces of UBC-76

TABLE 2 - COMPARISON OF THE MODEL AND THE PROTOTYPE
UNDER STATIC LOADING

Case	r_1^*	r_2^{**}	Fundamental Period (sec)	Top Displ. Ratio[+]	Base Mom. Ratio[+]
1	2.00	1.00	0.978	—	—
2	1.90	0.95	0.986	—	--
3	1.60	0.80	1.052	0.917	0.666
4	1.40	1.40	1.004	1.015	0.785
5	1.20	2.40	0.966	—	—
6	1.00	2.00	1.015	1.000	0.979
7	0.90	2.25	1.015	1.000	1.055

*r_1 is the ratio of model wall moment of inertia to prototype
wall moment of inertia, $r_1 = (I_{mod}/I_{prot})$wall

**r_2 is the ratio of model beam moment of inertia to prototype
beam moment of inertia, $r_2 = (I_{mod}/I_{prot})$beam

[+] Ratio of prototype results to model results

Berkeley and later modified by the Portland Cement Association.
The program has capabilities to analyze plane inelastic struc-
tures under seismic excitation.

The structural stiffness matrix is formulated by the direct
stiffness method, with nodal displacements as unknowns. Dynam-
ic response is determined using step-by-step integration by
assuming a constant response acceleration during each time step.

Several program modifications have been introduced by the
Construction Technology Laboratories of the Portland Cement
Association. These modifications range from input-output

changes to more substantive changes such as introduction of new hysteretic rules for moment-rotation and shear-distortion relationships.

Computer Program Modifications

Axial Force-Flexure Interaction

The major change to DRAIN-2D, implemented in relation to this phase of the project, is the modification of the moment-rotation hysteresis rules to include axial force-flexure interaction effects. Appropriate documentation of the changes, which also involved significant revisions of the input data format, has been prepared. The revisions in input format pertain mainly to plotting options and storage of output data on tapes.

The basic moment-rotation hysteretic model incorporated in the original version of DRAIN-2D follows an extended and modified set of rules based on those proposed by Takeda and Sozen[3]. This basic hysteresis loop for the decreasing stiffness beam element is shown in Fig. 4(a) and was developed for members under constant level of axial force. However, coupled walls generally undergo substantial changes in level of axial force during response to earthquake motions. Because of this continuous change in axial force and the interaction between axial force and bending moment, the yield moment changes continuously. This interaction not only alters the initial yield level, but also affects the effective stiffness of the structure in the post-yield range. Therefore, the basic decreasing-stiffness
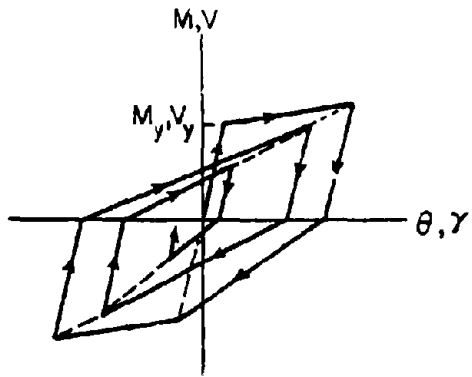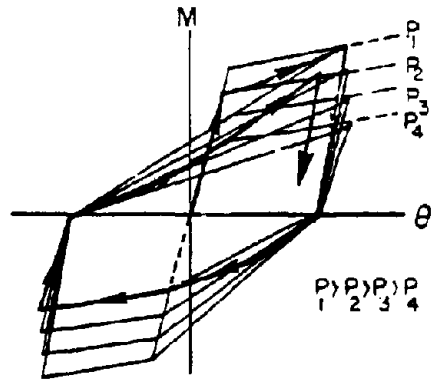
Fig. 4a Takeda's Hysteretic
Loop

Fig. 4b Hysteretic Loop Under
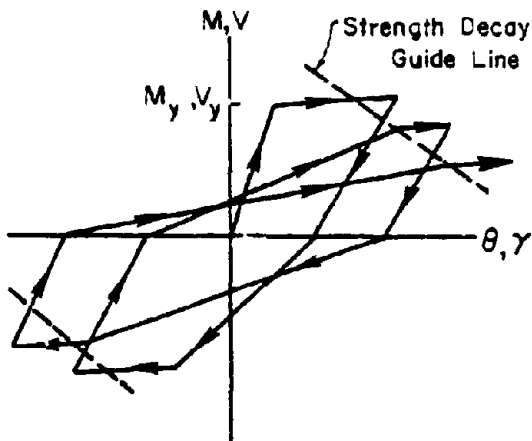Changing Axial
Forces

Fig. 4c Hysteretic Loop Showing
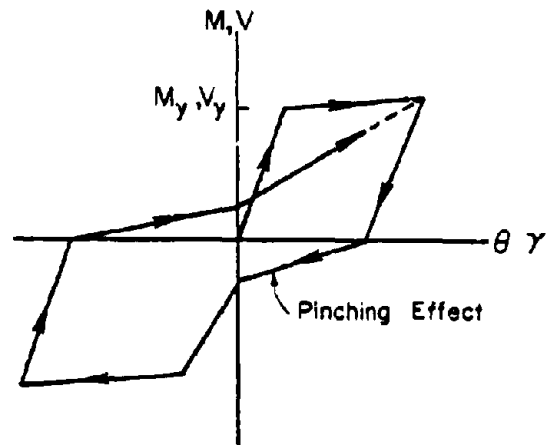Strength Decay Under
Reversed Load
Cycles

Fig. 4d Pinching of Hysteretic
Loop

beam element in DRAIN-2D model is modified to include axial force-flexure interaction. The modified model is shown in Fig. 4(b) and details are discussed in Appendix A.

Inelastic Shear

Inelastic shear model, previously implemented into DRAIN-2D by Buckle & Powell has been modified by Takayanagi and Derecho[4] at the Portland Cement Association. The model is based on hysteresis rules proposed by Takeda. A major feature of inelastic shear mechanism is the coupling of shear yielding with flexural yielding, a phenomenon observed in wall tests [5, 6].

Strength Loss and Pinching in Hysteresis Loops

Two additional features have been incorporated into hysteretic loops. One is a gradual loss of strength with repeated load reversals and the other is a pinching action in reloading branches. Figures 4(c) and 4(d) illustrate the strength loss and pinching features, respectively of the hysteresis loop.

The significance of these mechanisms on dynamic response of coupled walls was investigated and is discussed under "Dynamic Analyses."

MODELING FOR COMPUTER ANALYSIS

Proper modeling of a structure for computer analysis cannot be overemphasized if reliable results are to be obtained. The coupled wall structure analyzed in this investigation is modeled by means of line elements. Each wall and beam member
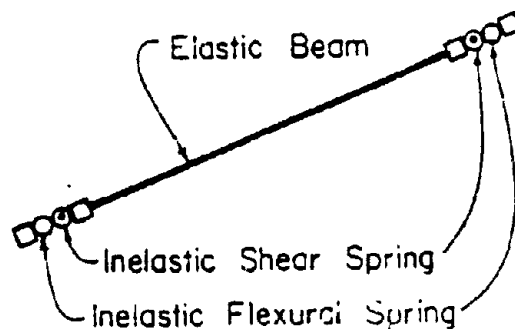
Fig. 5 Computer Idealization of a
Member

between joints is represented by a line element. It is extremely important to specify properties of these line elements properly so that both elastic and inelastic behavior of individual members can be simulated accurately. While the load deformation relationship for the elastic region is straightforward, representation of hinging regions of walls and beams requires special attention.

DRAIN-2D accounts for inelastic action by allowing the formation of plastic hinges at the ends of line elements. Thus, each element consists of an "elastic beam" and two potential "point hinges" at each erd as shown in Fig. 5. Stiffness of elastic beam and point hinges should be specified, such that total chord rotation of a line element in the model is equal to chord rotation of the real member.
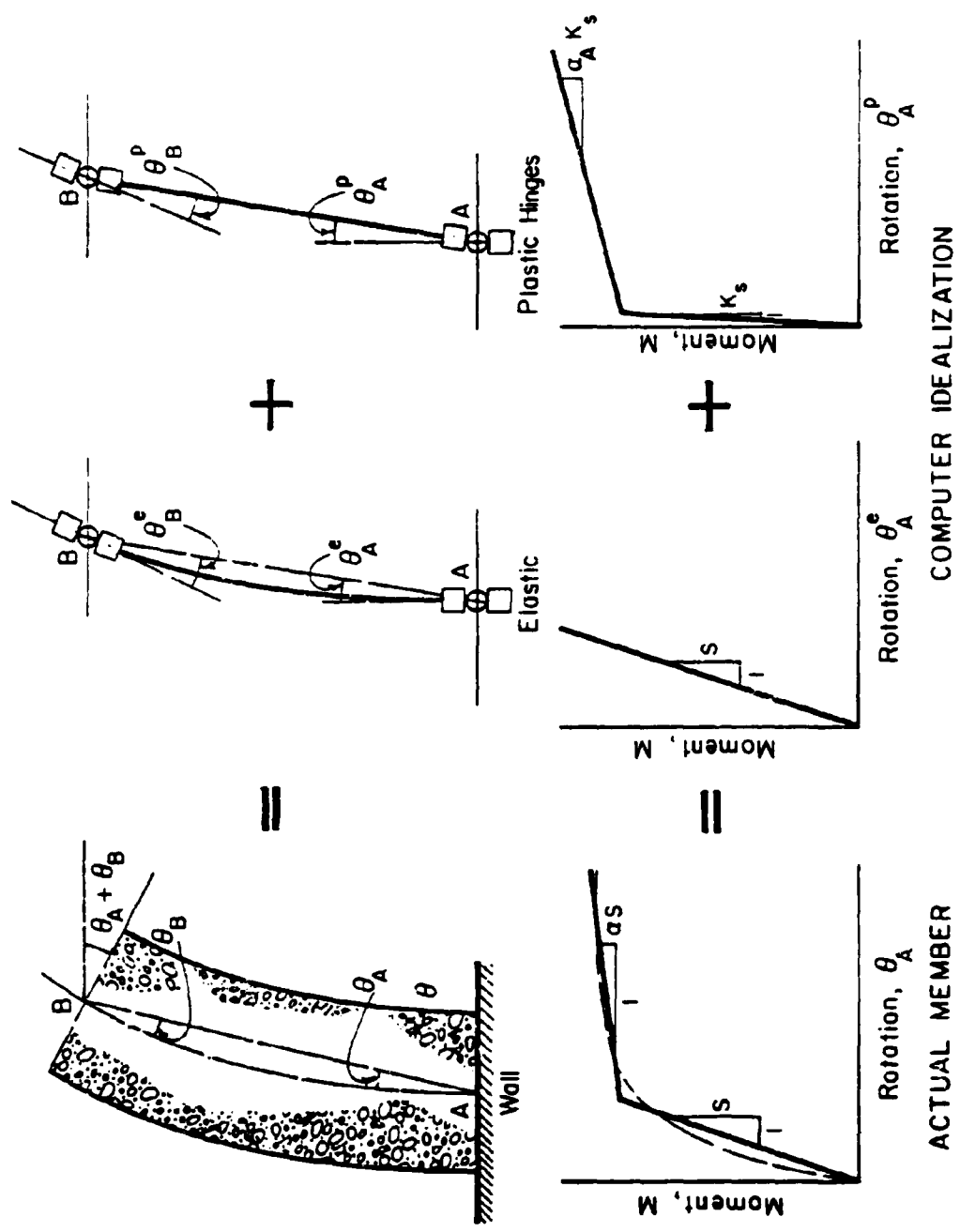
Fig. 6 Modeling Wall Members

Modeling for Flexure

If moment-rotation characteristics of a member are known, then flexural properties of the elastic beam and the point hinges can be determined. Primary moment-rotation relationship of a reinforced concrete member can be simplified as a bilinear relationship. This means that the primary curve of a typical member consists of two linear segments, one representing the elastic range and the other the post-yield or inelastic range. Figure 6 shows a representation of a moment-rotation diagram of a wall element in terms of moment-rotation diagrams of its idealized components, i.e., the elastic beam element and the point hinges.

In DRAIN-2D chord rotation of a member is calculated as the sum of elastic beam rotation and plastic hinge rotations. Thus,

$$\Delta\theta_A = \Delta\theta_A^e + \Delta\theta_A^p$$

$$\Delta\theta_B = \Delta\theta_B^e + \Delta\theta_B^p$$

where $\Delta\theta_A^e$ and $\Delta\theta_B^e$ are increments of chord rotations due to bending of elastic beam, $\Delta\theta_A^p$ and $\Delta\theta_B^p$ are increments of rotations of point hinges at ends "A" and "B", respectively. For an element AB, incremental moment-rotation relationships for elastic and plastic components are given by:

$$\begin{bmatrix} \Delta\theta_A^e \\ \Delta\theta_B^e \end{bmatrix} = \begin{bmatrix} \dfrac{L}{3EI} & -\dfrac{L}{6EI} \\ -\dfrac{L}{6EI} & \dfrac{L}{3EI} \end{bmatrix} \begin{bmatrix} \Delta M_A \\ \Delta M_B \end{bmatrix} \tag{1}$$

$$
\begin{bmatrix} \Delta\theta^P_A \\ \\ \Delta\theta^P_B \end{bmatrix} = \begin{bmatrix} \dfrac{1}{\alpha_A K_S} & 0 \\ \\ 0 & \dfrac{1}{\alpha_B K_S} \end{bmatrix} \begin{bmatrix} \Delta M_A \\ \\ \Delta M_B \end{bmatrix} \tag{2}
$$

The quantity K_S is specified as having a very large value within the elastic range, implying that the point hinges do not rotate prior to yielding. This leaves only the elastic beam component to rotate to simulate behavior of an actual concrete member in the elastic range. Then, the increments of total flexural chord rotations can be written from Eq. (1).

$$
\Delta\theta_A = \Delta\theta^e_A = \frac{L}{3EI} \Delta M_A - \frac{L}{6EI} \Delta M_B \tag{3}
$$

$$
\Delta\theta_B = \Delta\theta^e_B = -\frac{L}{6EI} \Delta M_A + \frac{L}{3EI} \Delta M_B \tag{4}
$$

Equations (3) and (4) indicate that it is sufficient to specify the effective elastic stiffness parameter (EI) to establish the moment-rotation relationship in the elastic range.

If the moment level exceeds the prescribed yield level, then the point hinges at member ends become active and start rotating to simulate yielding. Within the inelastic range, chord rotation at one end is equal to the sum of elastic beam rotation and plastic hinge rotation at that end. Total incremental flexural rotations at member ends can be written by adding Eqs. (1) and (2).

$$
\Delta\theta_A = \frac{L}{3EI} \Delta M_A - \frac{L}{6EI} \Delta M_B + \frac{1}{\alpha_A K_S} \Delta M_A \tag{5}
$$

$$
\Delta\theta_B = -\frac{L}{6EI} \Delta M_A + \frac{L}{3EI} \Delta M_B + \frac{1}{\alpha_B K_S} \Delta M_B \tag{6}
$$

Where α_A and α_B are ratios of the slope of the post-yield branch to the slope of the elastic branch of the bilinear moment-rotation curves characterizing the point hinges at member ends "A" and "B", respectively These two ratios can be determined by imposing the condition that total chord rotation of the model be equal to chord rotation in the real member.

Increments of flexural chord rotation of a real member beyond yielding can be written as:

$$\Delta\theta_A = \frac{L}{3\alpha EI}\,\Delta M_A - \frac{L}{6\alpha EI}\,\Delta M_B \tag{7}$$

$$\Delta\theta_B = -\frac{L}{6\alpha EI}\,\Delta M_A + \frac{L}{3\alpha EI}\,\Delta M_B \tag{8}$$

Where " αEI " is the effective stiffness parameter of the member beyond yielding. This effective stiffness represents a uniform member stiffness and corresponds to the slope of inelastic branch of bilinear moment-rotation idealization, as shown in Fig. 6. Ir the same idealization, "α" denotes the ratio of inelastic stiffness to elastic stiffness.

Equating $\Delta\theta_A$ and $\Delta\theta_B$ from Eqs. (5) and (6) (which were developed for the computer model) to the corresponding values from Eqs. (7) and (8) (which were developed for real member), yields expressions for "α_A" and "α_B":

$$\alpha_A = \frac{3EI}{L}\ \frac{\alpha}{(1 - \frac{\xi}{2})\ (1 - \alpha)\ K_S} \tag{9}$$

$$\alpha_B = \frac{3EI}{L}\ \frac{\alpha}{(1 - \frac{1}{2\xi})\ (1 - \alpha)\ K_S} \tag{10}$$

where $\xi = M_B / M_A$.

Equations (9) and (10) can be used to determine stiffness ratios of point hinges in the computer model if the bilinear moment-chord rotation relationship of the real member is known. The procedure for specifying stiffness properties of point hinges in program DRAIN-2D is explained in Appendix B.

The procedure described previously is concerned mainly with establishing the primary force-deformation relationship. The rules for hysteretic loops are obtained by substantially modifying the rules proposed by Takeda and Suzen[3]. Figure 4 illustrates different features of the hysteretic loops.

Modeling Wall Elements

Variation of moment along the height of structural walls is generally gradual and can be regarded as almost uniform between any two floors. Figure 7 shows a moment diagram of a wall element at the base. Since the moment in an element can be considered uniform, the sectional moment-curvature relationship has the same shape as the moment-chord rotation relationship. Therefore, general characteristics of the moment-curvature diagram can be used in specifying bilinear idealization of moment-chord rotation relationship. This implies that the inelastic stiffness ratio "α" required to solve Eqs. (9) and (10) can be obtained from moment-curvature relationship. For walls of the coupled wall structure considered in this investigation, the ratio of inelastic to elastic slopes of bilinear moment-curvature relationship "α" is taken as 0.05.

In solving Eqs. (9) and (10), "ξ" can be taken as approximately -0.8. It should be noted that according to the sign

-22-

Simulated Forces on a Wall Element
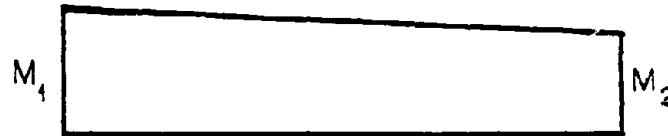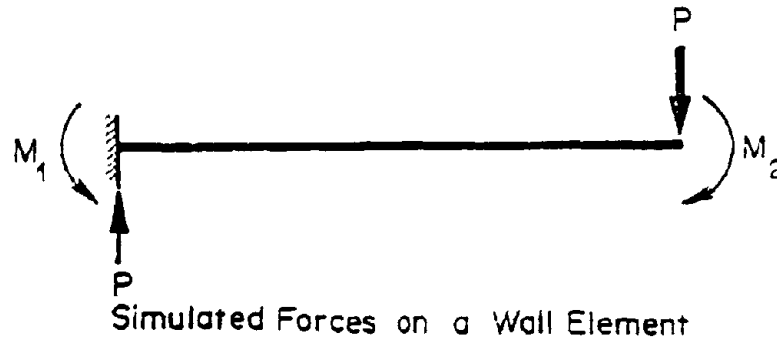
Moment Diagram

$$\xi = \frac{M_2}{M_1} \approx 0.8$$

Fig. 7 Moment Diagram of Wall Element at the Base

convention used in deriving the expressions for chord rotations, clockwise moments at member ends are positive. Therefore ratio of moments at ends of a wall element bent in single curvature has a negative sign. The stiffness parameter of point hinges in the elastic range is "K_S". This parameter is assigned a very large value to prevent rotation of point hinges during elastic action. A value of $K_S = EI \times 10^8$ is used for modeling wall elements.

Modeling Beam Elements

Coupling beams behave differently than wall elements. The main difference is the double curvature configuration that occurs in beams when the structure displaces laterally under earthquake-induced inertia forces. This implies that in the absence of gravity loads, the moment diagram for coupling beams shows a linear variation with opposite signs at each end. Consequently, formation of hinges may take place at two ends. These hinges rotate in opposite directions.

For a symmetric wall system with symmetrically reinforced coupling beams, it is reasonable to assume a symmetric moment distribution. Figure 8 illustrates a moment diagram and formation of hinges in coupling beams.

To determine properties of the point hinges at member ends, it is necessary to establish a bilinear idealization of the moment-chord rotation relationship. Although coupling beams do not exhibit uniform member stiffness beyond yielding, it is possible to assume an effective inelastic stiffness corresponding to the post-yield range of the linear idealization of the moment-chord rotation diagram. For beams of the coupled wall structure selected for this investigation, the ratio of inelastic to elastic slopes of bilinear moment-chord rotation relationship "α" is taken as 0.06.

In solving Eqs. (9) and (10), the moment ratio "ζ" is taken as 1.0 due to symmetry in the moment diagram. As in the case of wall elements, K_S is taken equal to $EI \times 10^8$.
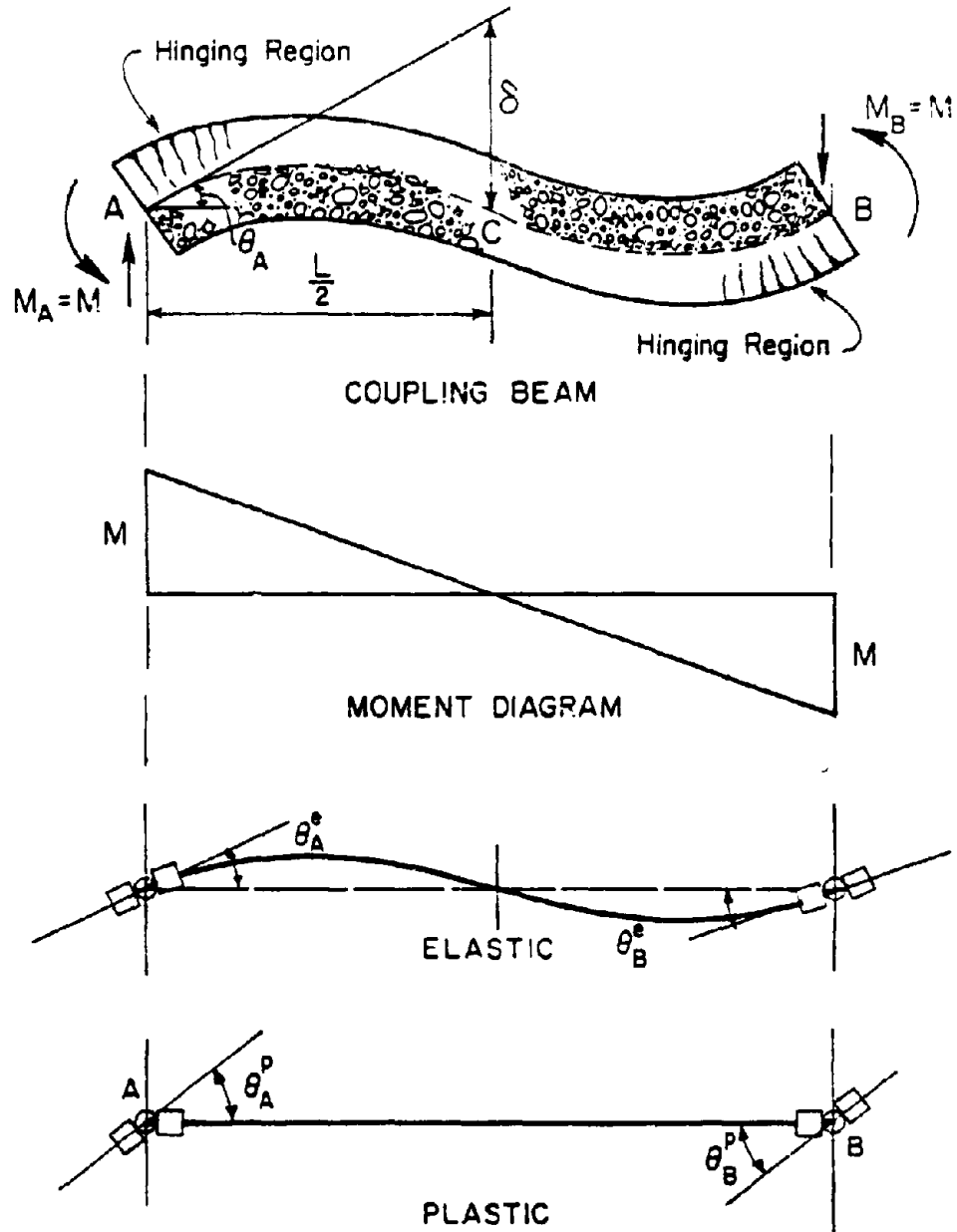
Fig. 8 Modeling Beam Members

Modeling for Shear

Modeling for shear is done in much the same manner as for flexure. Shear stiffnesses of the elastic beam and the point hinges are formulated in terms of flexibility equations. If the shear force-shear distortion relationship of a member is known, then characteristics of the primary shear-shear distortion curve for the analytical model can be determined. The following equations are used to determine total chord angle at member ends due to elastic and plastic shear distortion.

$$\Delta\gamma_A = \Delta\gamma_A^e + \Delta\gamma_A^p$$

$$\Delta\gamma_B = \Delta\gamma_B^e + \Delta\gamma_B^p$$

Where $\Delta\gamma_A^e$ and $\Delta\gamma_B^e$ are increments of chord angle rotations due to elastic shear distortions in the elastic beam and $\Delta\gamma_A^p$ and $\Delta\gamma_B^p$ are the corresponding increments due to plastic shear distortions in the point hinges at ends "A" and "B," respectively. The following shear-versus-shear distortion relationships can be written for the elastic and plastic components of an element AB.

$$\begin{bmatrix} \Delta\gamma_A^e \\ \Delta\gamma_A^e \end{bmatrix} = \begin{bmatrix} \frac{1}{GA} & 0 \\ 0 & \frac{1}{GA} \end{bmatrix} \begin{bmatrix} V_A \\ V_B \end{bmatrix} \tag{11}$$

$$\begin{bmatrix} \Delta\gamma_A^p \\ \Delta\gamma_B^p \end{bmatrix} = \begin{bmatrix} \frac{1}{\beta_A K_s} & 0 \\ 0 & \frac{1}{\beta_B K_s} \end{bmatrix} \begin{bmatrix} V_A \\ V_B \end{bmatrix} \tag{12}$$

Where β_A and β_B are ratios of the slope of post yield branch to the slope of elastic branch of the bilinear shear-shear distortion curves for the point hinges at member ends "A" and "B"

-26-

respectively. Stiffness of the shear spring (point hinge) in the elastic range is K_S. This quantity is typically very large prior to yielding so that the point hinges remain undeformed until yielding. Increments of shear forces at member ends are denoted ΔV_A and ΔV_B.

Stiffness ratios " β_A " and " β_B " can be determined by imposing the condition that the total chord angle due to shear be the same in both model and real member. The procedure used to derive expressions for these ratios in terms of the stiffness ratio of the real member, " β ", is similar to the procedure described previously for flexure.

Moments and shears in a member are directly related to each other through equilibrium equations. In DRAIN-2D, flexural and shear stiffnesses are combined as follows:

$$
\begin{bmatrix} \Delta\theta_A \\ \Delta\theta_B \end{bmatrix} = \begin{bmatrix} \dfrac{L}{3EI} + \dfrac{1}{\alpha_A K_s} + \dfrac{1}{LGA} + \dfrac{1}{\beta_A K_s} & -\dfrac{L}{6EI} + \dfrac{1}{LGA} \\ -\dfrac{L}{6EI} + \dfrac{1}{LGA} & \dfrac{L}{3EI} + \dfrac{1}{\alpha_B K_s} + \dfrac{1}{LGA} + \dfrac{1}{\beta_B K_s} \end{bmatrix} \begin{bmatrix} \Delta M_A \\ \Delta M_B \end{bmatrix} \tag{13}
$$

In this equation, $\Delta\theta_A$ and $\Delta\theta_B$ are "total" incremental chord angles at element ends "A" and "B" respectively, i.e., including elastic and plastic flexural and shear deformations.

The modeling procedure discussed above is used to establish the primary force-deformation relationship. Rules for hysteretic loops are obtained by modifying those proposed by Takeda and Sozen[3]. Figure 4 illustrates different features of hysteretic loops.
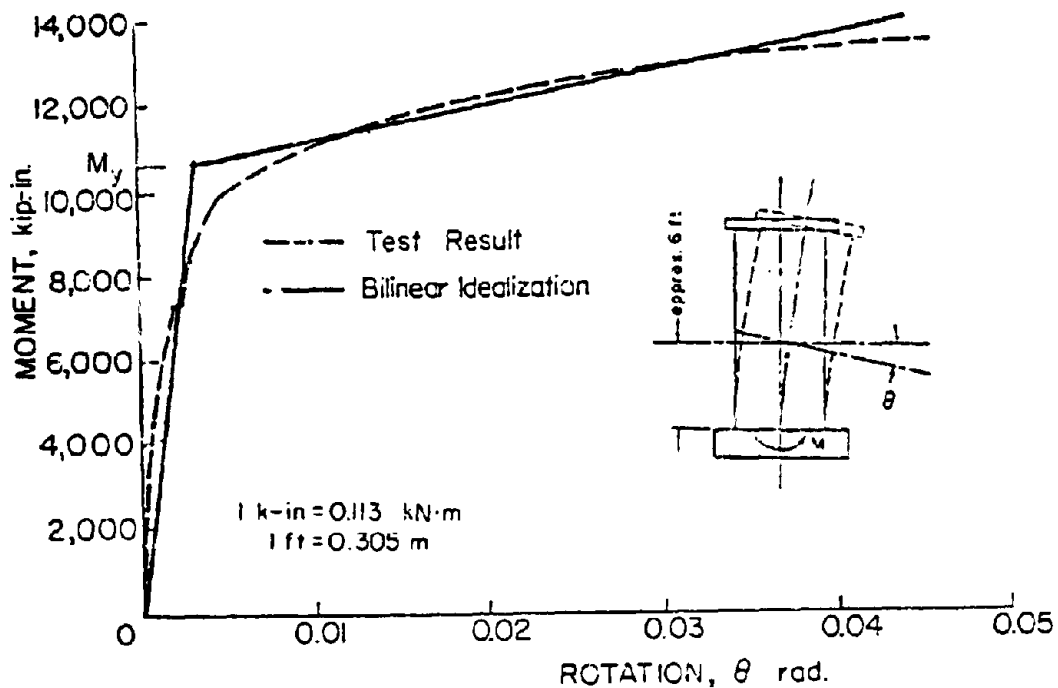
Fig. 9 Bilinear Idealization of Moment-Rotation
Relationship

Bilinear Idealization

A number of assumptions are made in modeling nonlinear
behavior of members. Most of these assumptions are related to
idealization and modeling of nonlinear force-deformation
relationships.

Moment-rotation relationships of members are idealized as
bilinear curves. Figure 9 illustrates a typical primary
moment-rotation relationship for reinforced concrete members
and its idealization as two line segments. The first line
segment represents effective stiffness in the elastic range,
and the second line segment represents post yield stiffness.

Depending on specifics of a given moment-rotation relationship, a number of rules may be devised to select slopes of these line segments and corresponding magnitude of yield moment. Member section details, especially locations of reinforcing bars, may have a significant effect on the general character of moment-rotation relationship. Thus members with the bulk of flexural reinforcement concentrated near ends of the section exhibit a relatively well-defined break (yield point) in their moment-rotation relationship. Some members, on the other hand, show progressive yielding and do not exhibit a clear yield point.

In arriving at a bilinear idealization of a particular force-displacement relationship, a number of approaches can be used. The simplest and most obvious would be a visual "sketched-in" approximation to the given curve. However, more specific quantitative criteria are desirable in the interest of reproducibility. Such rules can then be applied uniformly to any number of widely varying cases. For instance, best fit lines in the least squares sense could be obtained for specific ranges of deformation.

A more commonly used method applies the criterion of equal area under the actual and idealized curves over a reasonable range of deformation. In this case the intersection of effective elastic and post-yield line segments defines the yield point. The actual force-displacement curve will include effects of cracking as well as any softening due to bond slip.

A large number of moment rotation curves have been examined
in an effort to determine the range of variation of the ratio
of inelastic stiffness to effective elastic stiffness. For
example, members subjected to a uniform moment develop hinging
along the entire length once yield level is reached. In this
case, inelastic stiffness is almost uniform along the member
length. Wall elements at the base of coupled wall structures
are in this category. Inspection of moment-rotation relation-
ships for this case reveals that 5% of the effective elastic
stiffness can be used as a realistic approximation of inelastic
post-yield stiffness. The significance of variations in this
ratio is investigated and discussed under "Dynamic Analyses".

Beam elements show a slight difference in the magnitude of
their inelastic stiffness when compared to walls. This is due
mainly to the relatively steep moment gradient across the
span. Under a lateral wall displacement, coupling beams are
bent antisymmetrically and hinges can form at each end of a
beam. These hinges are usually localized and do not extend
beyond midspan. This implies that beams are partially elastic
even after formation of hinges at member ends. For this
reason, slightly higher effective inelastic member stiffness
should be used to account for the elastic portion of the beam.
In this investigation, 6% of the effective elastic stiffness is
taken as the effective inelastic stiffness for the coupling
beams. This value may be higher for shallow and slender beams

since the hinging region usually does not extend beyond a distance from the end equal to the effective depth of the beam.

The ratio of inelastic to elastic slopes of idealized moment-chord rotation relationship will vary with individual member properties. However, this variation is usually small and therefore is not expected to have any significant effect on dynamic response[7, 8]. The significance of variation in the inelastic slope of primary moment-rotation curve is investigated and discussed in detail under "Dynamic Analyses". Results indicate that small variations do not affect most response quantities. However, if considerable inelastic action takes place, as in the case of some coupling beams, then this effect becomes more pronounced. Any affect on coupling beams is transmitted to the walls in the form of changes in wall axial forces.

MEASURES OF INELASTICITY

The general concept of inelastic design against earthquake forces is well accepted in current design practice. The aim in inelastic design is to design critical regions of structures so that the required inelastic action can take place without significant loss of strength or excessive deformation. A measure of this inelastic action is difficult to define if it is to cover all aspects of inelastic deformation capacity.

A commonly accepted measure of inelastic deformation is ductility factor or ratio. In a general sense ductility is defined as the ratio of maximum deformation to yield deformation. Although this measure indicates maximum deformation

produced in a member, it does not qualify how this maximum deformation is obtained. More importantly, it does not indicate the number of times that this maximum deformation, or deformations of comparable magnitude, are imposed on a particular member. Because members subjected to repeated cycles of inelastic deformation can fail at force and deformation levels lower than those associated with static monotonic loading (i.e., low-cycle fatigue), it is important to include information on the number of cycles of large amplitude that can be expected in defining deformation requirements or capacity.

Other measures of inelastic action are based on energy. Energy, by definition, considers deformations as well as forces producing the deformations. Dissipated energy is the irrecoverable part of the total strain energy and is associated with plastic deformations. Cumulative dissipated energy, on the other hand, is the sum of the inelastic energy over the entire response period. As such it reflects the history of loading.

In this investigation, rotational ductility is used as a measure of inelastic action. However, cumulative dissipated energy is also computed for comparative purposes.

Rotational Ductility Factors

The rotational ductility factor is defined as:

$$\mu_r = \frac{\theta_{max}}{\theta_y}$$

Where θ_{max} is maximum rotation and θ_y is yield rotation. Generally, the rotations referred to here are the rotations of the hinging region. Generally, width of walls is equal to or greater than floor-to-floor height. If we assume the hinging region to have a height approximately equal to the wall width[5,6], then an entire wall element between floors in the model would form part of the hinging region. For this case, it would be appropriate to speak of ductility associated with the entire element. In terms of rotational deformation, the total rotation in the element would be given by the sum of chord rotations at both ends of an element. This total rotation in an element is made up of the sum of point hinge rotations and elastic chord rotations at both ends as shown in Fig. 6. Yield rotation is taken as the sum of elastic chord rotations at both ends when the moment in member is equal to the yield moment.

The same basic definition of ductility is used for coupling beams. However, because coupling beams are generally bent in double curvature, as compared to single curvature prevalent in walls, a slightly different method is used in calculating ductility. In a coupling beam bent in an antisymmetrical mode, hinges can form at each end but rotate in opposite directions. Because of this, hinges in coupling beams are generally limited in extent to one-half the span. In this case, ductility at one end is based on chord rotation at that end rather than the sum of the chord rotations at both ends used for walls.

Further clarification of the definition of ductility for coupled wall structures may be in order due to the nature of hysteretic loops for this kind of structure. Because of the

coupling action between the walls, magnitudes of axial forces at yielding and at the point of maximum rotation may be different. In this investigation, yield rotation corresponding in sign to the maximum rotation is used in defining ductility, irrespective of corresponding axial force levels. Thus, if maximum rotation is positive, rotation at first yield when the moment is positive is used to calculate the ductility ratio. This is illustrated in Fig. 10.

Another feature of the hysteretic loop for coupled walls is the loss of symmetry in wall behavior under reversed loading. Thus, axial force in a coupled wall can be tensile when bending in one direction and compressive when loaded in the opposite direction. Because yield moment of a section changes with magnitude of the concurrent axial force, different values of yield moment and rotation generally result for each direction. In this investigation, the ductility factor is based on the maximum and yield rotations in the same direction. This is done even if first yield occurs in one direction and maximum rotation is recorded in the opposite direction, although this case rarely occurs. Usually both initial yield and maximum rotation occur while loading in the same direction. Maximum rotation generally occurs during the "tension phase" when the flexural yield level of the wall is reduced due to tension.

Energy Dissipation

Dissipated energy is the irrecoverable portion of total strain energy. It is therefore associated with plastic deforma-

$$\mu_r^+ = \frac{\theta_{max.}^+}{\theta_y^+}$$

$$\mu_r^- = \frac{\theta_{max.}^-}{\theta_y^-}$$
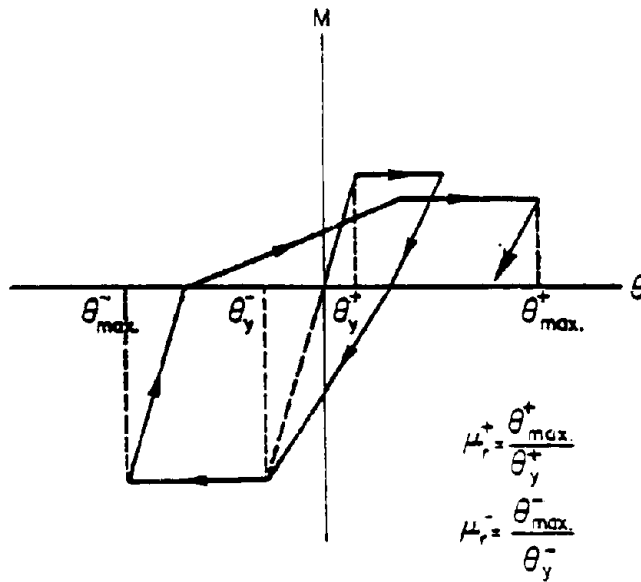
Fig. 10 Definition of Rotational Ductility Factors

$$e = \frac{Shaded \ Area}{\frac{1}{2} M_y \ \theta_y}$$
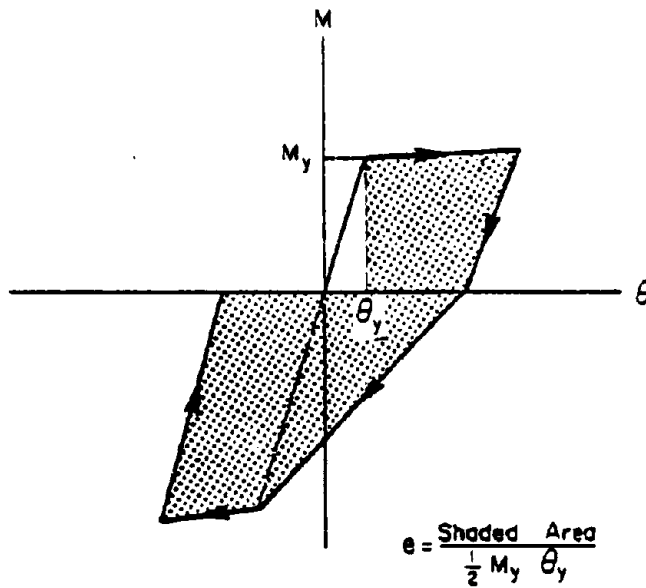
Fig. 11 Definition of Energy Dissipation Factors

tions. In computer program DRAIN-2D, plastic deformations are simulated by inelastic point hinges. Dissipated rotational energy can then be calculated from the area under moment-rotation curve of the point hinges.

Cumulative dissipated energy can be determined by summing the absolute value of inelastic energy for each time increment. In this investigation, cumulative dissipated energy as a measure of inelastic action is normalized by dividing it by the corresponding elastic energy up to yield. "Energy Dissipation Factor" is then defined as the ratio of cumulative dissipated energy to elastic energy up to yield, as shown in Fig. 11.

DYNAMIC ANALYSES

A series of dynamic analyses was carried out to answer several questions mainly relating to modeling techniques. The coupled wall structure previously selected, having an initial fundamental period of 1.0 second was analyzed. The structure was assumed to be fully fixed at foundation level, and assumed to have 5% of critical damping*. Basic properties of the structure are listed in Table 1 and were used unless otherwise noted.

Selection of Ground Motion

For preliminary dynamic analysis it was desirable to use an input motion that was critical in terms of frequency content with respect to the particular structure considered.

---

*Viscous damping assumed in this investigation is a linear combination of stiffness-proportional and mass-proportional damping. Percentage of the critical damping for the first and second modes were used.
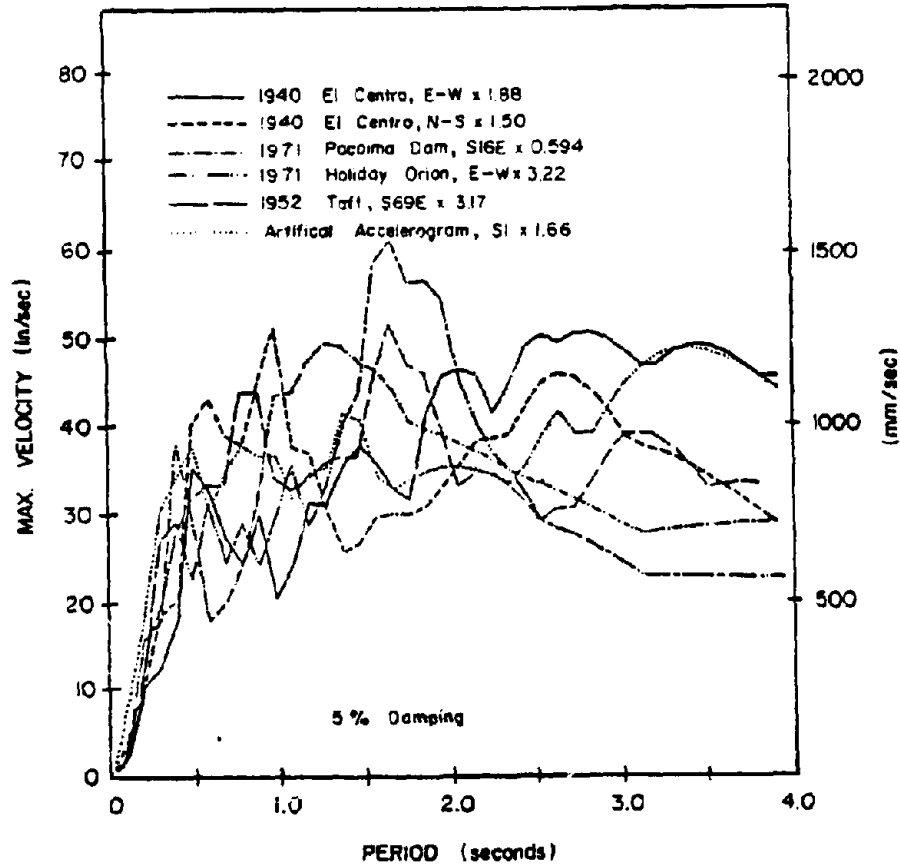
Fig. 12 Relative Velocity Response Spectra for First
Ten-Seconds of Normalized Input Motions

Six different accelerograms were examined for this purpose.
Response spectra of single-degree-of-freedom systems were used
as basis for the preliminary selection. Figure 12 shows the
5%-damped response spectra for the first 10 seconds of the
accelerograms considered. In all cases, intensity of each
input motion was adjusted to yield a spectrum intensity* equal
to 1.5 times the spectrum intensity of the N-S component of the
1940 El Centro record.

---

*5%-damped spectrum intensity for the period range of 0.1 sec.
to 3.0 sec. corresponding to first 10 seconds of input motions
considered.

The initial fundamental period of the 20-story structure and possible softening (lengthening in period) in the structure due to yielding were considered in selecting three potentially critical accelerograms from Fig. 12. The structure was analyzed under 10 seconds of each input motion. Figures 13 and 14 illustrate response envelopes of the 20-story coupled wall structure. Based on this comparison, the 1971 Pacoima Dam S16E record was selected for use in most cases during dynamic analysis.

It can be observed from the response histories that the maximum response under the 1971 Pacoima Dam S16E record occurs early in the analysis. Therefore, in cases where this feature of the response did not allow the effect of a particular parameter investigated to show up clearly, a different input motion was used. A good example of this is the investigation of effect of strength decay in hysteretic loops. If the maximum response is governed by initial maximum loading on the primary curve then gradual loss of strength in later cycles does not show up in response envelopes. For this reason, in some cases the E-W component of 1940 El Centro record was used to create a condition in which the investigated parameter was affected most.

In all the analyses reported here, a 10-second duration of input motion was used. Unless otherwise noted, the input motion used was the 1971 Pacoima Dam S16E record.
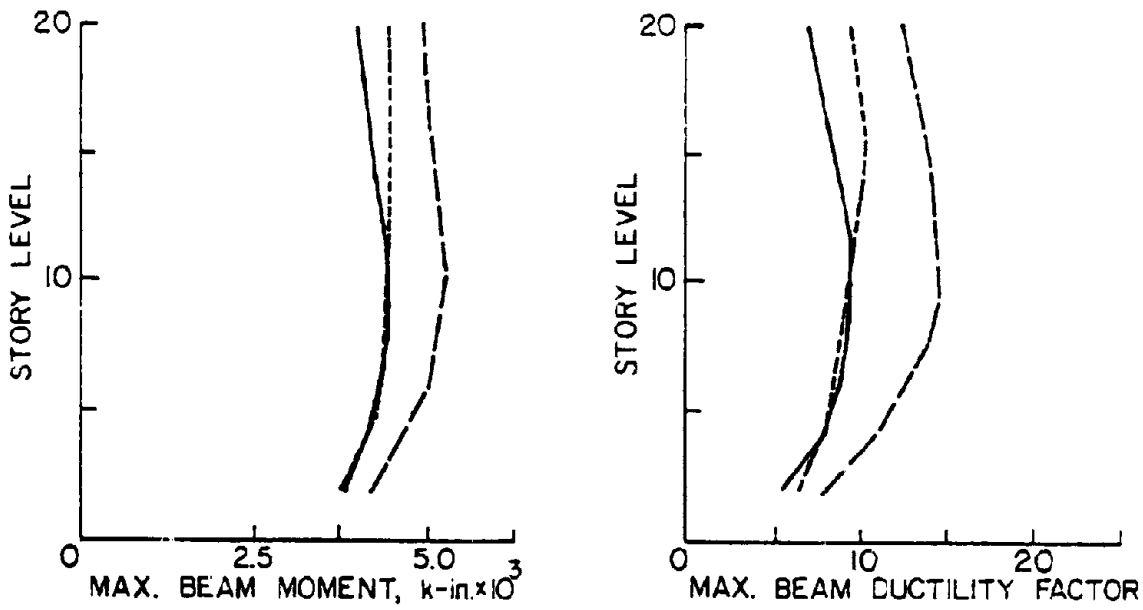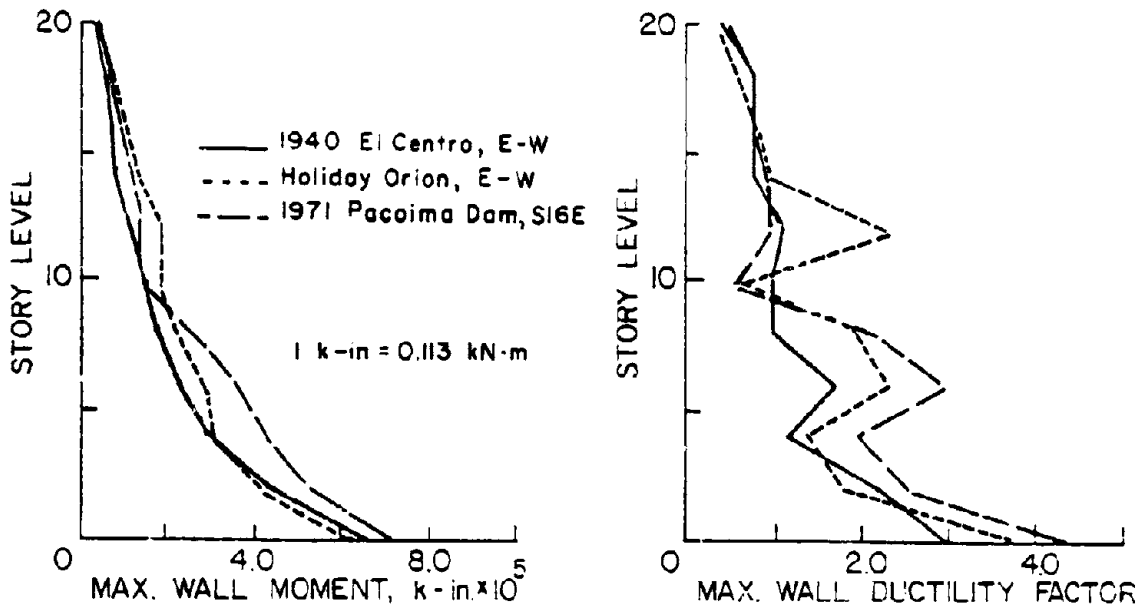
Fig. 13 Response Envelopes Showing the Effect of Earthquake
Frequency Characteristics
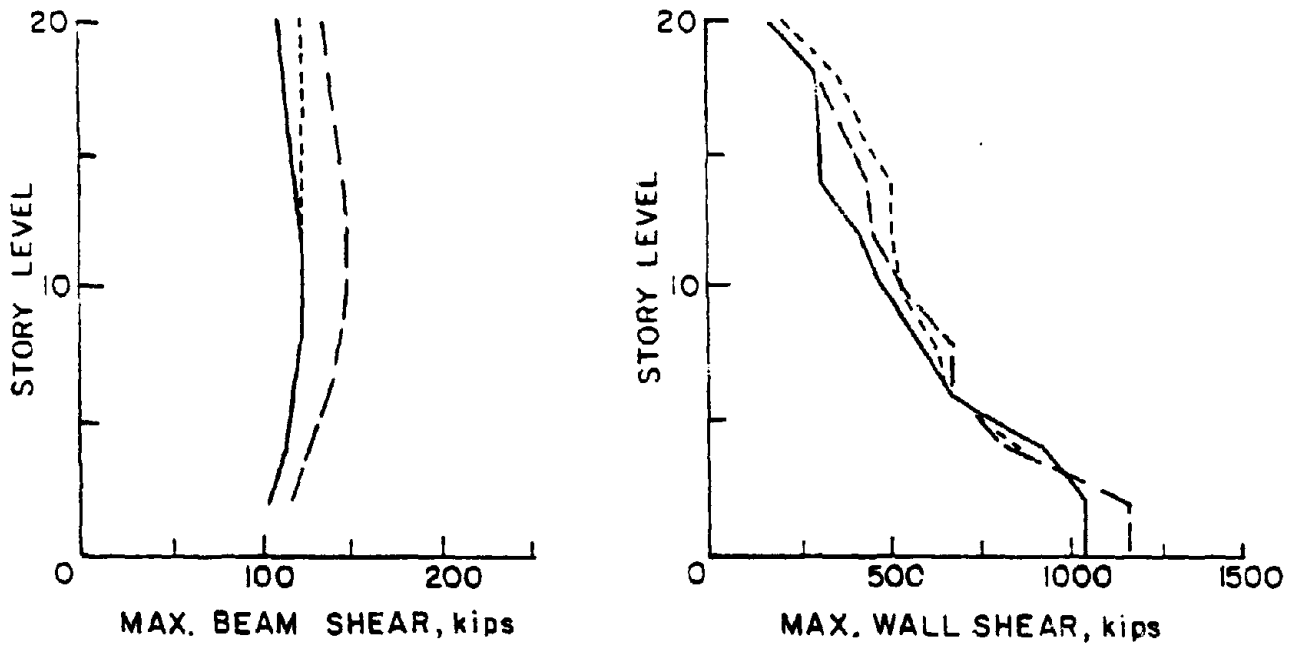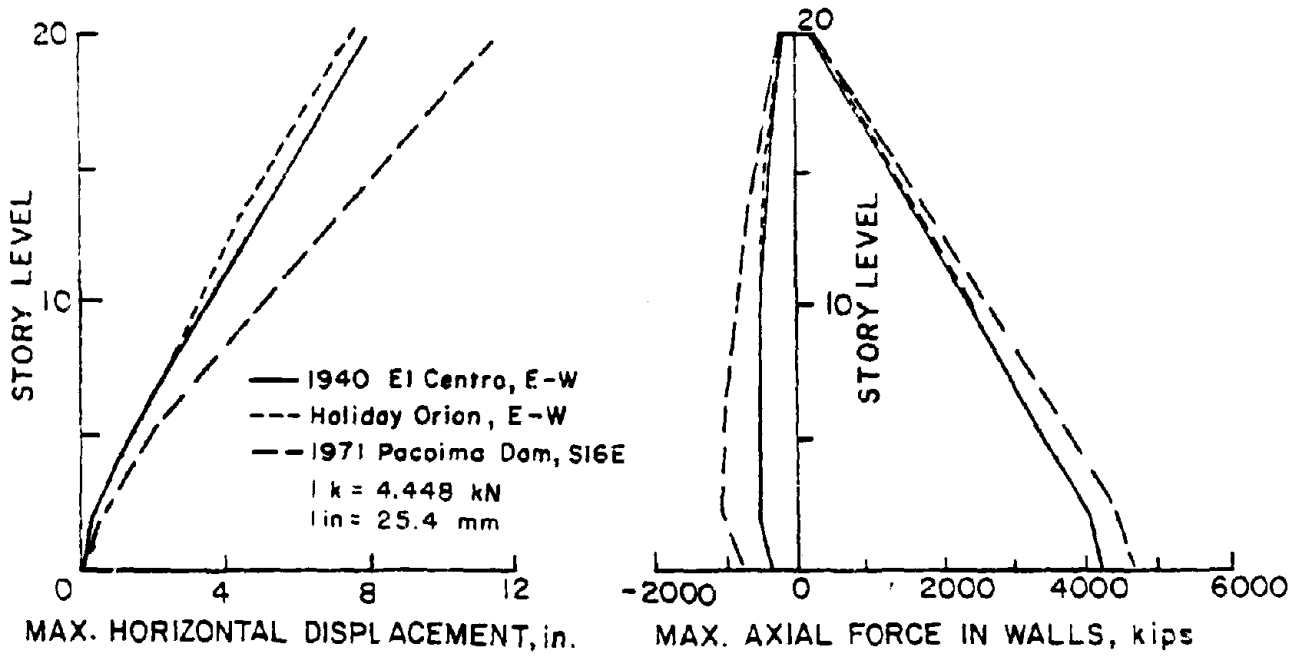
Fig. 14 Response Envelopes Showing the Effect of Earthquake
Frequency Characteristics

Vertical Lumping

As outlined under "Selection of a Structure", the 20-story prototype was reduced to a 10-story model to reduce the computer time required for analysis. The 10-story model was obtained through static, elastic analysis. To verify equivalence between model and prototype under dynamic inelastic response conditions, a comparison is made between the 20-story prototype and the 10-story model under earthquake excitation. Response envelopes for the two structures show good agreement as indicated in Figs. 15 and 16.

These analyses confirm that the 10-story model provides a good representation of the 20-story prototype.

Integration Time Step

The integration time step used in the dynamic analysis is of primary concern as it plays an important role in accuracy of results and cost of computer runs. The 10-story model structure, which has a fundamental period of 1.0 second, was analyzed using integration time steps of 0.005 sec. and 0.01 sec. The results show excellent agreement. Top displacement, base maximum moment, base maximum shear, and ductilities are all within 5% of each other.

Based on these results, an integration time step of 0.01 sec. was selected for use throughout this investigation.

Strength and Stiffness Taper

As discussed under "Selection of a Structure", wall cross sectional dimensions and percentages of reinforcement were
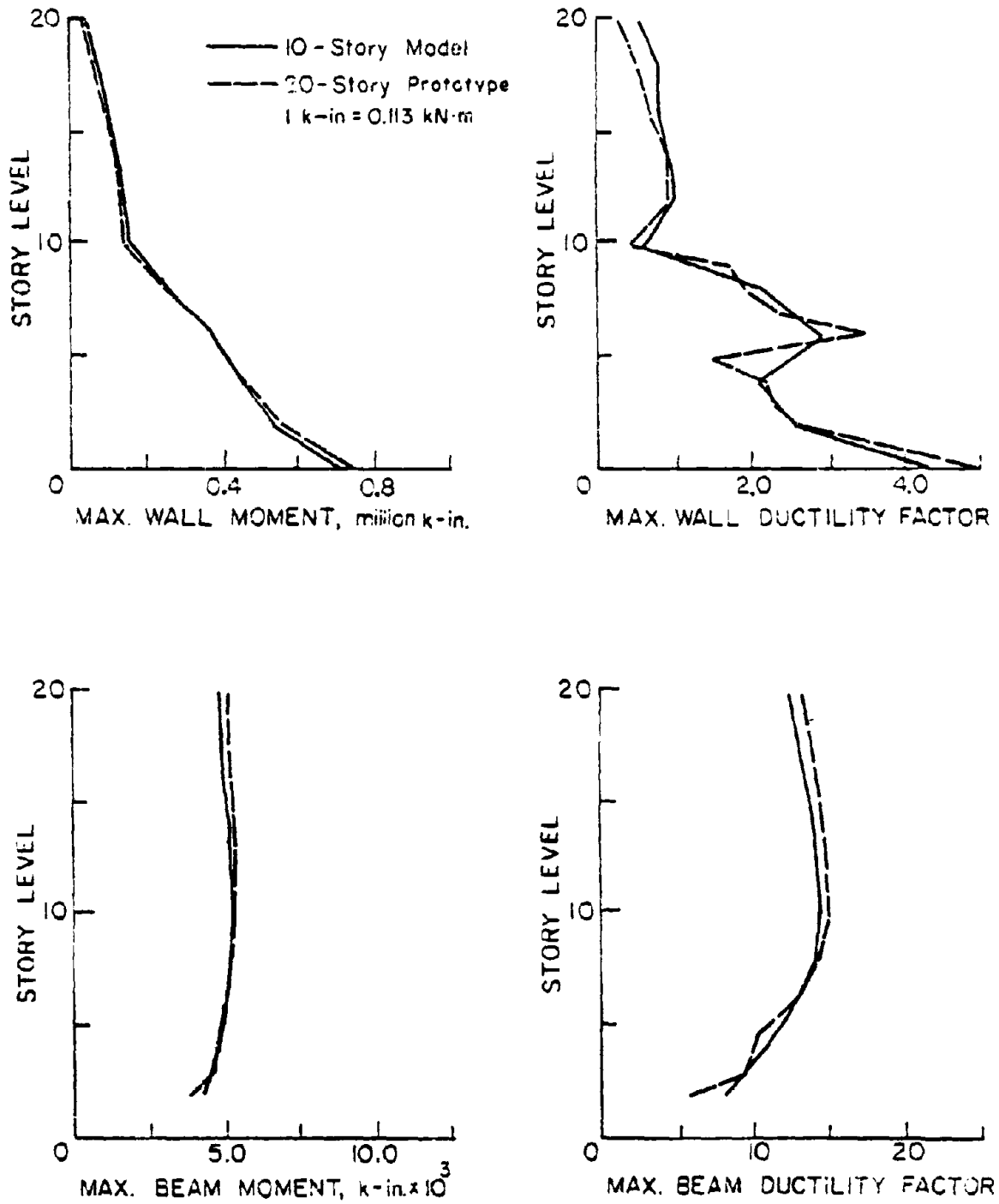
Fig. 15 Response Envelopes Showing the Effect of Vertical
Lumping
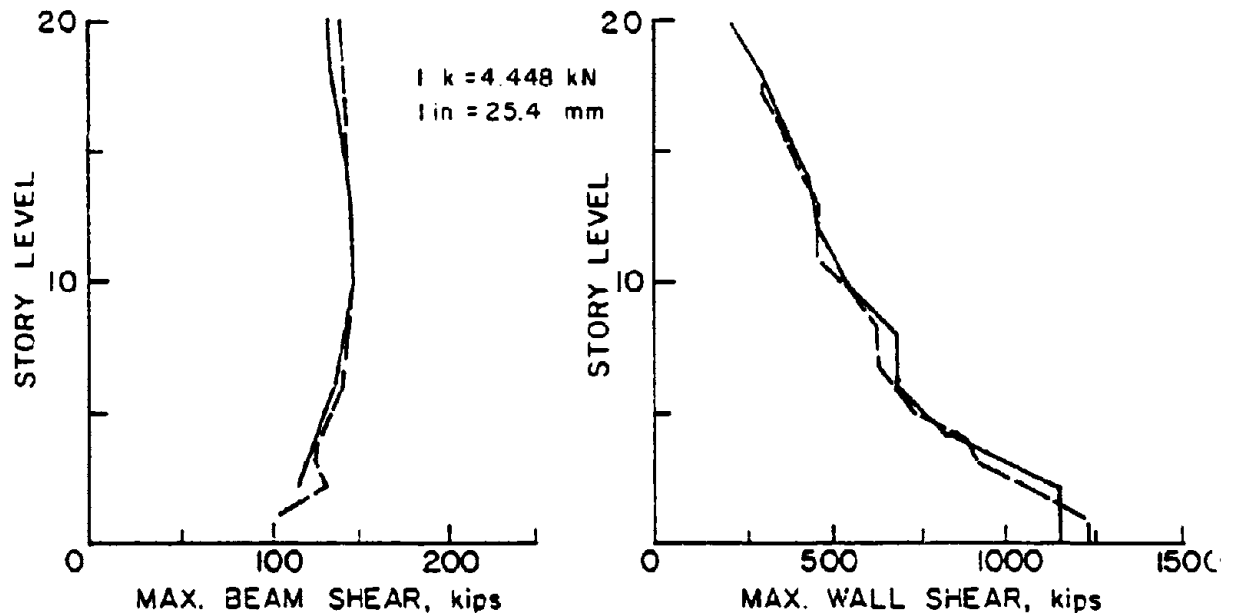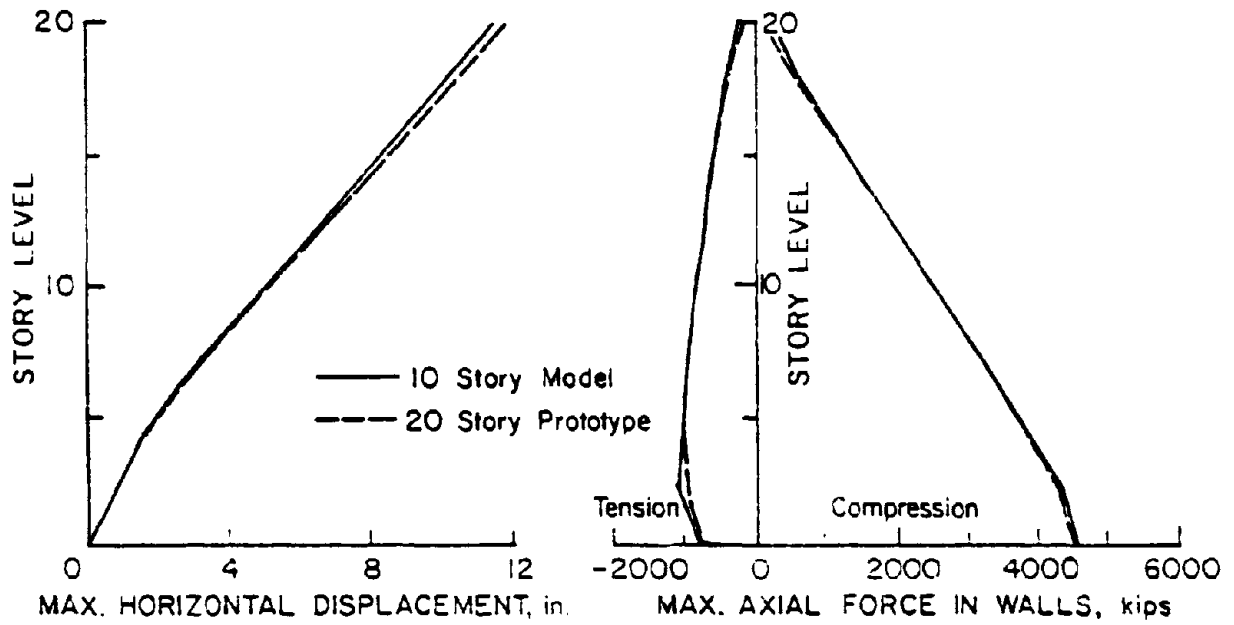
Fig. 16 Response Envelopes Showing the Effect of Vertical
Lumping

TABLE 3 - POSSIBLE VARIATION IN WALL THICKNESS
OF A 20-STORY STRUCTURE

Floors	Wall Thickness (in.)						% Variation
$15^{th} - 20^{th}$	8	10	13	16	18	20	65
$9^{th} - 14^{th}$	10	13	16	20	23	27	80
$1^{st} - 8^{th}$	12	15	20	24	28	32	100

changed twice along the structure height. This introduced a stiffness and strength taper. In practice, this is done for tall structures to save material and can be justified from the point of view of static gravity loads.

The significance of taper in walls on dynamic response was investigated and is discussed in this report. Possible variation in wall thickness for a 20-story structure was reviewed. Table 3 lists selected wall thicknesses and percentages of variation in moments of inertia of rectangular cross sections. Although Table 3 does not necessarily cover all the countless possibilities in practice, it does provide a practical variation in wall thickness in view of general variation of moment along the structure height. Based on this review, effective elastic stiffnesses equal to 80% and 65% of that of the walls at the base were used at two locations along the height of the structure considered, as indicated in Table 1.

Changes in reinforcement also occur at locations where wall thickness changes. This is done by specifying different flexural strengths. The amount of taper is determined on the basis of static design under equivalent static forces. The

strength taper, introduced at two locations along the wall height, results in reductions to 75% and 50% of wall strength at the base as shown in Table 1. It is important to note that wall flexural strength is further adjusted at every floor for effect of axial loads due to gravity load on the structure. This is done by specifying a moment-axial force interaction diagram and dead load of structure at every floor. This strength adjustment for gravity load effects also introduces a natural strength taper along the height. Further changes in flexural strength of walls occur during dynamic response due to effect of axial forces associated with lateral displacement of the structure.

To investigate the effect of taper, the structure was subjected to two different recorded earthquake motions, namely the 1971 Pacoima Dam S16E component and the 1971 Holiday Orion E-W component*. The Pacoima Dam record produced the more severe response in all cases except for the ductility at midheight which was greater for the Holiday Orion record.

The same structure having same fundamental period but without the strength and stiffness taper was analyzed under the same two earthquake motions. Strength taper due to structure weight was present in these analyses. Response envelopes are compared in Figs. 17 and 18. Force envelopes for walls and beams, and ductility envelopes for beams are not significantly affected by

---

*The E-W Component of the record was taken at the ground floor of the Holiday Inn on Orion Boulevard, Los Angeles, during the 1971 San Fernando earthquake.
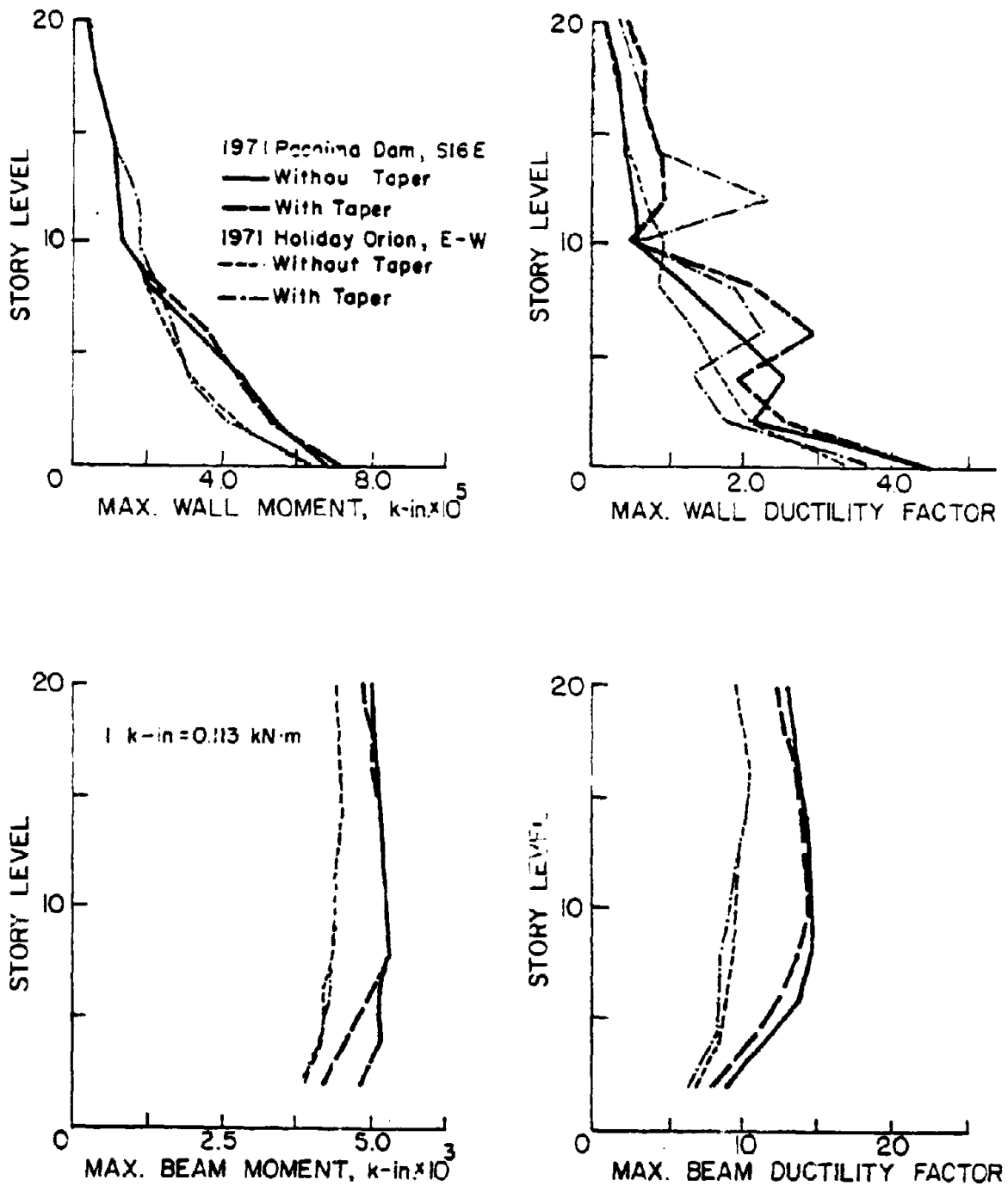
Fig. 17 Response Envelopes Showing the Effect of Stiffness and
Strength Taper Along the Height of the Walls
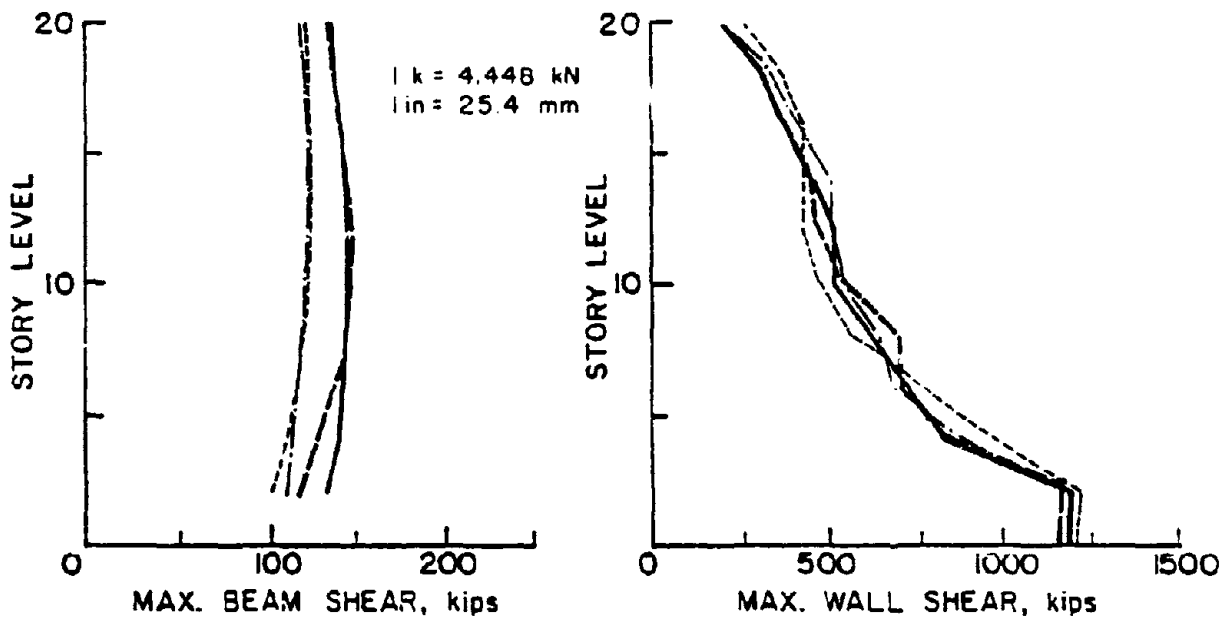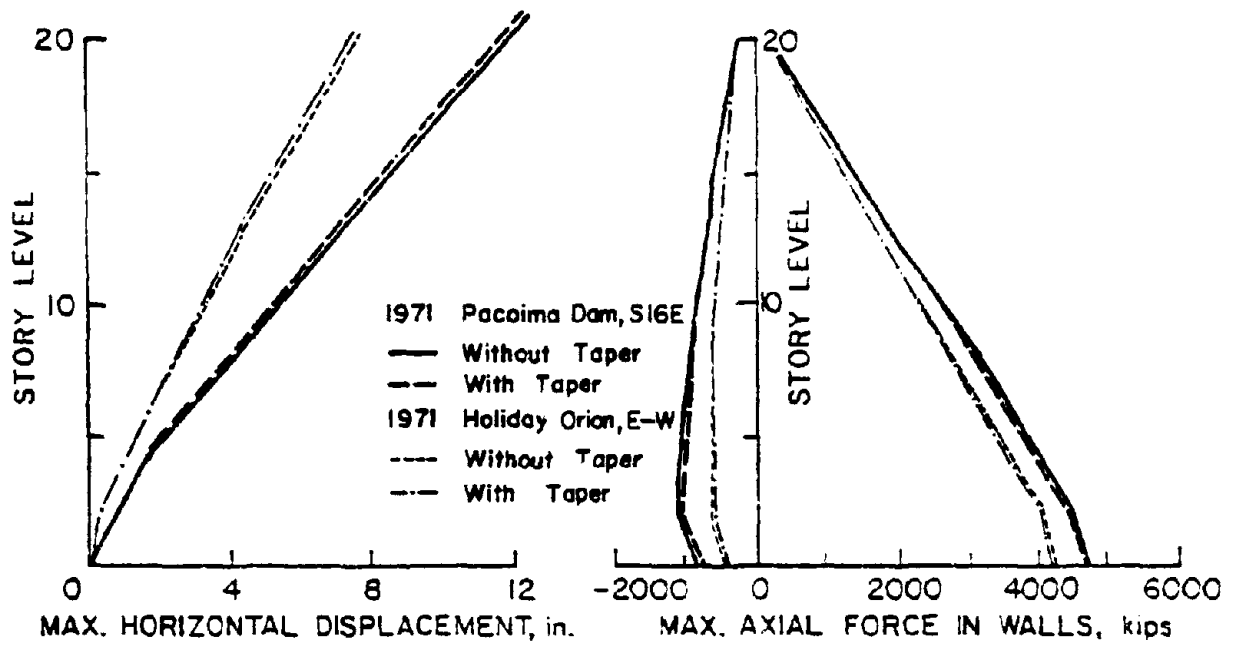
Fig. 18 Response Envelopes Showing the Effect of Stiffness and
Strength Taper Along the Height of the Walls

strength and stiffness taper. Wall ductility envelopes, on the other hand, show a considerable effect of strength and stiffness taper.

As can be seen in Fig. 17, walls with taper show yielding not only at the base, but also at locations where changes in strength occur, i.e., at points of discontinuity. Inelastic action in upper story walls is reduced to a great extent by eliminating taper. In this respect, a structure with uniform strength and stiffness produces superior behavior under earthquake forces. In all cases, inelastic action at upper stories is less severe than that at the base. This can be observed from the ductility envelopes of walls given in Fig. 17.

Axial Force Effects

The original DRAIN-2D model for reinforced concrete members with moment-rotation hysteretic loops exhibiting decreasing stiffness characteristic was developed for constant axial force. In coupled wall systems, substantial axial forces can be induced in walls during dynamic response as a result of the coupling action of linking beams. Because of the significant effect that axial forces in coupled walls can have on their flexural yield levels[9], it was deemed necessary to include this axial force-flexure interaction effect in the analytical model. Modification of Program DRAIN-2D to incorporate this feature was the first step in this investigation. A detailed description of the model is given in Appendix A.

Changes in level of axial forces in walls during dynamic response has direct influence on force-deformation characteristics of walls. The presence of compressive forces can increase flexural strength as well as stiffness. Tensile forces, on the other hand, produce the reverse effect. This results in shifting of forces from one wall to another during dynamic response and may subject individual walls to critically high shears and moments.

Figure 19 illustrates the effect of axial forces on hysteresis loops of "tension" and "compression" walls. Increase in strength (yield level) and stiffness during loading and reloading of compression wall can be observed in Fig. 19. The reverse effect is shown in the same figure for tension wall. Had the axial force effect in wall behavior been neglected, a symmetric behavior would be observed in "tension" and "compression" walls as indicated by broken lines in Fig. 19.

To investigate the effect of axial force-flexure interaction, the structure was analyzed first by neglecting this effect and then a second time with the effect considered. The results are shown in Figs. 20 and 21. These results indicate that maximum forces in the walls can be affected significantly by axial force-flexure interaction. The analysis which ignored the effect of axial force underestimates maximum shear and moment at the base by as much as 50%. Moreover, the sequence of yielding observed in this analysis is not realistic since the yield level is affected by the concurrent axial force. It should be noted that the difference between the maximum wall ductilities

-49-
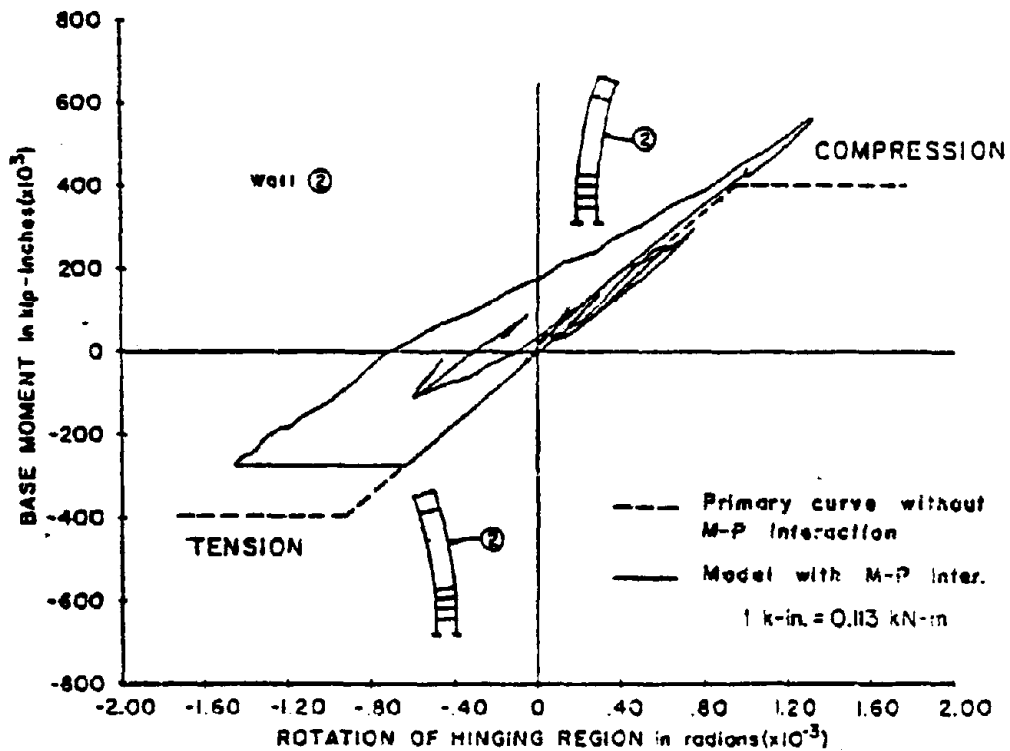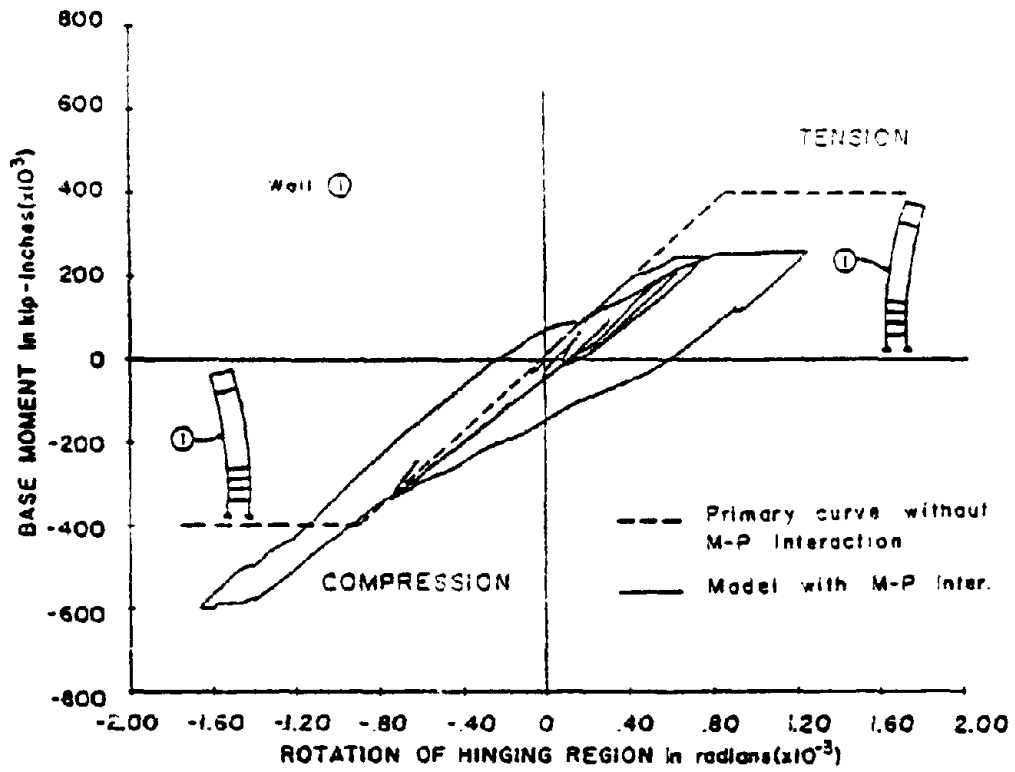
Fig. 19 M-P Interaction Effects on Hysteresis Loops
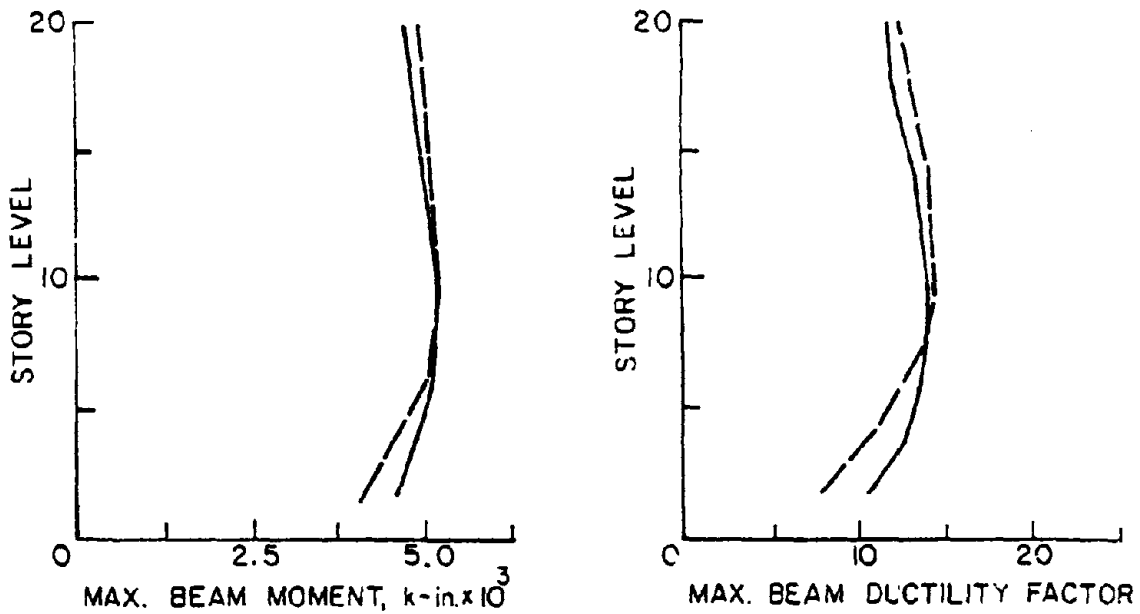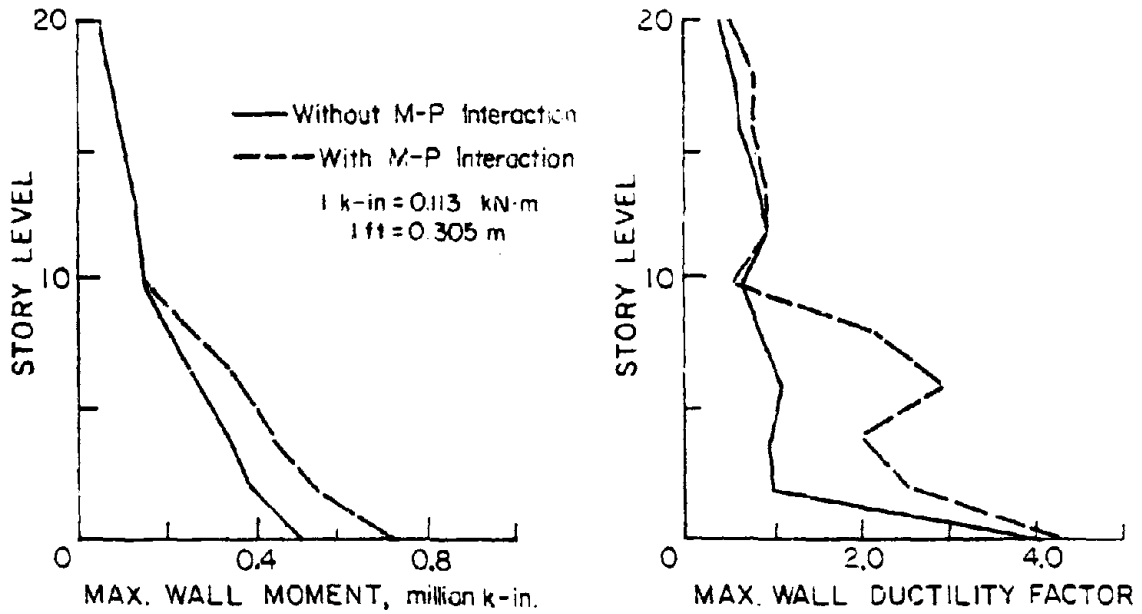
Fig. 20 Response Envelopes Showing the Effect of Changing
Axial Forces (M-P Interaction) on Walls
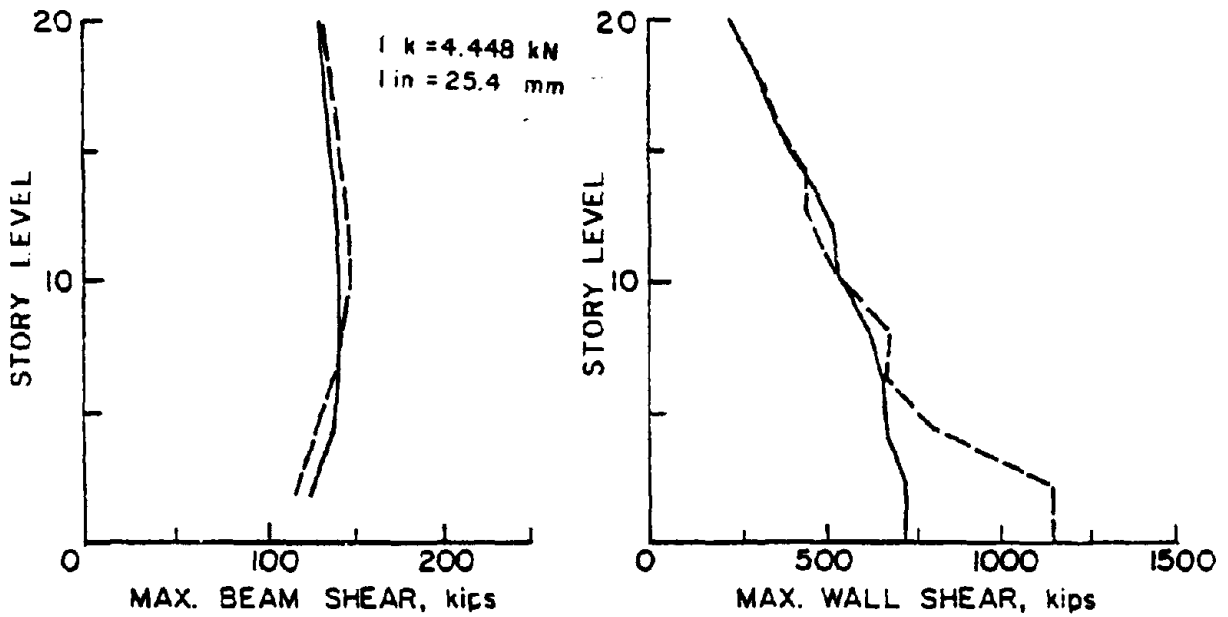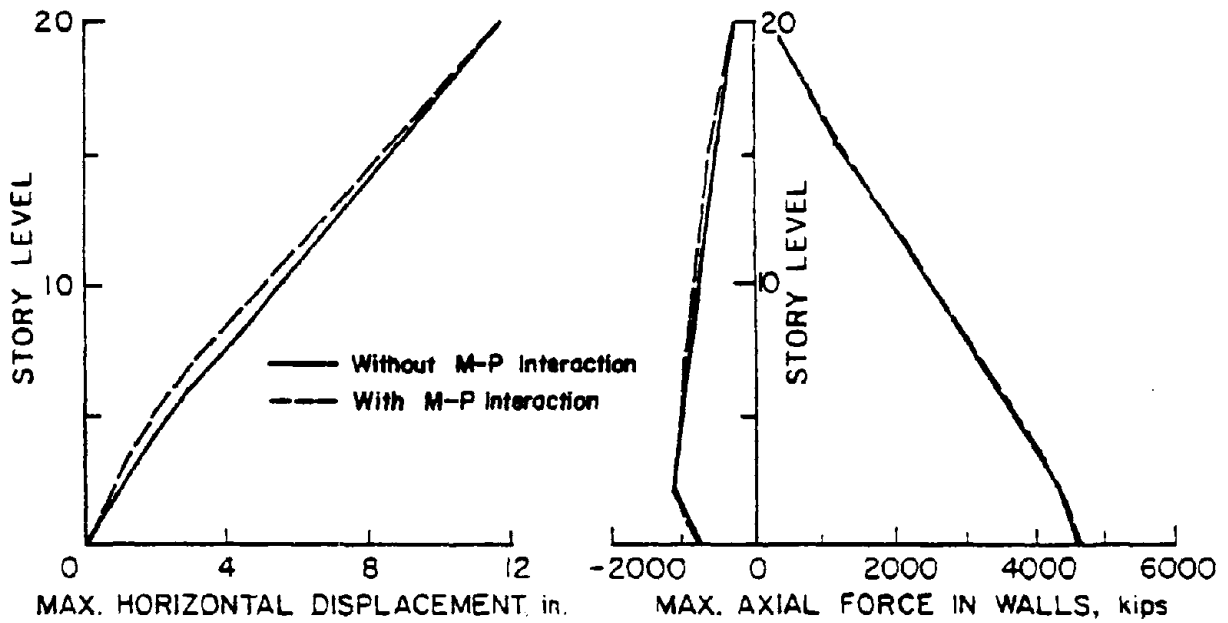
Fig. 21 Response Envelopes Showing the Effect of Changing
Axial Forces (M-P Interaction) on Walls

of the two cases compared in Fig. 20 is due to the lower yield
level in tension walls. It does not necessarily imply increased
horizontal displacement of tension walls. Maximum horizontal
displacements are shown in Fig. 21.

Inelastic Shear Effects

Structural walls in multistory buildings, like most rein-
forced concrete members, are generally designed so that shear
strength does not control their behavior, i.e., adequate shear
strength is provided so that flexural yielding can occur prior
to shear distress. Under this condition, a member is expected
to remain essentially elastic in shear at least until flexural
yielding occurs. Tests conducted at the Portland Cement Asso-
ciation, as part of this project, indicate that flexural
yielding is usually accompanied by shear yielding[5,6].

Estimation of the magnitude of inelastic action, in both
shear and flexure, is of primary interest in design. Because
of this and the potential effects that shear yielding ay have
on overall structural response, a simplified model of the
inelastic shear mechanism was introduced into Program DRAIN-2D
to allow examination of this effect. A brief description of
basic features of this model is given under "Computer Program
for Dynamic Analysis".

Figure 22 shows moment-versus-rotation and shear-versus-
shear distortion relationships of a test specimen subjected to
statically applied, slow load reversals[5]. This figure shows
that shear yielding takes place almost simultaneously with flex-
ural yielding. Investigation of the hinging region deformations

-53-

$1 \text{ k-in} = 0.113 \text{ kN} \cdot \text{m}$

$1 \text{ k} = 4.448 \text{ kN}$

$1 \text{ in} = 25.4 \text{ mm}$
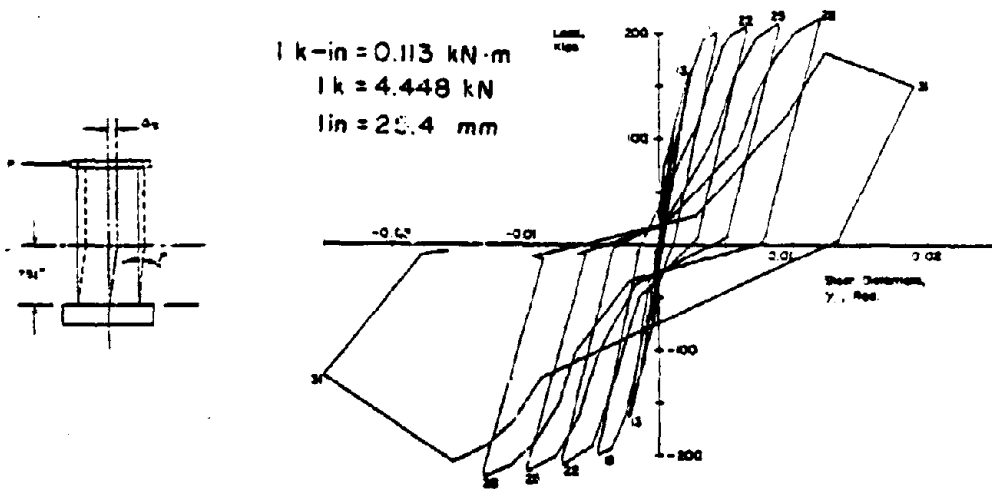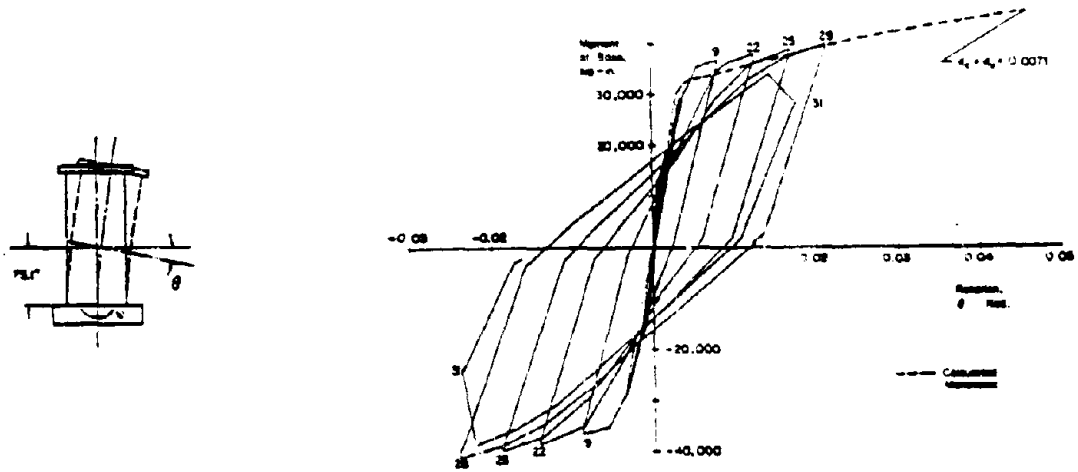
Fig. 22 Moment-Rotation and Shear-Distortion Relationships
of a Test Specimen

revealed that a substantial component of the horizontal displacement is due to inelastic shear action. Similar behavior was observed in the other 15 structural wall tests conducted at the Portland Cement Association[5, 6].

Another important phenomenon observed in the PCA wall tests was the substantial reduction in shear stiffness that occurs under increasing load. The effective elastic shear stiffness is reduced due to both flexural and shear cracking in concrete. This reduction results in effective elastic shear stiffnesses as low as 10% of its uncracked value. Wall tests under slow load reversals have also been reported by other investigators[10, 11, 12]. Considerable inelastic shear deformation and a substantial reduction in elastic shear stiffness were also observed in these tests.

The effect of inelastic shear deformation on dynamic response of a 20-story coupled wall structure was investigated using the structure shown in Fig. 2. Structural and ground motion properties are given in Table 1, except for stiffness properties, which are given in Table 4. The structure was analyzed three times: In the first analysis, the structure was not allowed to yield in shear throughout the response with stiffness equal to effective elastic shear stiffness. In the second analysis, shear yielding was allowed following flexural yielding. The inelastic shear force-versus-shear distortion relationship was modeled on the basis of rules proposed by Takeda and Sozen[3] as shown in Fig. 4(a). In the third analysis, shear yielding was allowed in the same manner as

TABLE 4 - STIFFNESS PARAMETERS

Floor level:	Walls			Beams*
	1st - 5th	6th - 12th	13th - 20th	All Floors
Effective Elastic "EI" (k-in².)	8.28×10^{10}	6.62×10^{10}	5.38×10^{10}	2.27×10^{7}
Post-Yield "EI" (Primary Curve, k-in².)	0.41×10^{10}	0.33×10^{10}	0.27×10^{10}	0.14×10^{7}
Effective Elastic "GA" (kips)	1.02×10^{6}	0.81×10^{6}	0.66×10^{6}	6.50×10^{4}
Post-yield "GA" (Primary Curve, kips)	0.61×10^{5}	0.49×10^{5}	0.40×10^{5}	3.90×10^{3}
Effective Elastic "EA" (kips)	1.42×10^{7}	1.14×10^{7}	0.93×10^{7}	9.20×10^{5}

*Stiffness values of beams in 10-story model are twice the value listed.

the second analysis. However, this analysis includes "pinching" action in the shear-shear distortion relationship, as shown in Fig. 4(d). Response envelopes for these three cases are compared in Figs. 23 and 24. In Fig. 23 the decrease in beam rotational ductility due to shear yielding can be attributed to an increase in shear component of total deformation which leads to a decrease in flexural component of chord rotation. The yielding sequence of members is shown in Fig. 25 and Table 5. The effect of pinching is discussed later in this report under "Pinching of Force-Deformation Relationship".

In addition to the comparison of response envelopes, a more detailed evaluation of analysis results was made to obtain a better understanding of inelastic shear behavior. For this purpose, the behavior of the wall hinging region was examined. The hinging region was taken as the lower 21-foot portion of the walls at the base. Under dynamic earthquake loading, moments and shears in structural members are not always in phase, this can be seen in Fig. 27. This means that in contrast to the usual conditions of slowly reversed tests, the maximum shear force and bending moment do not necessarily occur at the same time. Therefore, different times during response were considered to investigate the behavior of hinging regions. Tables 6 and 7 summarize displacement response of the hinging region at six different times during which either shear or moment was maximum. Results indicate that for the structure under consideration shear displacement constitutes about 50% of the total
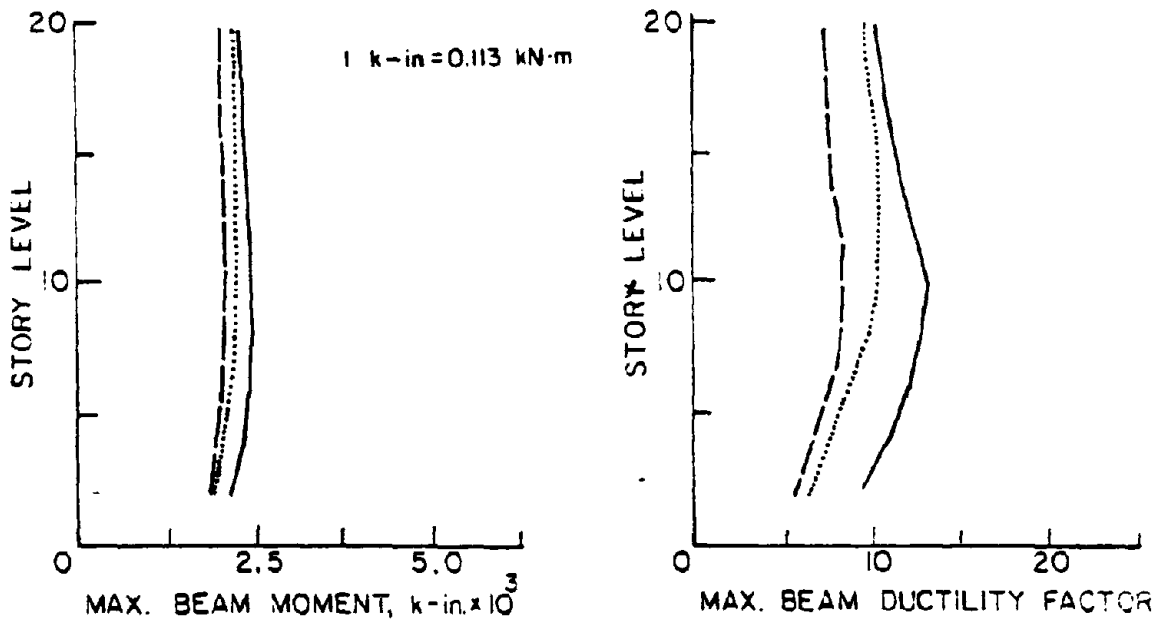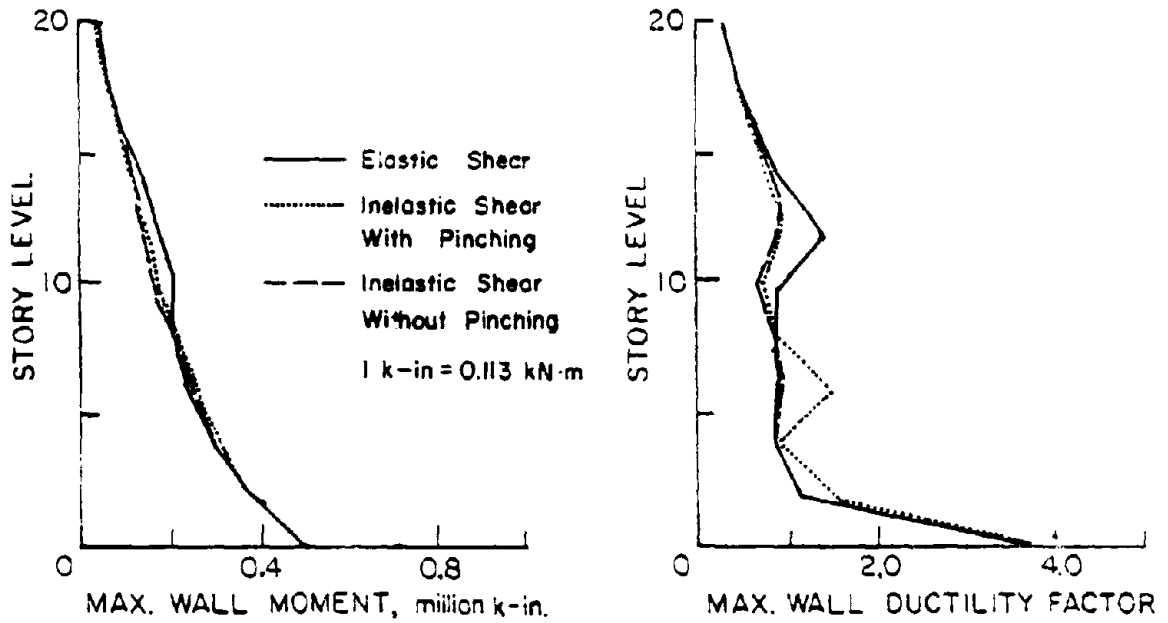
Fig. 23 Response Envelopes Showing the Effect of Shear Yielding
Under 1971 Pacoima Dam, S16E Record
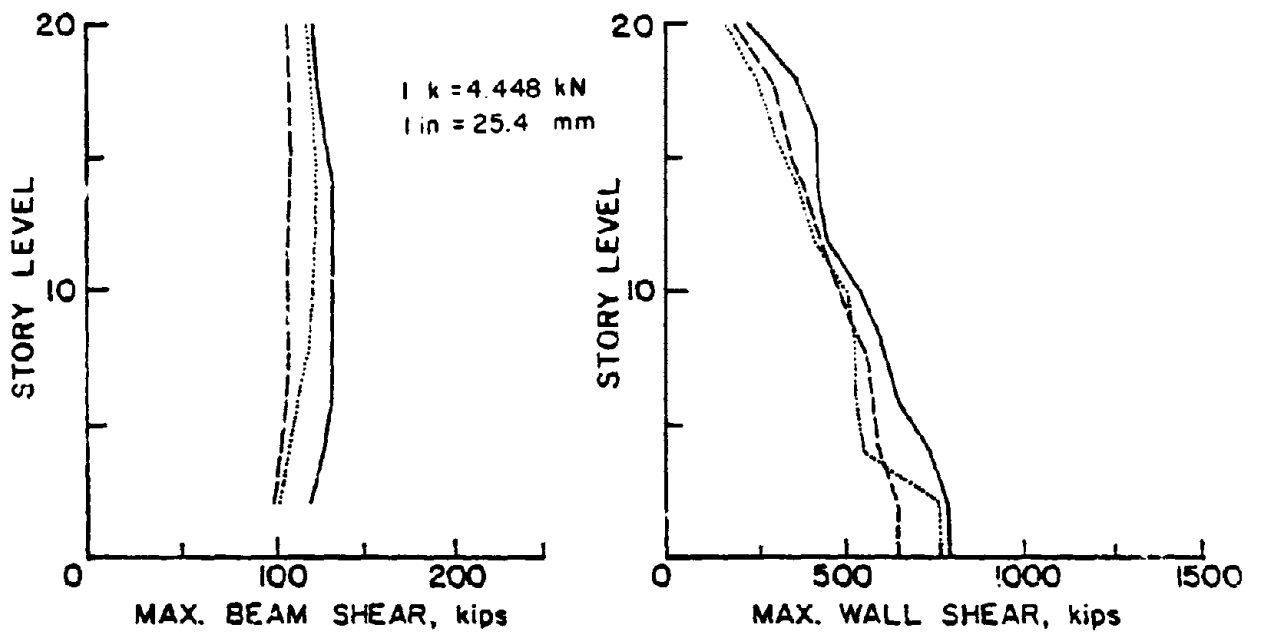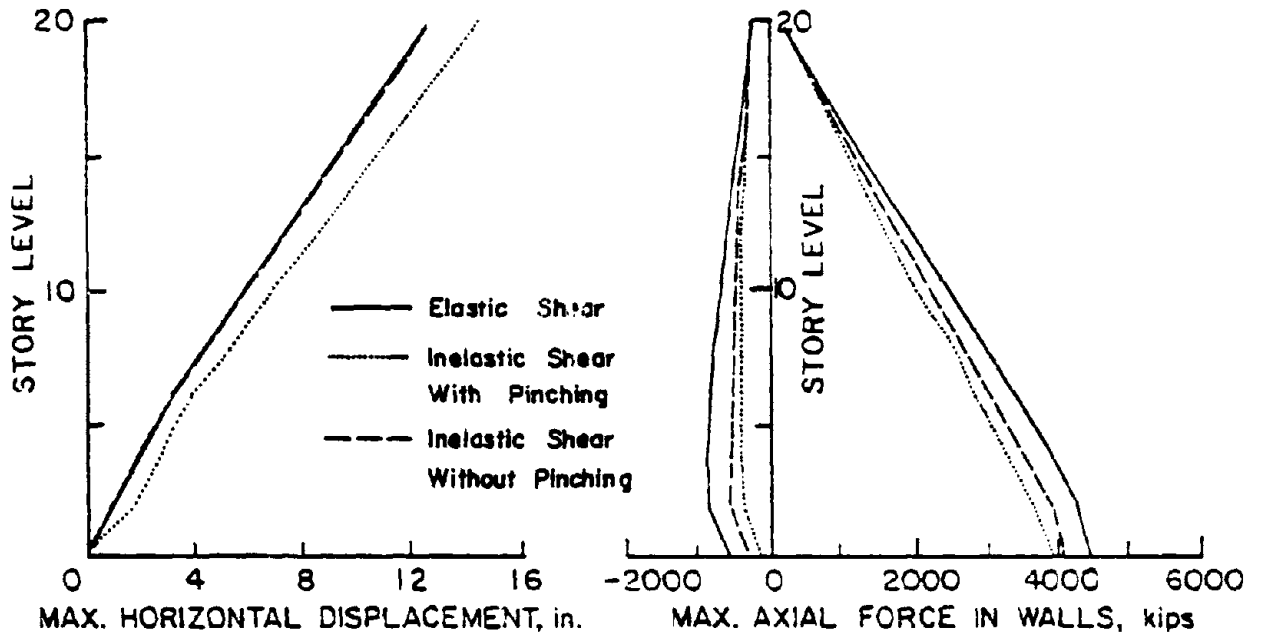
Fig. 24 Response Envelopes Showing the Effect of Shear Yielding
Under 1971 Pacoima Dam, S16E Record

● YIELD IN FLEXURE ● YIELD IN FLEXURE AND SHEAR
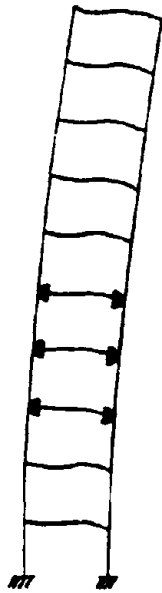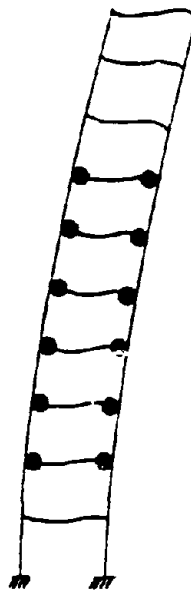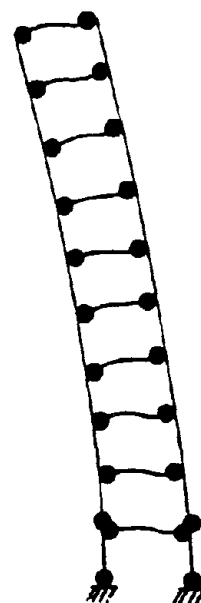
TIME = 2.77 sec.   TIME = 2.80 sec.   TIME = 2.84 sec.
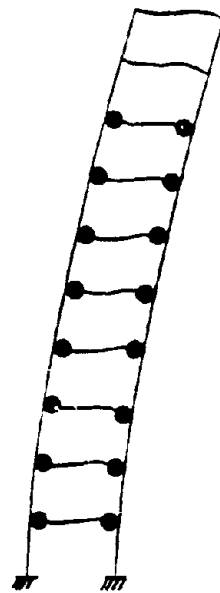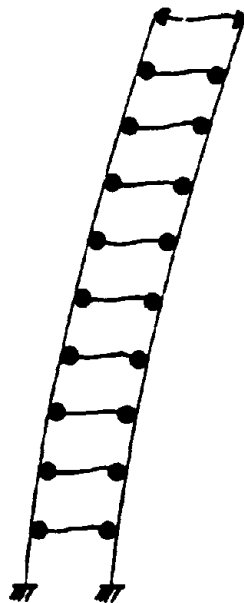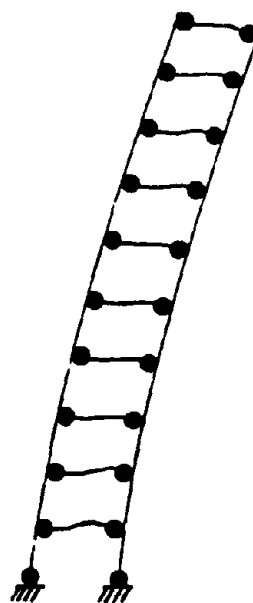
TIME = 2.88 sec.   TIME = 2.95 sec.   TIME = 3.80 sec.
(FINAL YIELDING PATTERN)

Fig. 25 Yielding Sequence

-60-

TABLE 5 - YIELDING SEQUENCE

Total Response Time: 10 Sec.

	Elastic Shear		Inelastic Shear (with and without Pinching)		
Time (sec.)	Member No.	Yielding Type	Time (sec.)	Member No.	Yielding Type
2.77	26, 27, 28	Flexure	2.77	26, 27, 28	Flexure
2.78	25, 29	"	2.78	25, 29	"
2.79	24	"	2.78	27, 28	Shear
2.81	23	"	2.79	24	Flexure
2.82	30	"	2.79	25, 26, 29	Shear
2.85	22	"	2.80	24	"
2.89	19, 20, 21	"	2.81	23	Flexure
3.76	17, 18	"	2.82	30	"
			2.83	23	Shear
			2.84	30	"
			2.85	22	Flexure
			2.87	22	Shear
			2.88	21	Flexure
			2.89	19, 20	"
			2.89	21	Shear
			2.95	19, 20	"
			3.76	17, 18	Flexure
			3.80	17, 18	Shear

21

1 | 22 | 2
3 | 23 | 4
5 | 24 | 6
7 | 25 | 8
9 | 26 | 10
11 | 27 | 12
13 | 28 | 14
15 | 29 | 16
17 | 30 | 18
19 | | 20
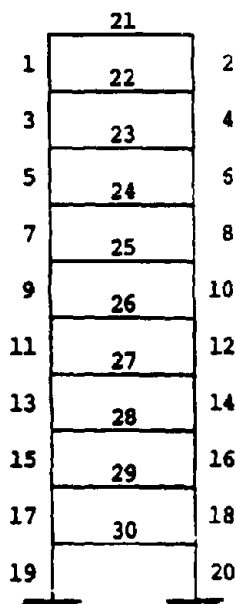
__10-Story Model of__
__20-Story Prototype__

Note: Effect of axial force on force deformation characteristics of members is not considered in this analysis. Therefore, symmetric behavior is obtained.

-61-

TABLE 6 - RESPONSE OF HINGING REGION AT SELECTED
LOADING STAGES - WITHOUT PINCHING

Time (Sec.)	Loading Stage*	Total Displ. (in.)	Flexural Displ. (in.)		Shear Displ. (in.)	
			Elastic	Plastic	Elastic	Plastic
2.82	Elastic - Deforming in Positive Direction $V = V^e_{max}$; $M = 86\% M^e_{max}$	0.256	0.113 (44.1%)	-	0.142 (55.9%)	-
2.86	Elastic - Deforming in Positive Direction $V = 83\% V^e_{max}$; $M = M^e_{max}$	0.256	0.137 (53.7%)	-	0.118 (46.3%)	-
3.05	Inelastic - Deforming in Positive Direction $V = 96.5\% V^{ie}_{max}$; $M = M^{ie}_{max}$	0.648	0.147 (22.7%)	0.205 (31.6%)	0.136 (21.0%)	0.160 (24.7%)
3.81	Inelastic - Deforming in Negative Direction $V = 95.1\% V^{ie}_{max}$; $M = M^{ie}_{max}$	-0.884	-0.169 (19.1%)	-0.589 (66.6%)	-0.133 (15.0%)	+0.008 (1.0%)
5.43	Inelastic - Deforming in Negative Direction $V = V^{ie}_{max}$; $M = 69\% M^{ie}_{max}$	-0.665	-0.112 (16.8%)	-0.416 (62.6%)	-0.140 (21.2%)	+0.003 (0.4%)
8.30	Inelastic - Deforming in Positive Direction $V = V^{ie}_{max}$; $M = 70\% M^{ie}_{max}$	0.772	0.095 (12.3%)	0.016 (2.1%)	0.162 (21.0%)	0.499 (64.6%)

* V^e_{max}: Maximum shear force within elastic range positive or negative.

M^e_{max}: Maximum moment within elastic range positive or negative.

V^{ie}_{max}: Maximum shear force within inelastic range positive or negative.

M^{ie}_{max}: Maximum moment within inelastic range positive or negative.

Time (Sec.)	Loading Stage*	Total Displ. (in.)	Flexural Displ. (in.)		Shear Displ. (in.)	
			Elastic	Plastic	Elastic	Plastic
2.82	**Elastic** - Deforming in Positive Direction $V = V^e_{max}$; $M = 86\% M^e_{max}$	0.256	0.113 (44.1%)	-	0.142 (55.9%)	-
2.88	**Elastic** - Deforming in Positive Direction $V = 83\% V^e_{max}$; $M = M^e_{max}$	0.256	0.137 (53.7%)	-	0.118 (46.3%)	-
3.03	**Inelastic** - Deforming in Positive Direction $V = V^{le}_{max}$; $M = 99.5 M^{le}_{max}$	0.647	0.145 (22.4%)	0.192 (29.7%)	0.149 (23.0%)	0.161 (24.9%)
3.05	**Inelastic** - Deforming in Positive Direction $V = 75.1\% V^{le}_{max}$; $M = M^{le}_{max}$	0.648	0.147 (22.6%)	0.205 (31.7%)	0.136 (21.0%)	0.160 (24.7%)
3.83	**Inelastic** - Deforming in Negative Direction $V = 85.7\% V^{le}_{max}$; $M = M^{le}_{max}$	-1.435	-0.169 (11.8%)	-0.652 (45.4%)	-0.160 (11.2%)	-0.453 (31.6%)
8.98	**Inelastic** - Deforming in Negative Direction $V = V^{le}_{max}$; $M = 80\% M^{le}_{max}$	-2.062	-0.124 (6.0%)	-0.590 (28.6%)	-0.187 (9.1%)	-1.160 (56.3%)

* V^e_{max}: Maximum shear force within elastic range positive or negative.

M^e_{max}: Maximum moment within elastic range positive or negative.

V^{le}_{max}: Maximum shear force within inelastic range positive or negative.

M^{le}_{max}: Maximum moment within inelastic range positive or negative.

horizontal displacement of the top of the hinging region before yielding.

Contribution of shear and flexural deformations to horizontal displacement during the inelastic phase of response varies depending on moment-to-shear ratio. When the structure is subjected to high moments and low shears during response, flexural deformations play the dominant role and vice versa. In the structure considered, shear contribution to horizontal displacement of the hinging region is as high as 85% when maximum shear deformation occurs. The inelastic shear component of the same displacement is 65% of total displacement.

Figure 26 shows time histories of displacement of the top of the structure and the top of the hinging region for the three cases considered. Note the shift in the axis of oscillation for the structure with pinching. Moment and shear response histories for the wall element at the base and the beam element at the eighth floor, is shown in Figs. 27 and 28. The same shift in the axis of oscillation for the case with pinching is also apparent in these figures, although to a lesser degree.

The same structure was also analyzed under a different earthquake motion. The input motion used this time was the E-W component of the 1940 El Centro record. Two cases were considered; one with, and the other without shear yielding allowed. In this set of analyses, no shear yielding was observed in walls. This appears to be mainly due to the frequency characteristics of the particular input motion used. Examination of response histories revealed that after flexural yielding in

(a) TOP DISPLACEMENT

Elastic Shear
Inelastic Shear, without Pinching
Inelastic Shear, with Pinching

1 in = 25.4 mm

(b) DISPLACEMENT OF HINGING REGION

TIME in seconds
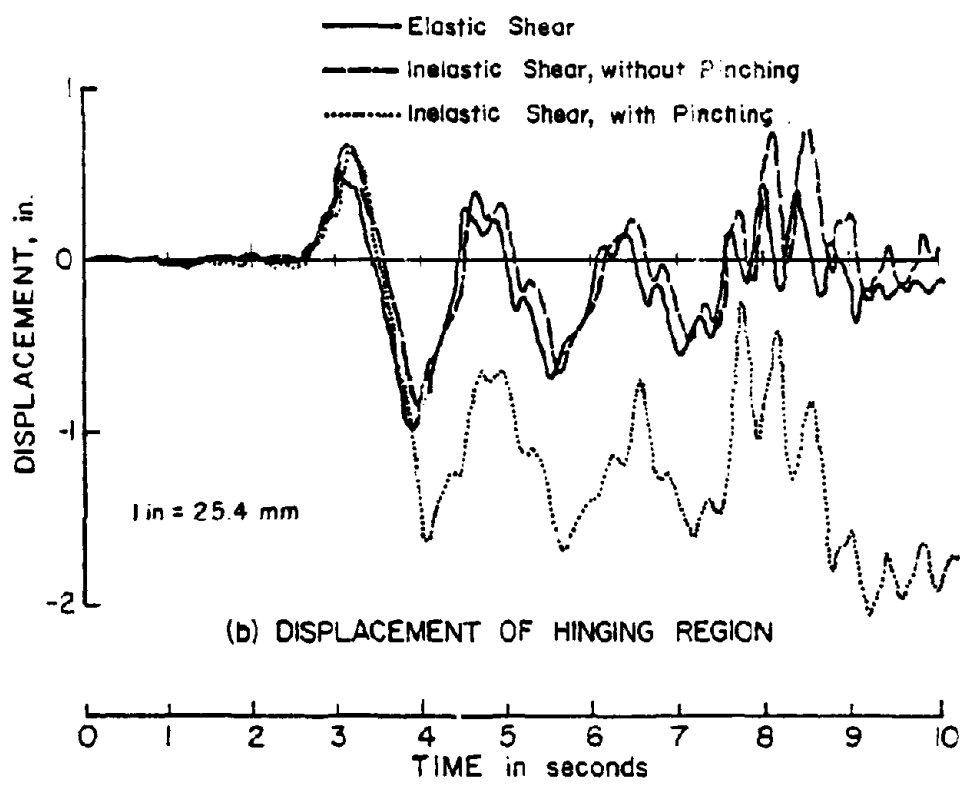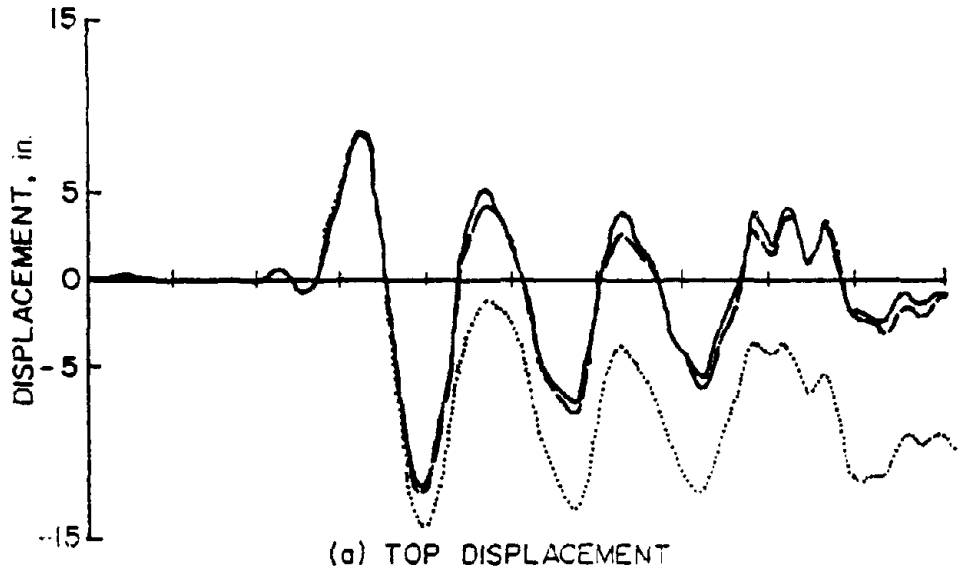
Fig. 26 Response Time Histories for Horizontal
Displacement
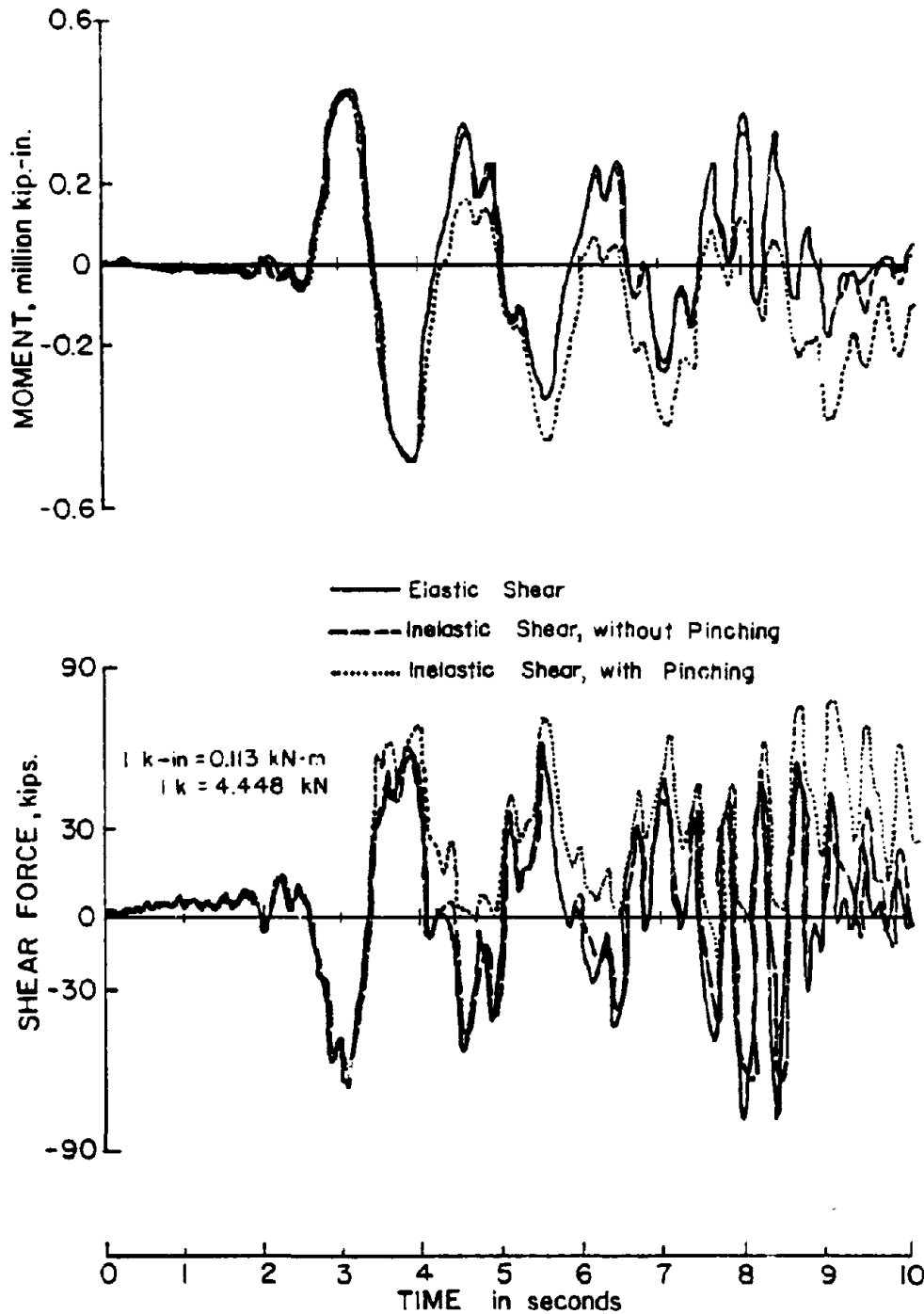
Fig. 27 Bending Moment and Shear Force Response Time
Histories of the Wall Hinging Region at
the Base
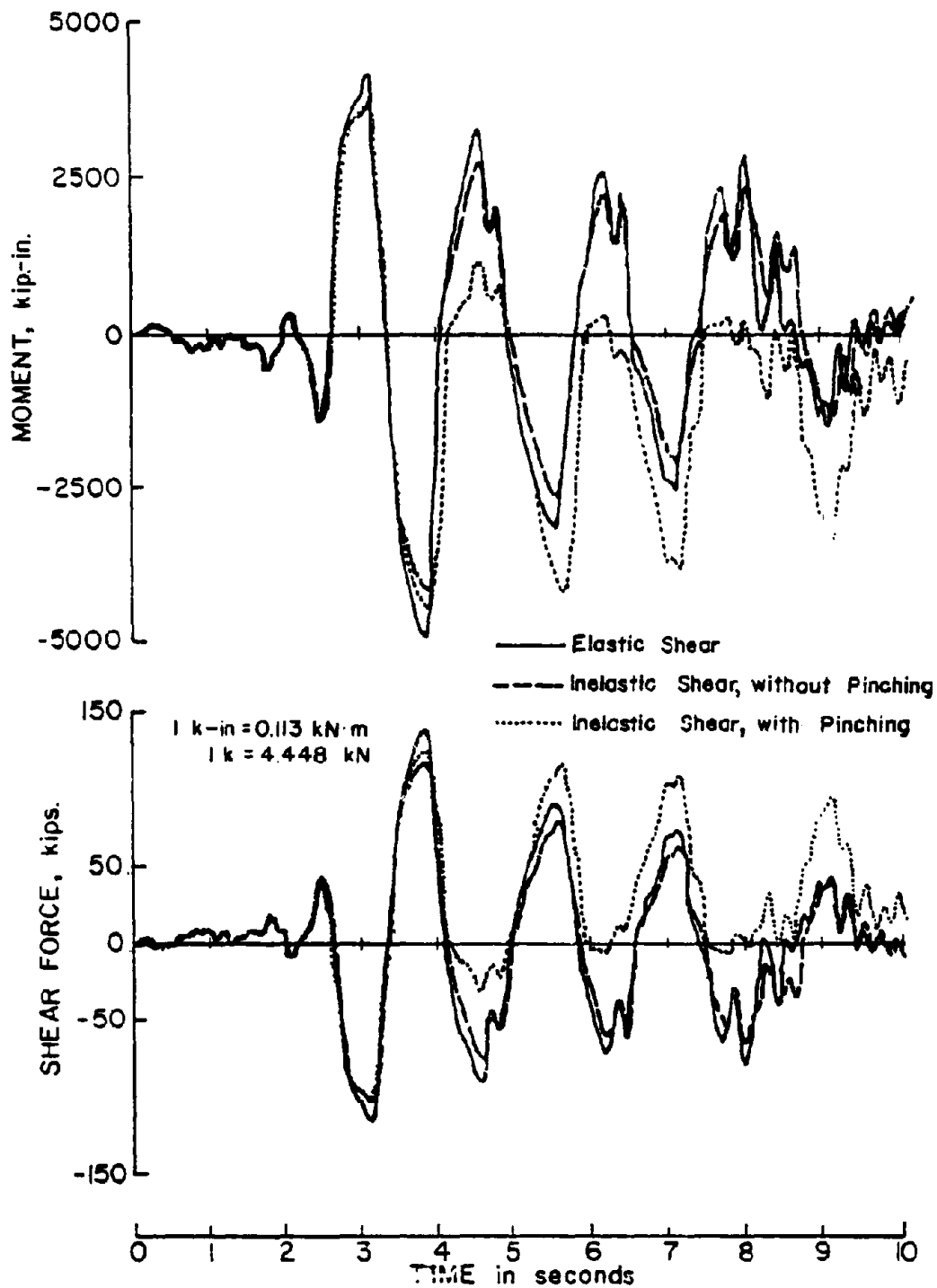
Fig. 28 Bending Moment and Shear Force Response Time
Histories of the Eighth Story Beam

walls takes place, a reduction in wall shear occurs. Beams, on the other hand, show simultaneous yielding in flexure and shear. Response envelopes for these two cases are compared in Figs. 29 and 30.

It is obviously essential to use reasonably accurate estimates of flexural and shear stiffnesses of members to establish primary curves for force-deformation relationships. Flexural stiffness prior to yielding is affected substantially by cracking in concrete. Tests indicate that effective flexural stiffness of cracked concrete members can be as low as 50% to 30% of the stiffness corresponding to the gross concrete area. Any additional rotation due to bond slip of reinforcement can be included in this value as a further reduction in rotational stiffness.

The problem of evaluating effective "elastic" stiffness of a member in terms of relevant factors still awaits further study. It is reasonable to assume that flexural and shear cracking affect shear stiffness. The contribution of each type of cracking to decrease in effective shear stiffness will in turn depend on the moment-to-shear ratio. Until this aspect of behavior is better defined and for purposes of this investigation, it is sufficient to eastablish the probable range of variation of effective shear stiffness for the bilinearly idealized shear-shear distorition relationship. An estimate of this range can be obtained by examining available test data. Tests on isolated walls [5, 6] conducted at the Portland Cement Association indicate that effective elastic shear stiffness can
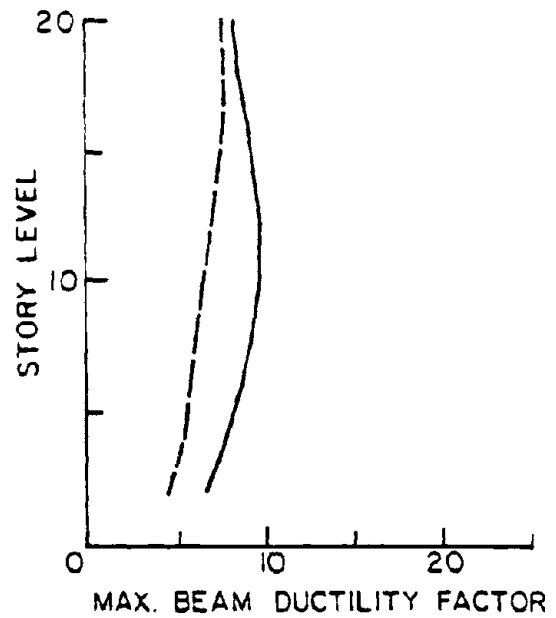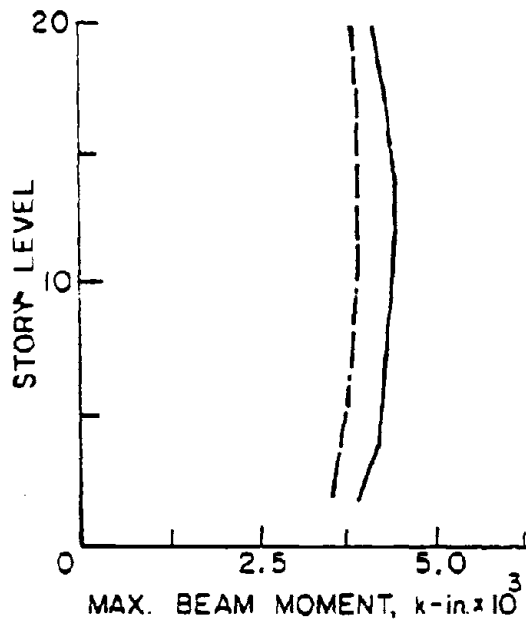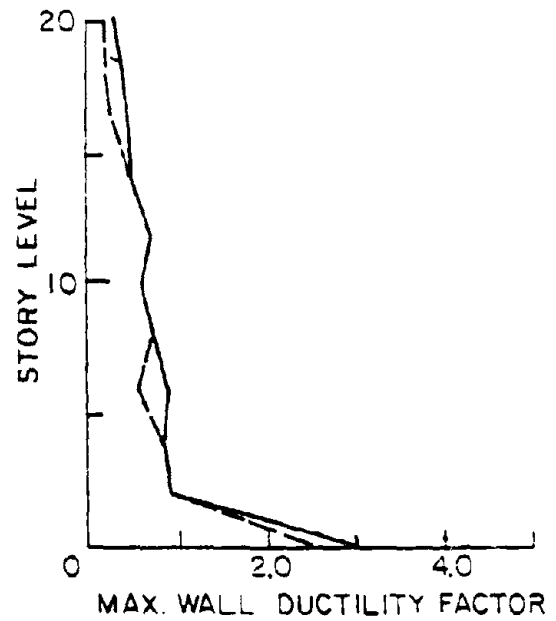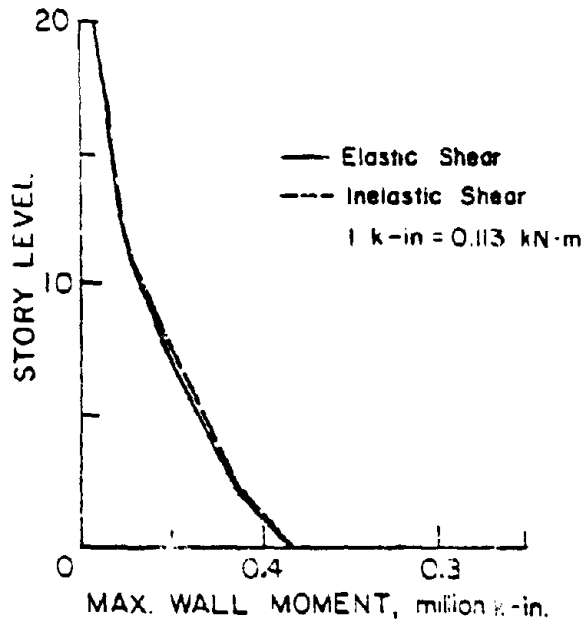
Fig. 29 Response Envelopes Showing the Effect of Shear Yielding
Under 1940 El Centro, E-W Record
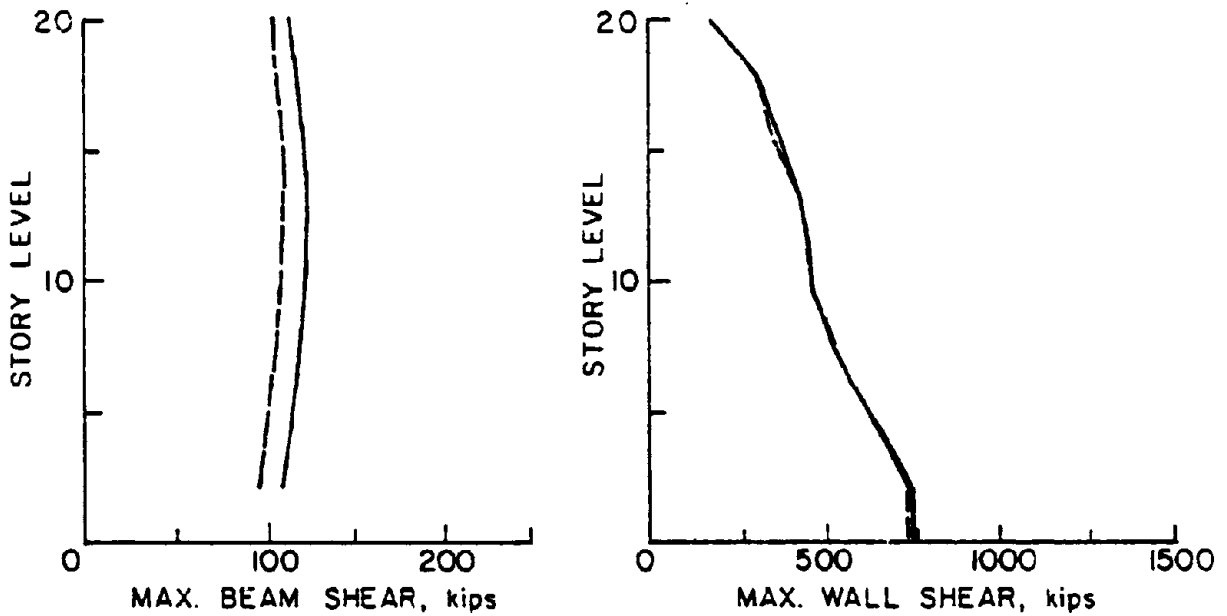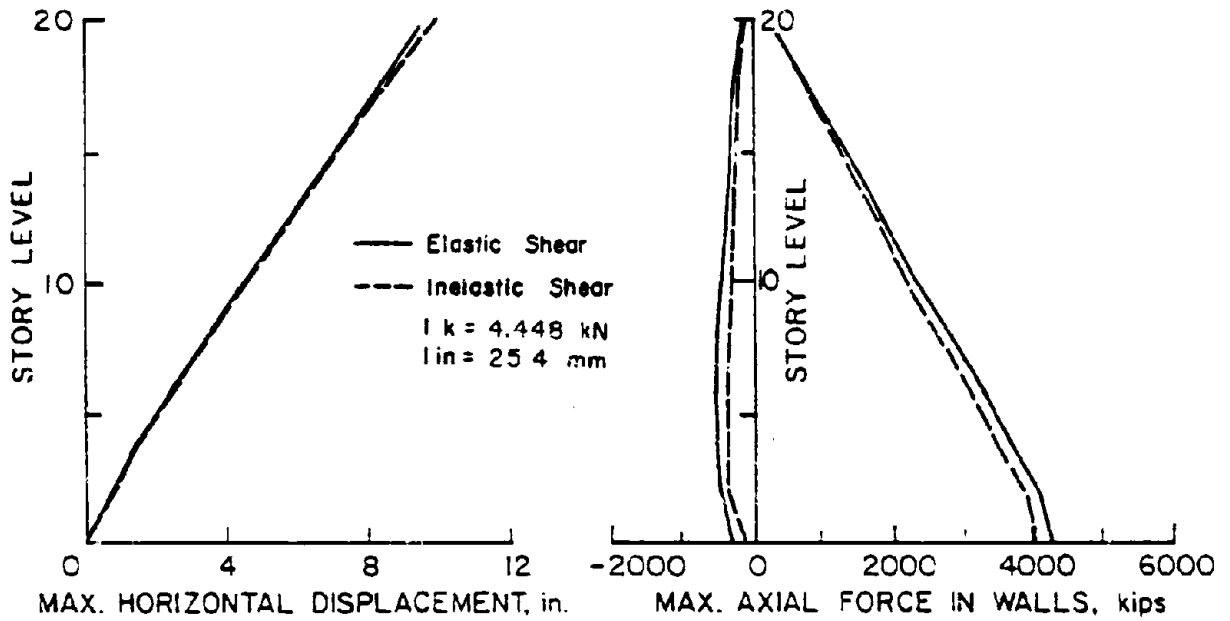
Fig. 30 Response Envelopes Showing the Effect of Shear Yielding
Under 1940 El Centro, E-W Record

be as low as 10% to 30% of the stiffness associated with the gross (uncracked) area. As might be expected, having low shear stiffness relative to their flexural stiffness show a higher percentage of total deformation due to shear. Results obtained from the analyses discussed above are valid for the structure that has stiffness properties listed in Table 4.

A third set of analyses was conducted on essentially the same structure considered earlier, but with high shear stiffness. Elastic and inelastic shear stiffnesses for this case were taken equal to five times the value given in Table 4, while flexural stiffness was kept constant. Two structures were analyzed using the 1940 El Centro record, E-W component; as in previous cases, one analysis did not allow shear yielding, while the other allowed yielding in shear. Comparison of response envelopes for the two cases indicate that effect of shear yielding for this set is very small. Response envelopes for the two cases agree within 5%.

Beam Strength Decay

In a coupled wall system, it is generally desirable to have the coupling beams dissipate most of the energy to limit inelastic action in the primary vertical-and-lateral-load-resisting elements, i.e., the walls. This implies that coupling beams are expected to have high ductility capacity. Experiments have shown that coupling beams exhibit varying degrees of strength decay at higher levels of ductility[13] Degree of strength decay depends on structure geometry, reinforcement detailing, confinement, and history of loading.
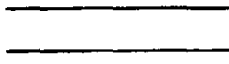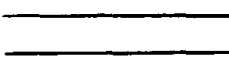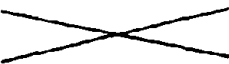
-71-
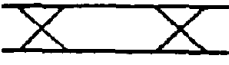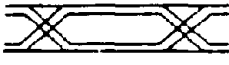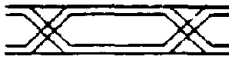
Eight coupling beam tests have been conducted at the Construction Technology Laboratories of the Portland Cement Association[13]. These tests were performed under statically applied slow load reversals. Variables in the test program were concrete core width, span length, and reinforcement detailing. Table 8 lists the specimens tested. Further details of the experimental program are discussed in Ref. 13.

Specimens C2 and C5 were short span specimens with conventional straight longitudinal reinforcement. Load-versus-deflection relationships for these two specimens are shown in Figs. 31 and 32. These hysteretic loops indicate that no strength decay occurs under load reversals up to a displacement ductility of about 6.0. It should be noted that even after this ductility level, decrease in load level does not necessarily indicate a strength loss. This is because loading was deflection controlled and applied load was released when a predetermined deflection was obtained. However, Figs. 31 and 32 show a clear trend for strength loss at higher ductility levels.

Specimen C7 was also reinforced by straight reinforcing bars but had a longer span. Figure 33 shows load versus deflection relationship for Specimen C7. For this specimen strength decay does not occur until after a deflection ductility of 10.0 is exceeded.

To improve specimen performance, full diagonal bars were used in specimens C6 and C8. Load-versus-deflection relationships for these specimens are shown in Figs. 34 and 35.

TABLE 8 — VARIABLES CONSIDERED IN COUPLING BEAM TESTS

Specimen	Core Width a (in.)	Span Length b (in.)	Primary Reinforcement
C1	2.63	16.67	
C2	2.63	16.67	
C3	2.63	16.67	
C4	3.50	16.67	
C5	3.50	16.67	
C6	3.50	16.67	
C7	3.50	33.33	
C8	3.50	33.33	

1 in. = 25.4 mm

-73-
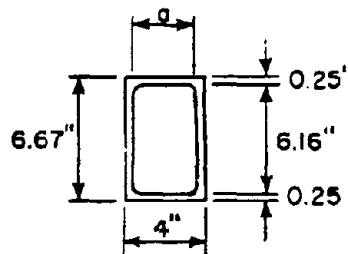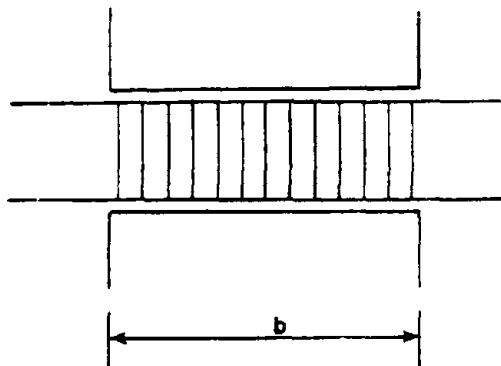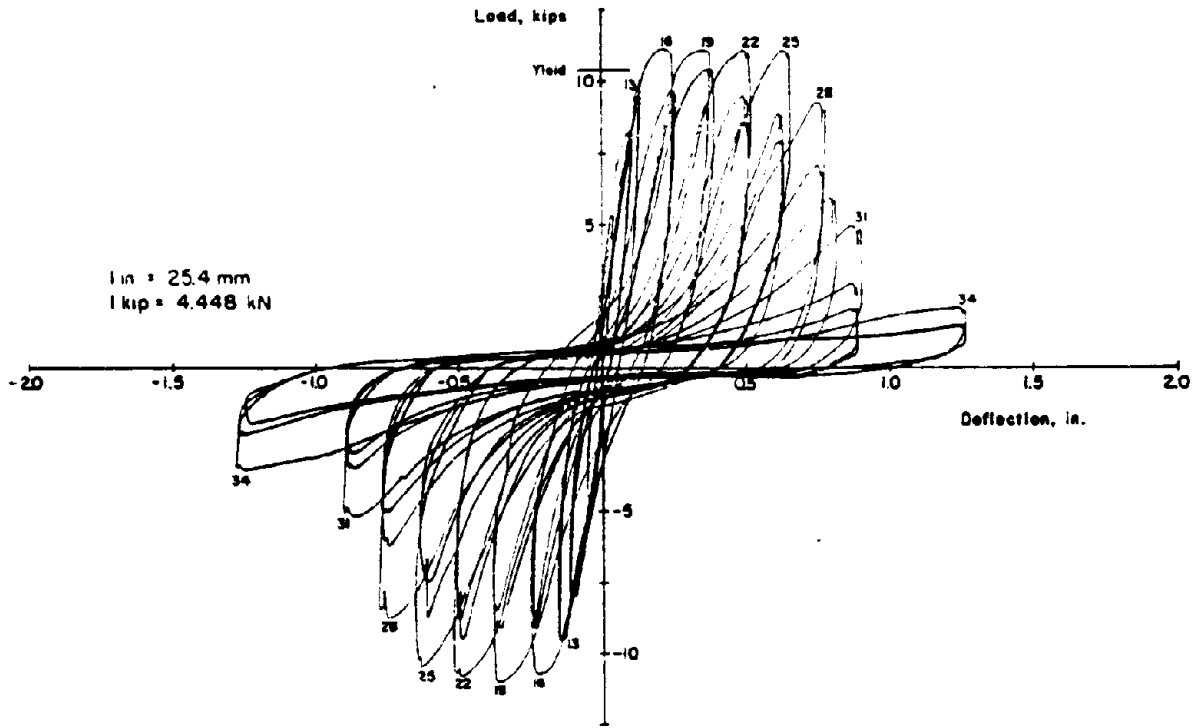
Fig. 31 Lcad-Deflection Relationship of Specimen C2[13]
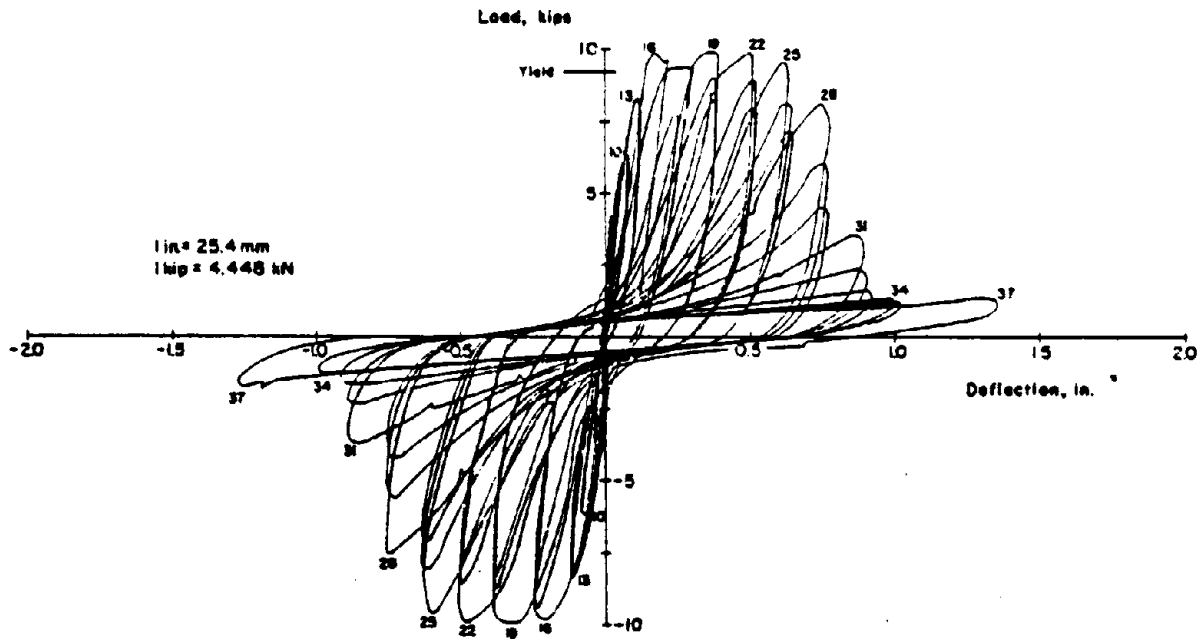
Fig. 32 Load-Deflection Relationship of Specimen C5[13]

-74-
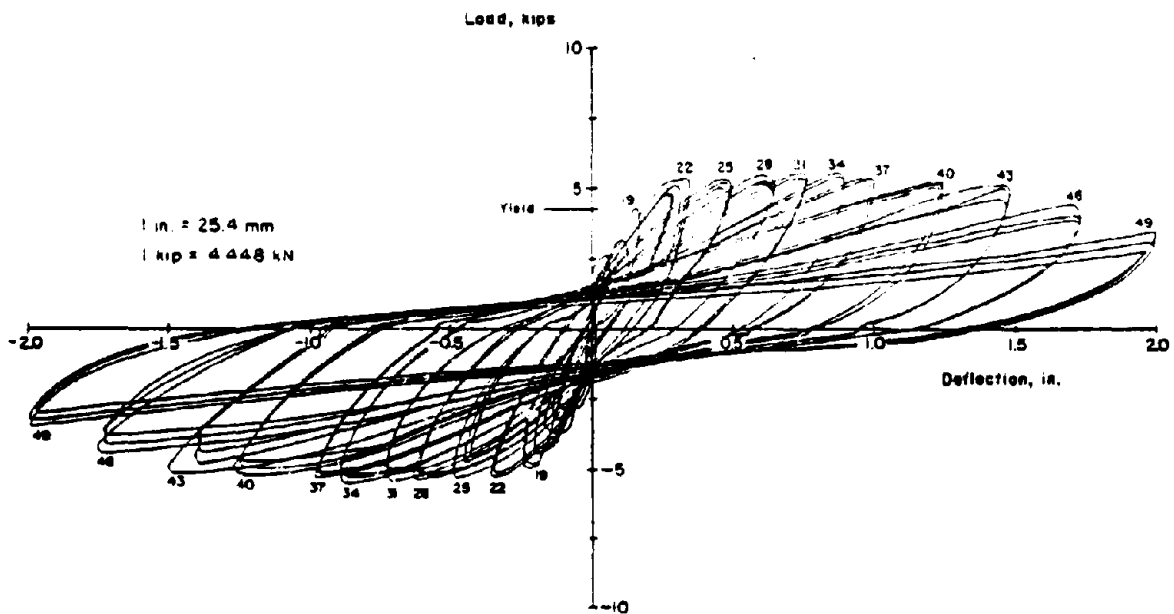
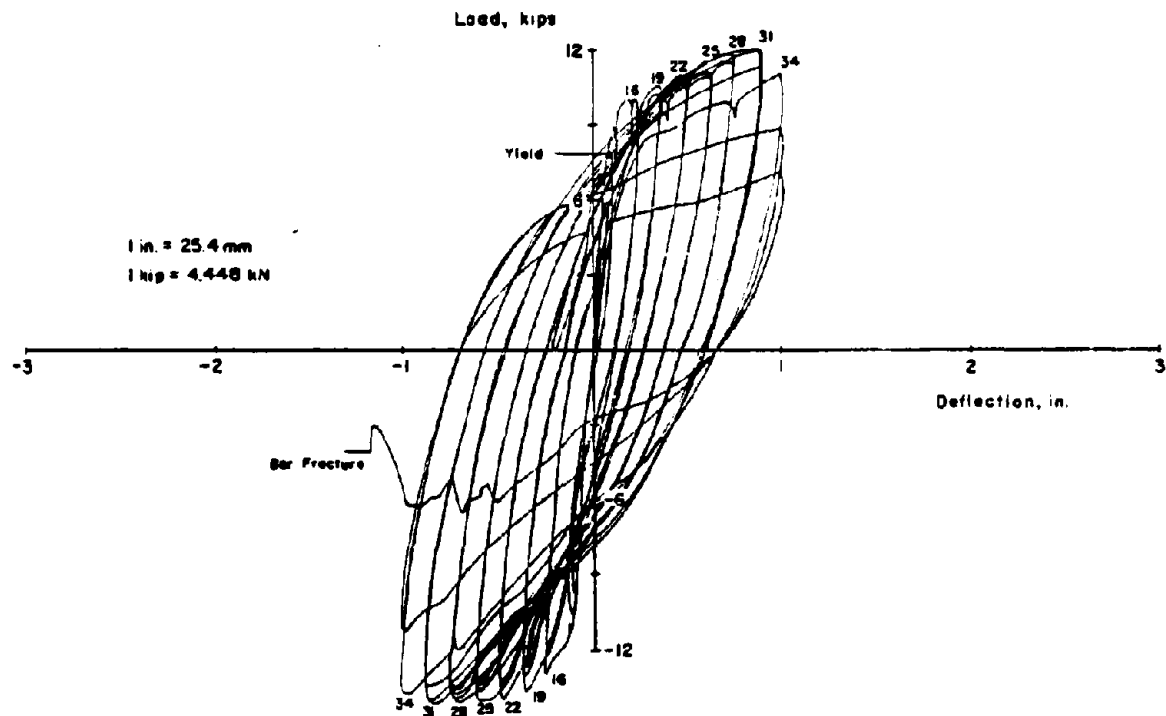Fig. 33 Load-Deflection Relationship of Specimen C7[13]

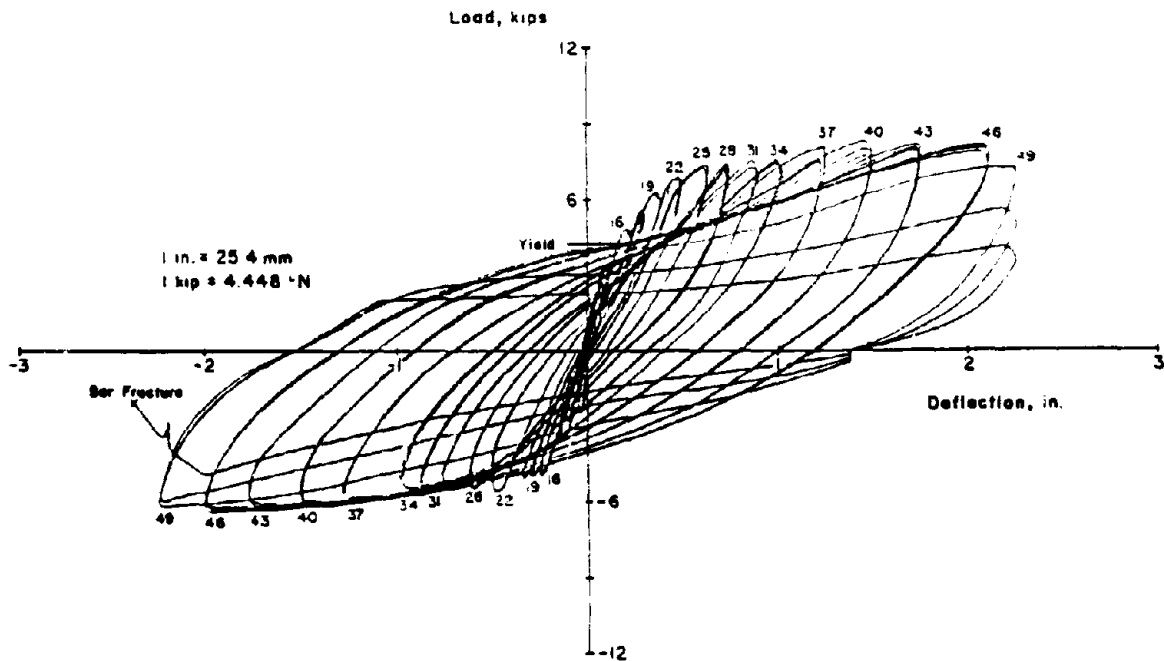Fig. 34 Load-Deflection Relationship of Specimen C6[13]

Fig. 35 Load-Deflection Relationship of Specimen C3[13]

Another reinforcement detailing included diagonal bars in the hinging region. Specimens C1, C3, and C4 are of this type.

Examination of load-versus-deflection relationships for this series of test specimens indicates that in most cases strength decay does not start until after a displacement ductility of 6.0. In some cases it is possible to improve beam performance so that a ductility of 10.0 can be achieved prior to strength decay. Although it is realized that these observations are only valid for beams similar to those tested, and for the specific loading history used, they do represent the general character of beam behavior under cyclic loading.

To investigate the effect of different degrees of strength decay in beams on overall dynamic response of coupled walls, a number of analyses were carried out. Experimentally observed phenomena, relating to rate of strength decay as well as level of deformation at which such decay starts, are modeled as described in the following paragraphs. It should be noted that "pinching" action in reloading branches of hysteretic loops and its effect on dynamic response is discussed later.

Force-deformation hysteretic loops of members are modeled as moment-rotation loops for dynamic analysis. Two different degrees of strength decay, shown in Fig. 36, were modeled. One is referred to as "mild" and has a "break-off line" slope, K_o, equal to 10% of the elastic slope while the other is referred to as "rapid" decay and has K_o = 20%. Two sets of analyses were carried out to study the effect of strength decay. The first set investigated the effect of rate of strength decay when this decay starts at a moderate value of ductility. The second set studied the effect of the level of deformation at which strength decay starts. In both sets, walls were assumed not to suffer loss of strength under load reversals. In all cases the structures were subjected to the E-W component of the 1940 El Centro earthquake.

In the first set, both mild and rapid rates of beam strength decay starting at rotational ductility ratio of 3.5 were considered, with no-decay case. Response envelopes for these two cases are compared in Figs. 37 and 38. Although maximum shear force and bending moment are only slightly affected, wall
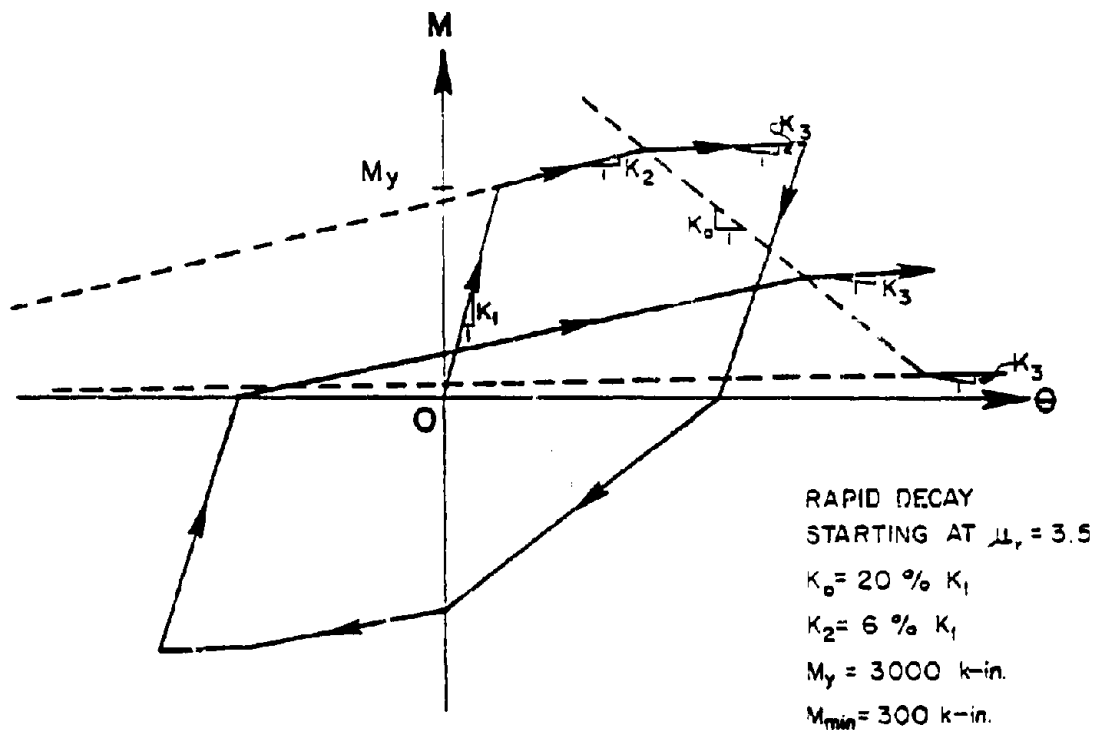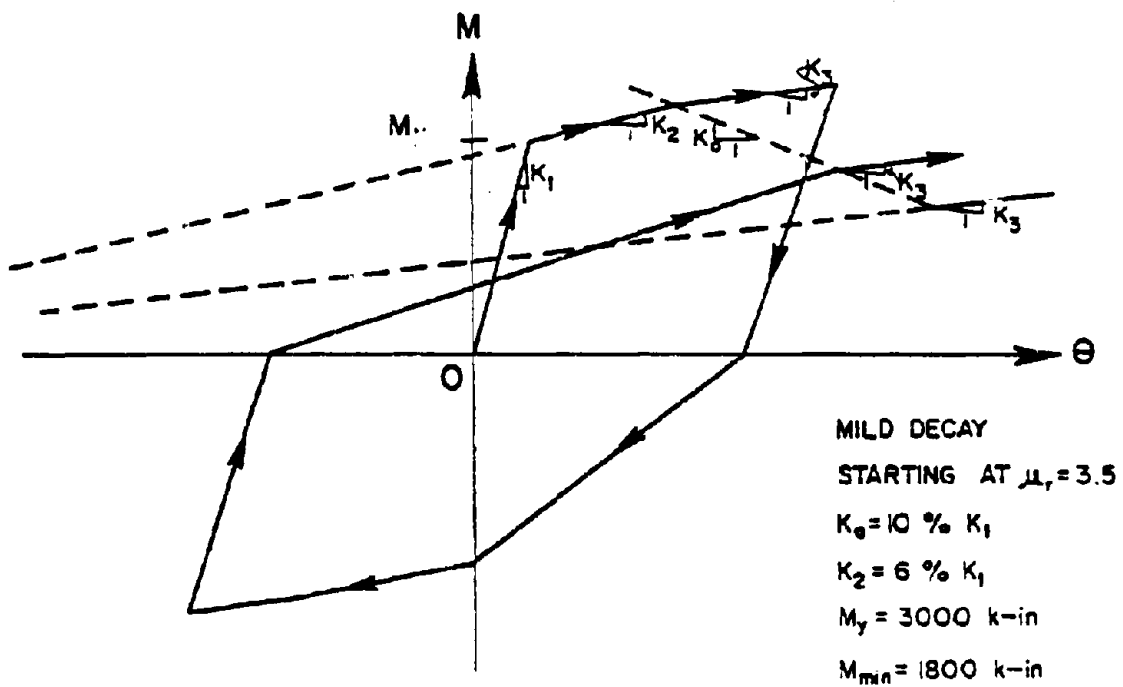
Fig. 36a Rapid Strength Decay

RAPID DECAY
STARTING AT $\mu_r = 3.5$
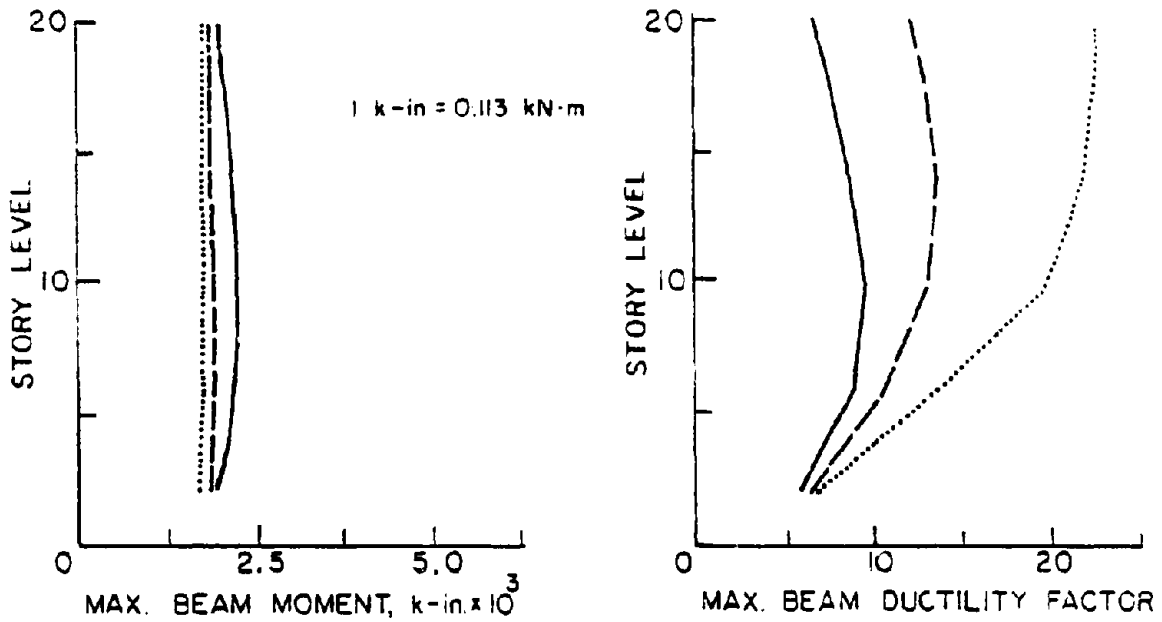$K_o = 20 \% \ K_1$
$K_2 = 6 \% \ K_1$
$M_y = 3000 \ k\text{-in.}$
$M_{min} = 300 \ k\text{-in.}$

Fig. 36b Mild Strength Decay

MILD DECAY
STARTING AT $\mu_r = 3.5$
$K_o = 10 \% \ K_1$
$K_2 = 6 \% \ K_1$
$M_y = 3000 \ k\text{-in}$
$M_{min} = 1800 \ k\text{-in}$

BEAM STRENGTH DECAY
—— No Decay
——— Mild Decay
······· Rapid Decay

Decay Starts at
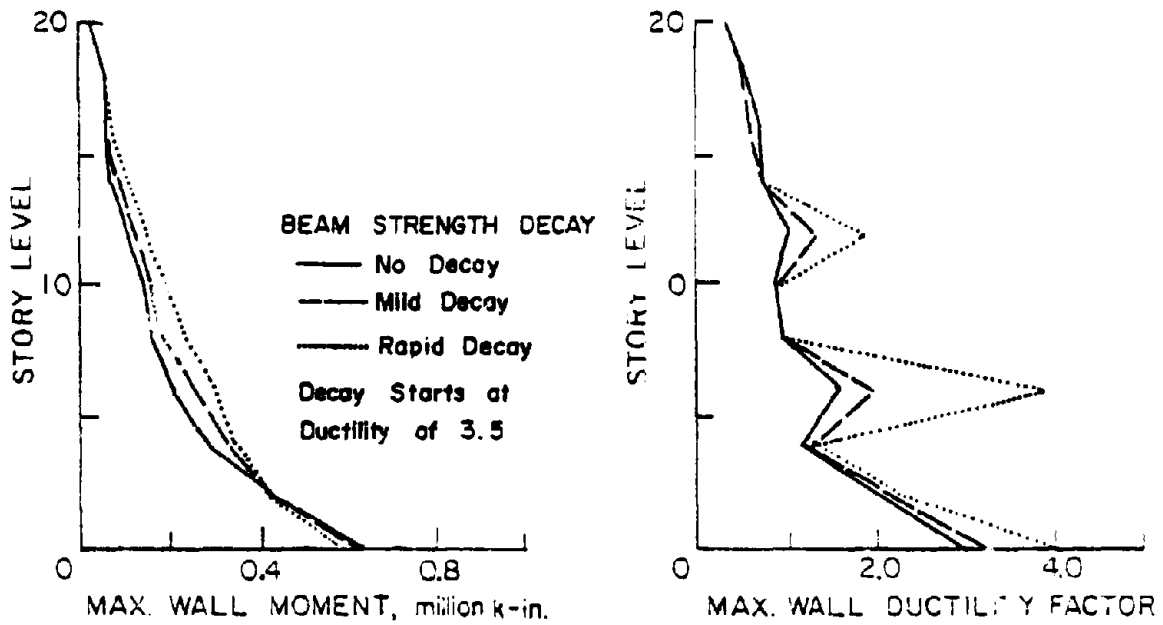Ductility of 3.5

1 k-in = 0.113 kN·m

Fig. 37 Response Envelopes Showing the Effect of Different
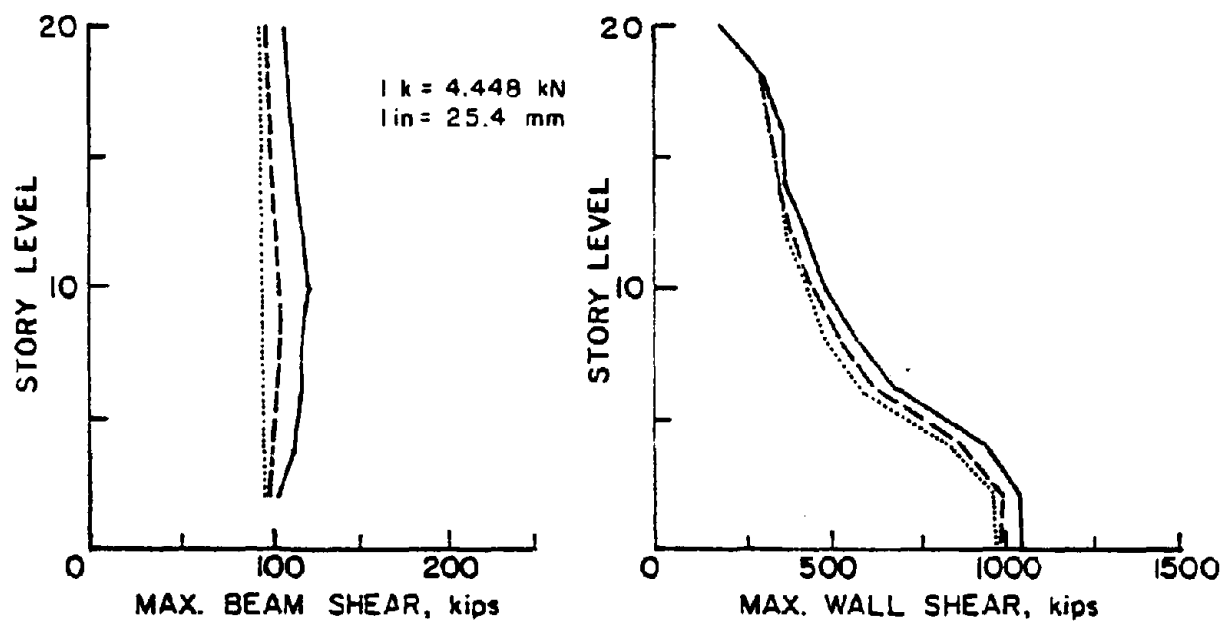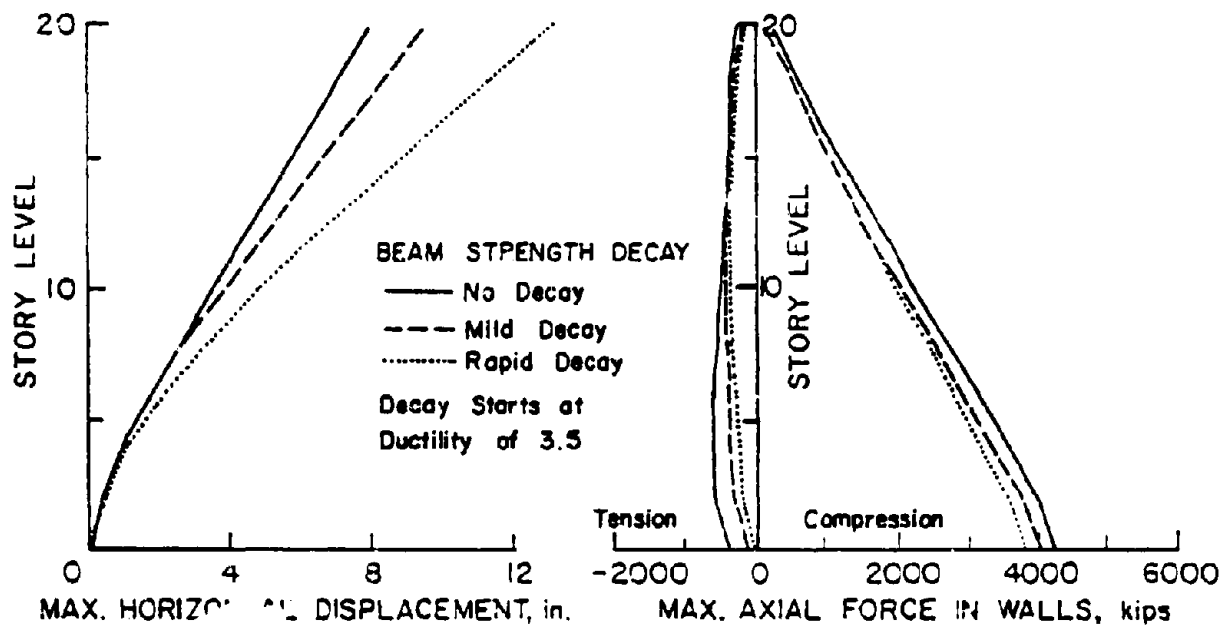Degrees of Strength Decay in Coupling Beams

Fig. 38 Response Envelopes Showing the Effect of Different
Degrees of Strength Decay in Coupling Beams

and beam rotational ductilities are significantly increased as a result of strength decay in beams. Maximum horizontal displacements also increase significantly. When the rapid strength decay is assumed in beams, maximum top horizontal displacement is increased by 70%, indicating considerable softening in the structure. Beam ductilities are also increased by an average of 100% over the structure height. Moment-versus-point hinge rotation (plastic component of total chord rotation) diagrams from computer analyses of the three cases are shown in Figs. 39, 40, and 41 for the sixth story beam.

The second set of analysis covers three structures with rapid beam strength decay, starting at different rotational ductility levels. First structure does not have strength decay,
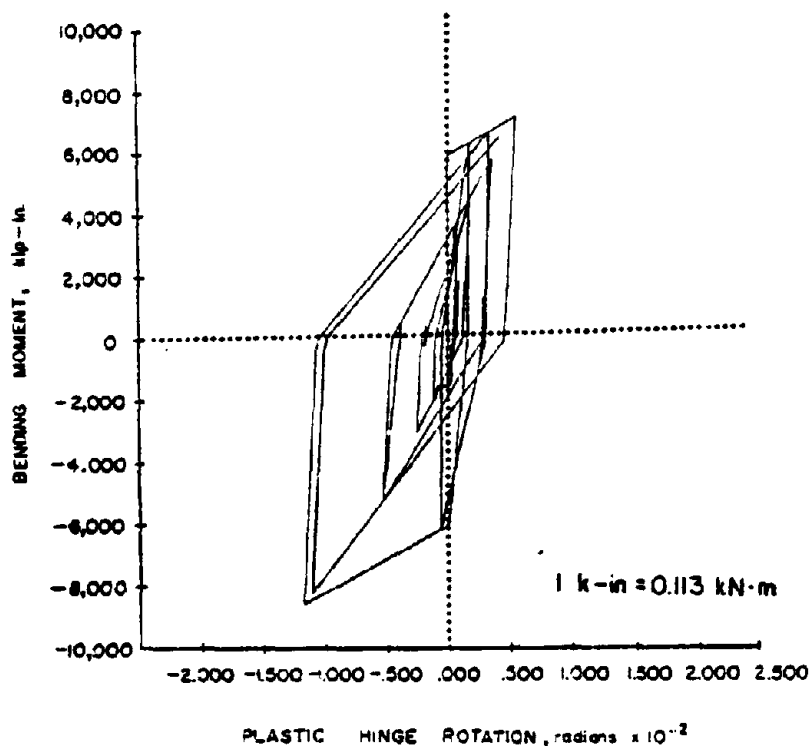

Fig. 39 Moment Versus Plastic Hinge Rotation of Sixth Story Beam Without Strength Decay
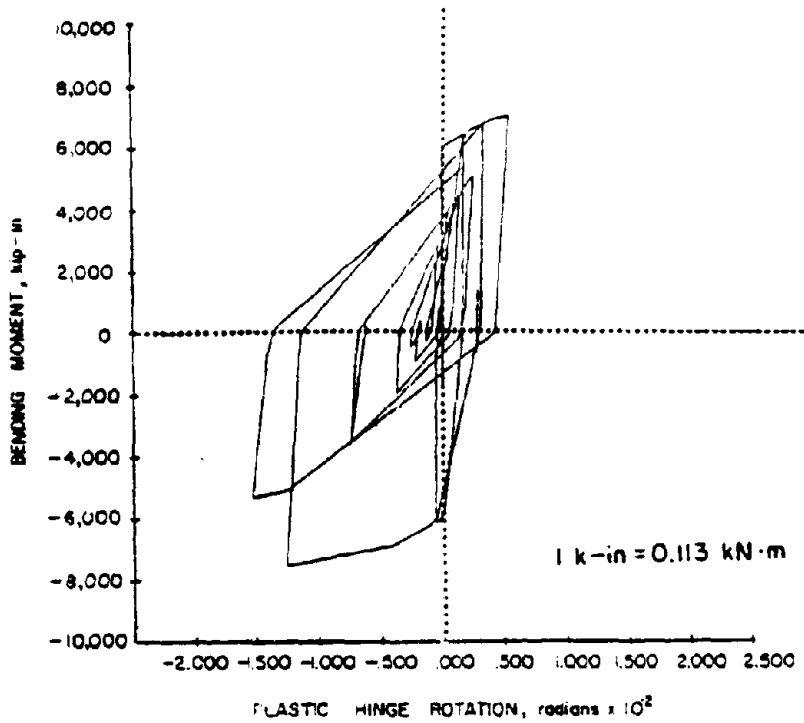
Fig. 40 Moment versus Plastic Hinge Rotation of Sixth
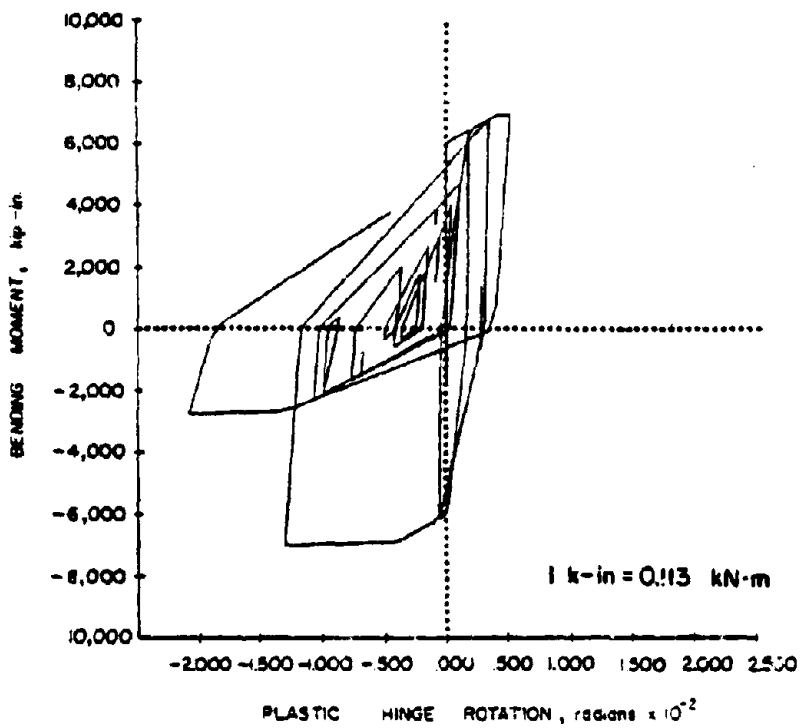Story Beam with Mild Strength Decay

Fig. 41 Moment Versus Plastic Hinge Rotation of
Sixth Story Beam With Rapid Strength Decay

implying that decay starts at a ductility level higher than demanded in this analysis. The other two structures have beam strength decay starting at rotational ductility levels of 3.5 and 6.0. The structure without beam strength decay shows maximum beam ductility demand of about 10.0. All three structures are subjected to the same ground motion previously described for the first set of analysis.

Response envelopes for this second set of analyses are shown in Figs. 42 and 43. Also shown for comparison are results for no-decay. The comparison indicates the expected trend. As the beginning of strength decay is delayed, its effect on dynamic response is reduced. The results indicate that for a rapid strength decay starting at ductility of 6.0, maximum horizontal displacement at the top is increased by about 10% and average beam ductility is increased by 25%. The moment-versus-point hinge rotation (plastic rotation) diagram for this case is shown in Fig. 44 for the sixth story beam.

The above comparisons indicate that when the combination of earthquake intensity and structure yield level are such as to produce ductility demands in coupling beams well into the range where strength loss occurs, significant effects can be expected in structure response. Effects of strength loss in coupling beams are most noticeable in increased horizontal displacements of the structure and coupling beam ductility requirements.
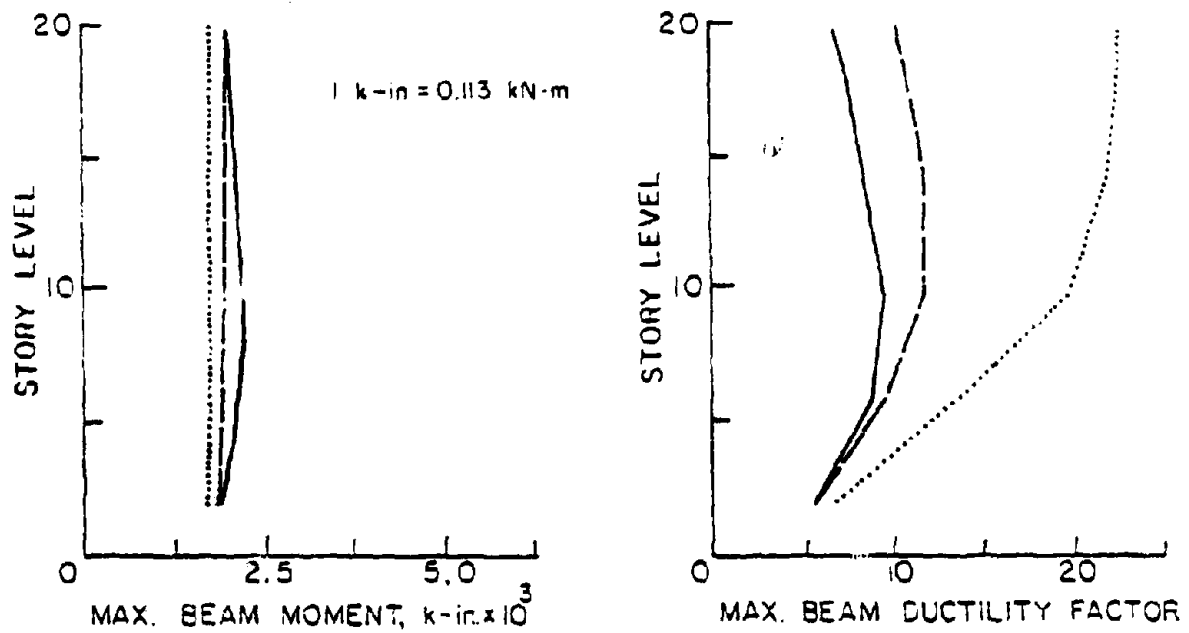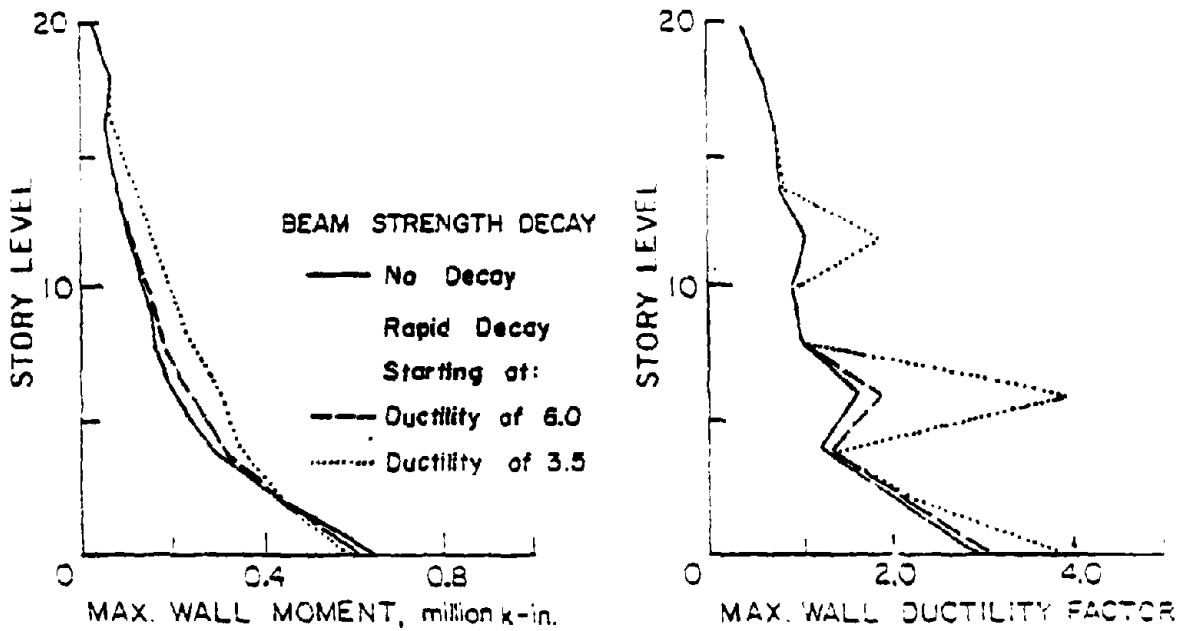
Fig. 42 Response Envelopes Showing the Effect of Strength Decay
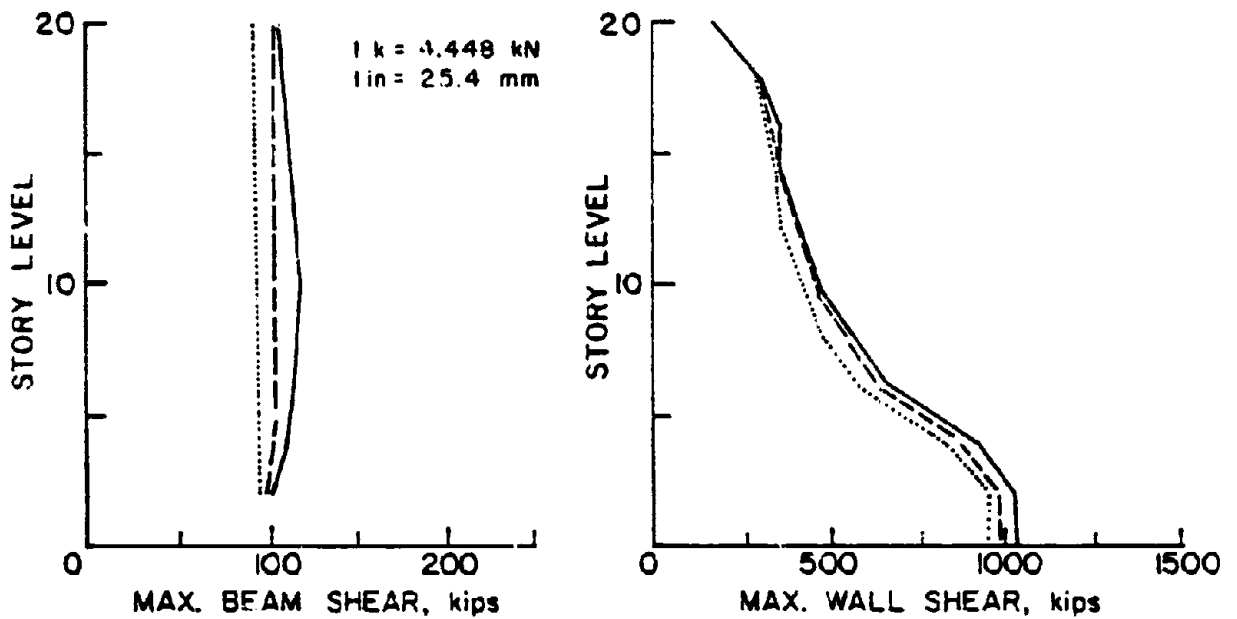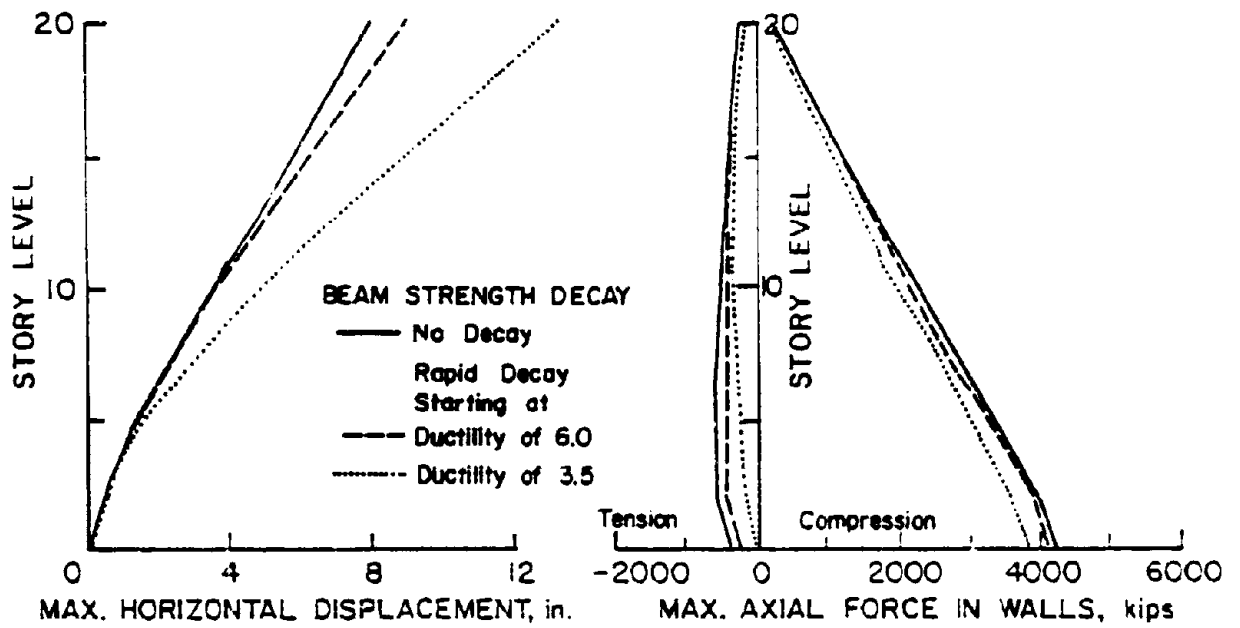in Coupling Beams Starting at Different Levels of
Rotational Ductility

Fig. 43 Response Envelopes Showing the Effect of Strength Decay
in Coupling Beams Starting at Different Levels of
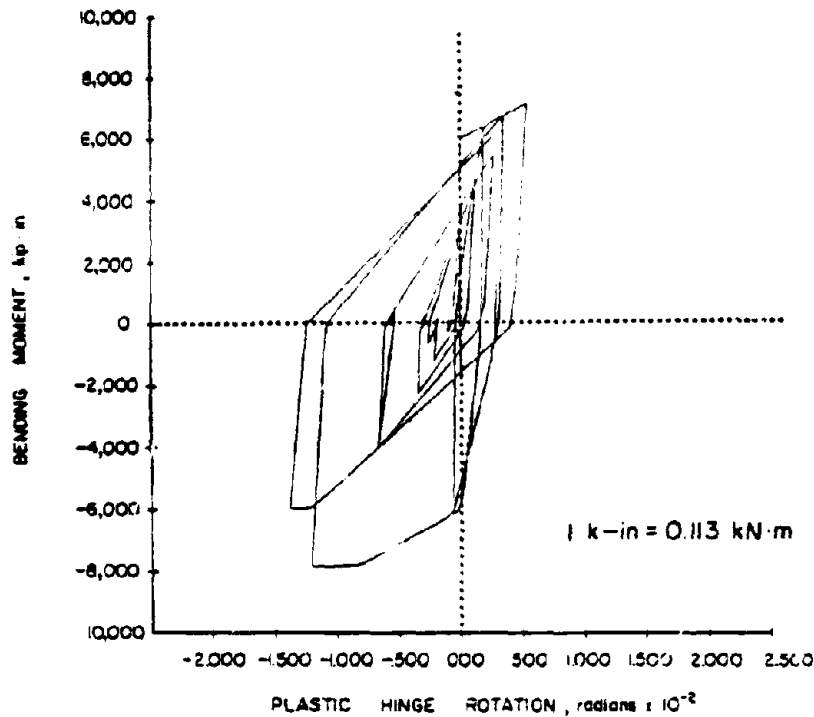Rotational Ductility

Fig. 44 Moment Versus Plastic Hinge Rotation of
Sixth Story Beam with Rapid Strength
Decay Starting at Ductility of 6.0

Pinching of Force-Deformation Relationship

The force-versus-deflection relationship of concrete mem-
bers under cyclic loading generally exhibits a "pinching" of
the hysteresis loop during reloading. This pinching represents
slippage that results mainly from degradation of the shear
transfer mechanism. Loss of shear stiffness during this phase
of loading is directly related to number of cycles of loading
as well as magnitude of forces. Sliding of concrete sections
takes place along the interface of a crack with little increase
in force. Subsequently the cracked surfaces come in full
contact, increasing load resistance. An idealization of the
pinching phenomenon is shown in Fig. 45.

Tests of specimens subjected to slow load reversals indicate that pinching is most apparent in shear force-versus-shear distortion relationship[5, 6]. Figure 22 shows moment-versus-rotation and shear force-versus-shear distortion relationships of a wall specimen. It is evident from this figure that pinching action is mainly due to the shear component of total deformation.

The same observation can be made with respect to deformations of two previously mentioned coupling beam specimens. Specimen C5 had a shorter span than Specimen C7; otherwise these two specimens were identical. Force-versus-deflection relationships of the two specimens are shown in Figs. 32 and 33. It can be seen in these figures that Specimen C5 shows more severe pinching than Specimen C7. The greater degree of pinching in Specimen C5, relative to C7, can be attributed mainly to the higher shear, or lower moment-to-shear ratio, that the specimen was subjected to. In the case of coupling beams bent antisymmetrically, the ratio of moment to shear is equal to half the span length. This translates into a moment-to-shear ratio of 8.34 for Specimen C5, and 16.67 for Specimen C7. Since both specimens have identical flexural capacity, at any level of moment during loading, shear force is greater for the case where moment to shear ratio is lower.

Pinching in Shear-Shear Distortion Relationship

To investigate the effect of pinching on dynamic response of coupled walls, the previously selected 20-story coupled wall
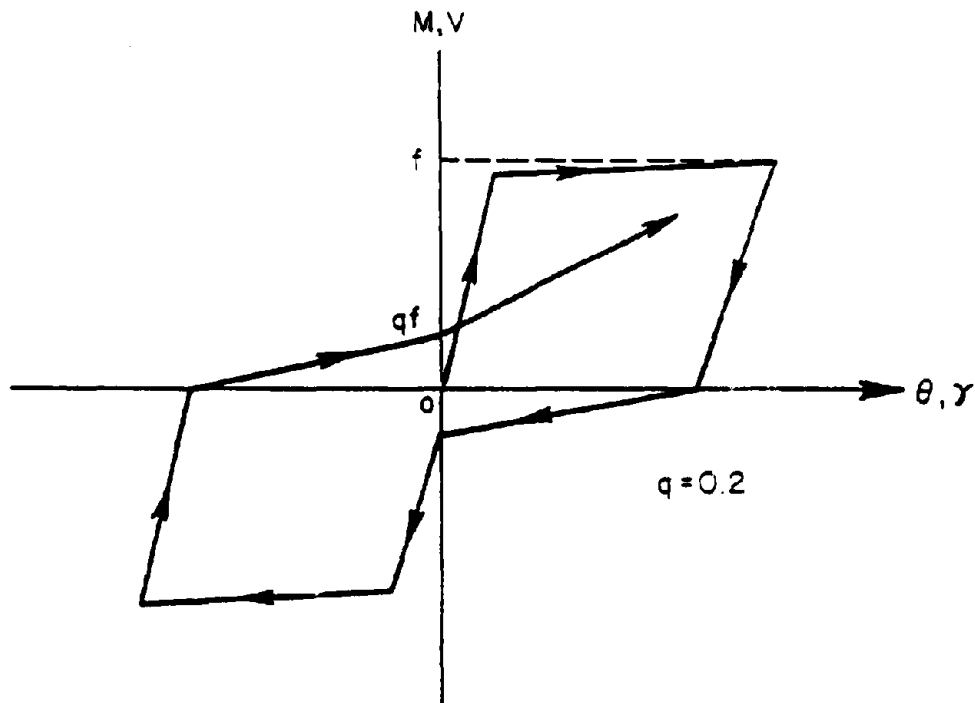
Fig. 45 Degree of Pinching Used in Dynamic Analysis

structure was analyzed with pinching in shear-distortion rela-
tionship. Stiffness properties of the structure are given in
Table 4. The degree of pinching is determined on the basis of
avaialable test data[5, 6]. Figure 45 illustrates the degree
and the manner in which pinching in shear-distortion relation-
ship is specified in the computer program. No pinching in the
moment-rotation relationship was considered. Response envelopes
for the case with pinching are compared with the case without
pinching in Figs. 46 and 47. Time history plots of selected
response quantities for this case were previously shown in
Figs. 26, 27, and 28.

Examination of the results indicate that for the degree of
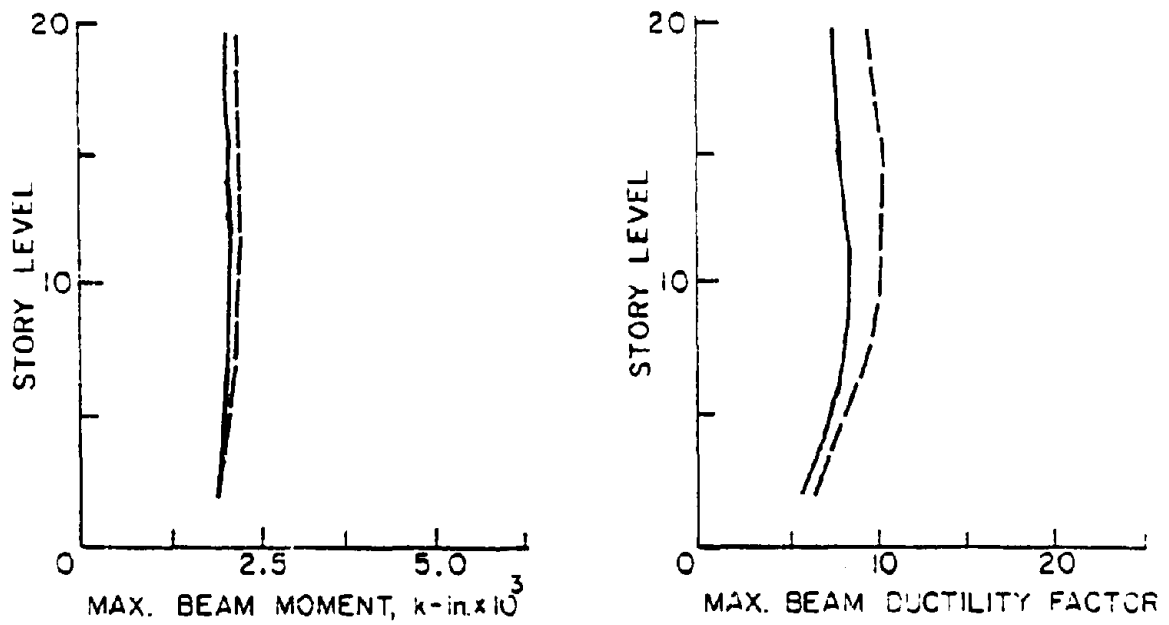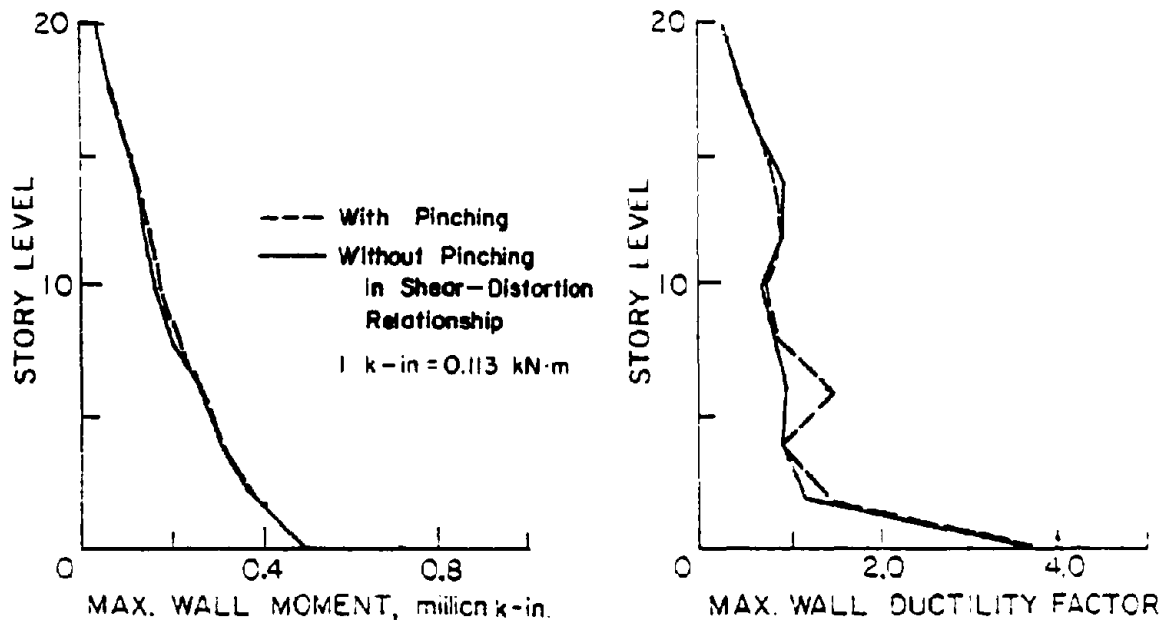pinching assumed, a significant shift in the axis of oscillation

Fig. 46 Response Envelopes Showing the Effect of Pinching in
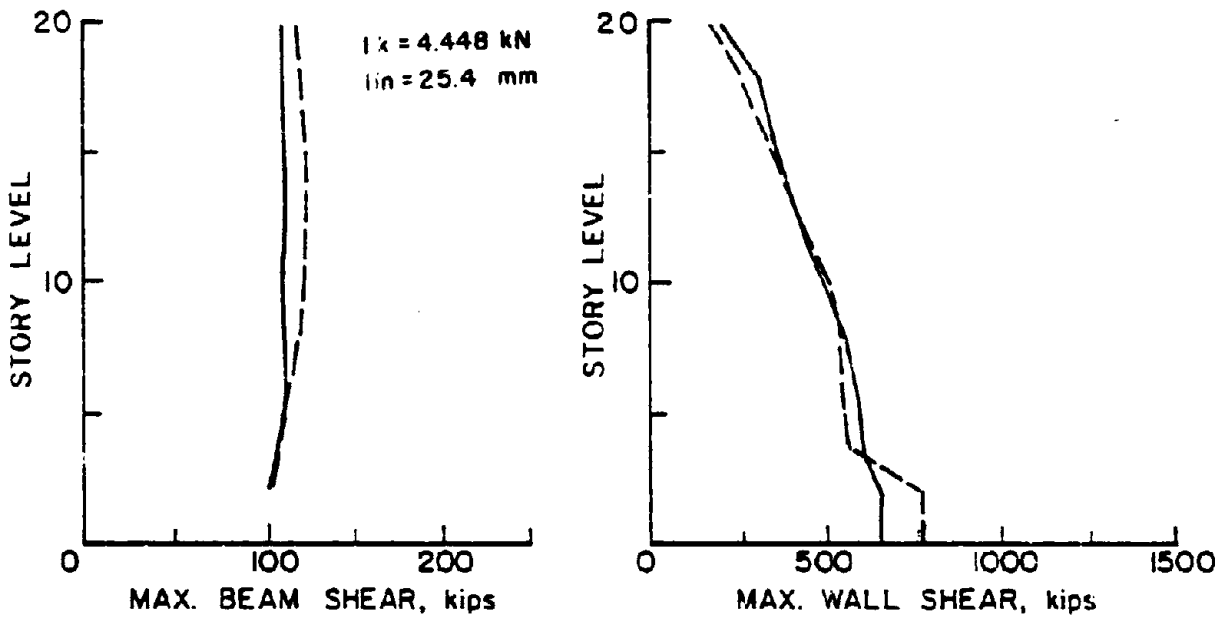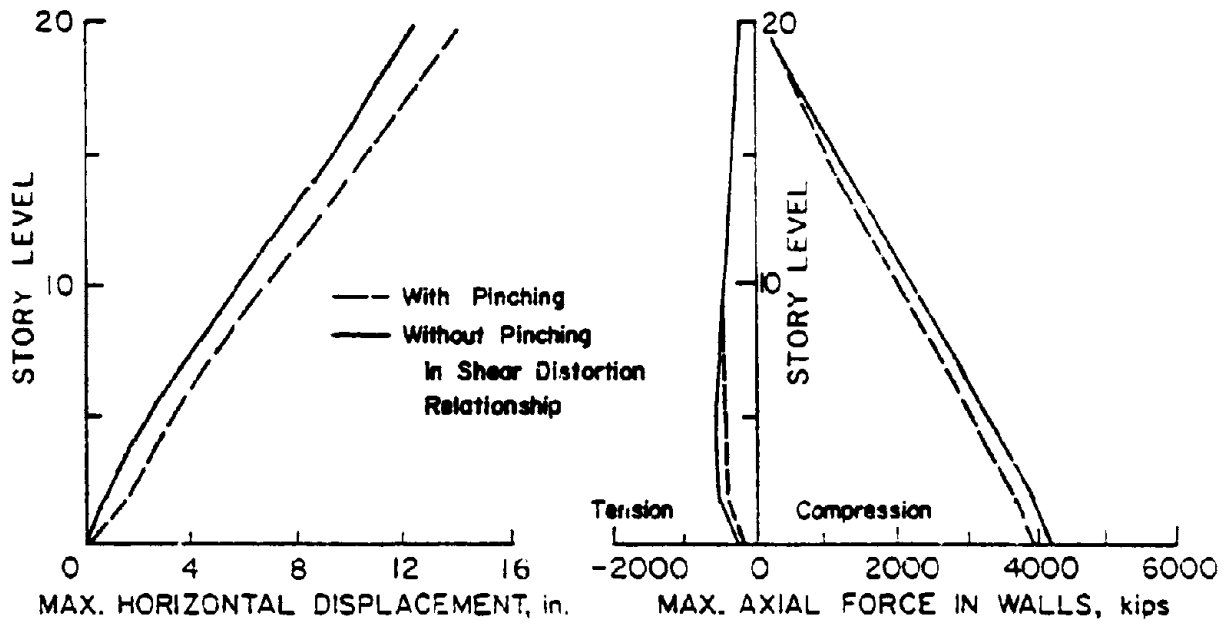Shear-Distortion Relationship

Fig. 47 Response Envelopes Showing the Effect of Pinching in
Shear-Distortion Relationship

can occur under input motions with specific frequency charac-
teristics. The structure considered shows a substantial sway
in one direction that is not recovered in subsequent response.
Response force envelopes, on the other hand, show little effect
of pinching action.

Pinching in Moment-Rotation Relationship of Coupling Beams

To examine the effect of pinching in moment-rotation loops
of coupling beams, another analysis was made using essentially
the same structure considered in the preceding case. This time
elastic shear behavior was considered. Pinching was assigned
to the moment rotation relationship of coupling beams. The
same degree of pinching used in the previous analysis ($q=$
0.20) was assumed. Properties of the structure, including mem-
ber stiffness parameters, are listed in Table 1. El Centro 1940
E-W record was used as input acceleration. Response of this
structure is compared with response of a companion structure
without pinching action. Plots of moment-plastic hinge rotation
relationships for the sixth story beam of the two cases are
shown in Fig. 50. Response envelopes shown in Fig. 48 and 49
indicate that except for beam rotational ductilities which
increase by about 20%, maximum forces and displacements are not
significantly affected by pinching in M-θ loops of beams.

Post-Yield Slope of Primary Moment-Rotation Curve

In program DRAIN-2D, the force-displacement relationship of
members is specified in terms of the bilinear primary curve.

Fig. 48 Response Envelopes Showing the Effect of Pinching in
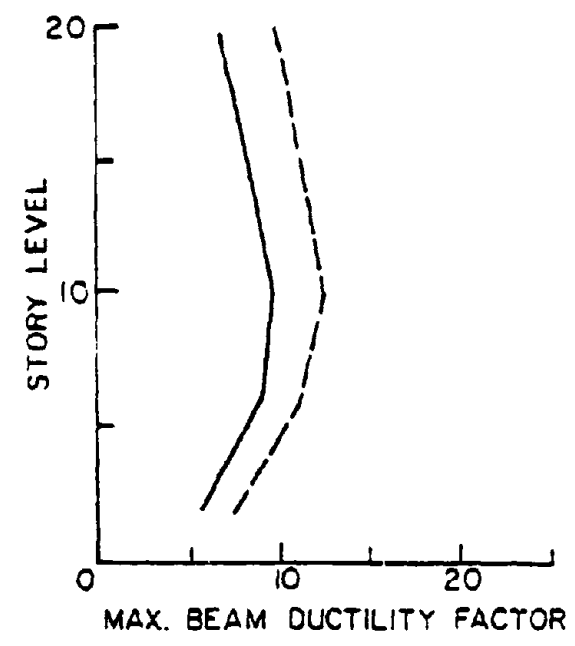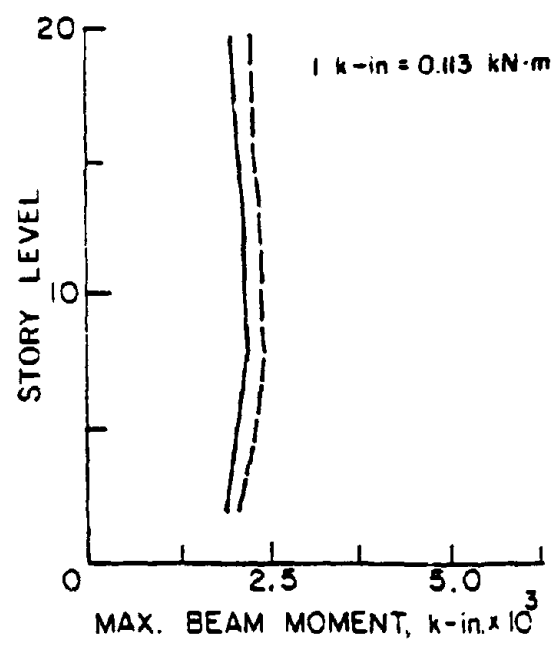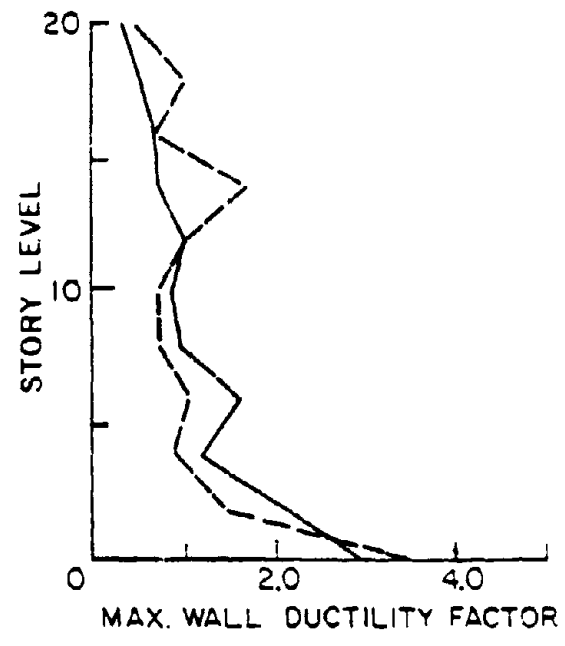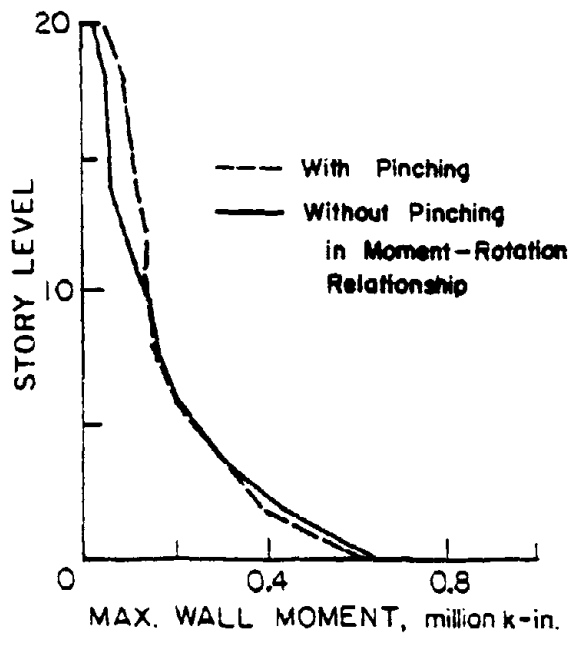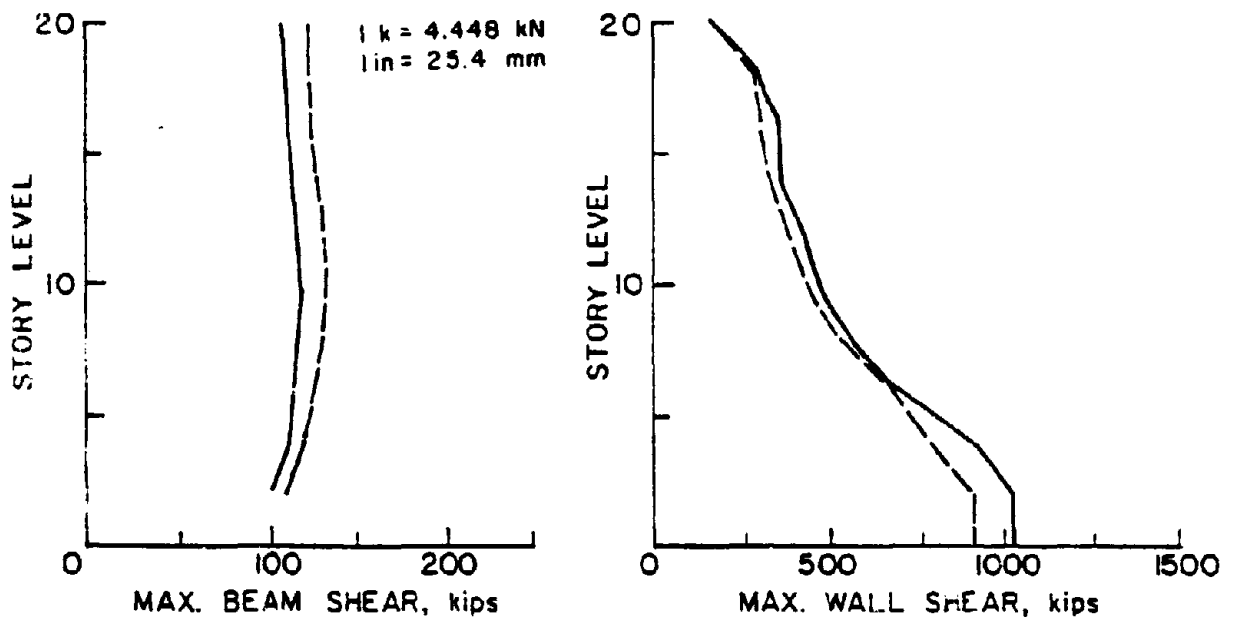Moment-Rotation Relationship of Coupling Beams
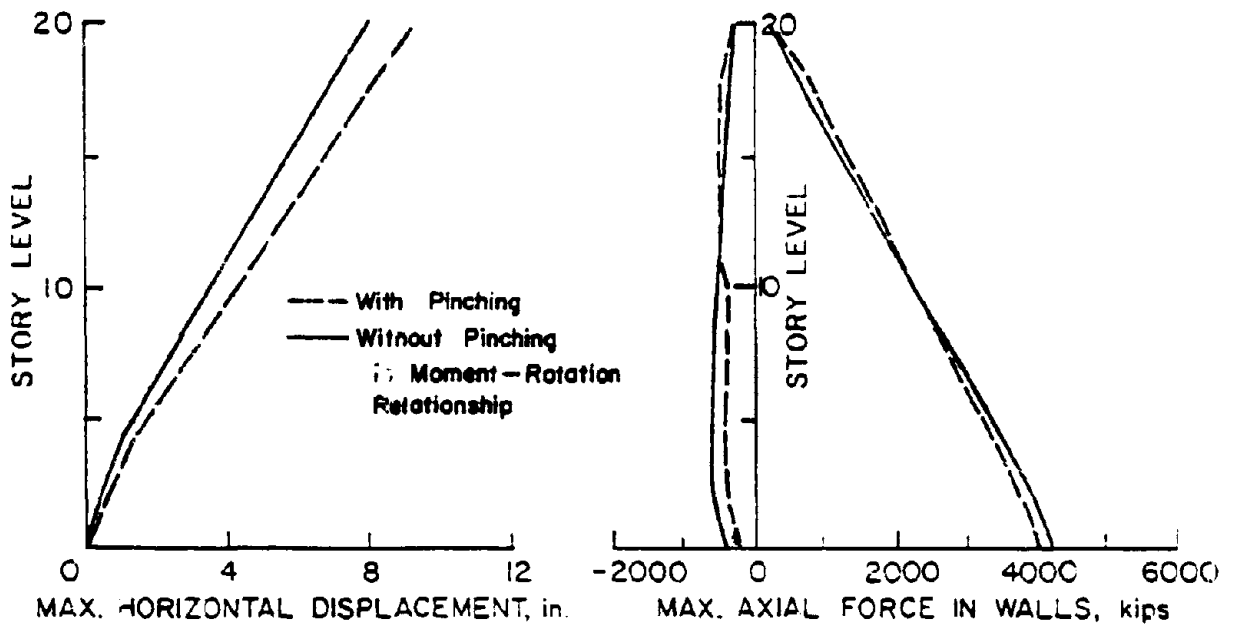
Fig. 49 Response Envelopes Showing the Effect of Pinching in
Moment-Rotation Relationship of Coupling Beams
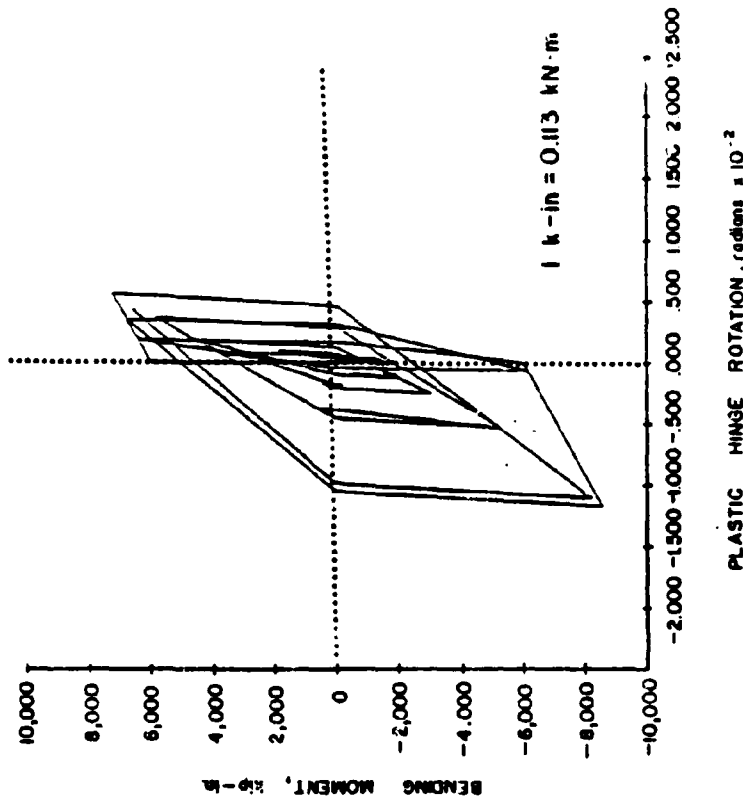
Fig. 50a Moment Versus Plastic Hinge Rotation Relationship of Sixth Story Beam Without Pinching
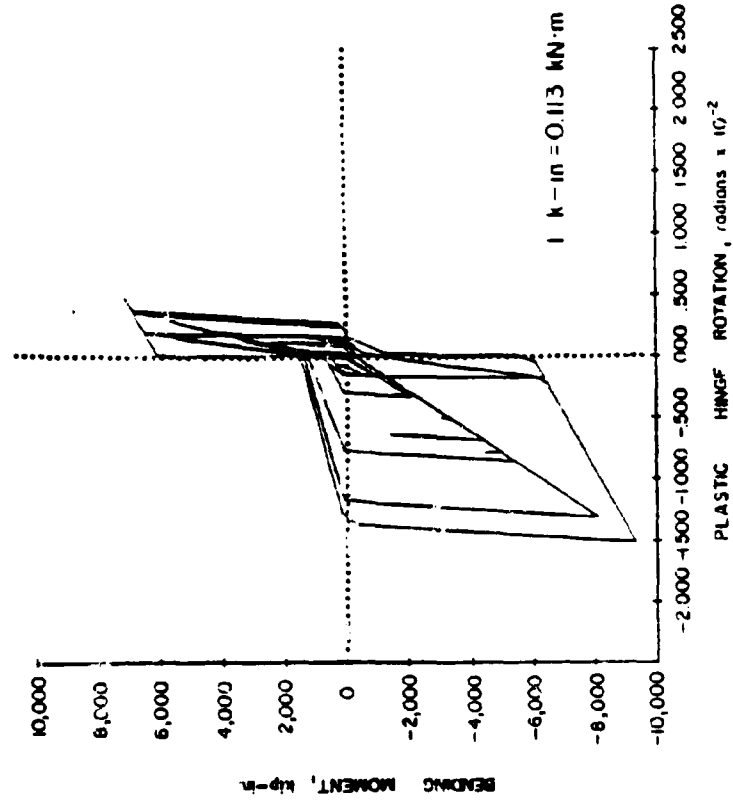
Fig. 50b Moment Versus Plastic Hinge Rotation Relationship of Sixth-Story Beam With Pinching

The initial elastic branch of this bilinear idealization repre-
sents effective stiffness of the member prior to yield and is
directly associated with the initial fundamental period of
vibration. The slope of the second, post-yield branch of the
primary curve is usually defined as a percentage of the slope
of the elastic branch.

A series of dynamic analyses was performed to investigate
the sensitivity of dynamic response to varying values of the
second slope. Cases analyzed considered four combinations of
post-yield stiffness of walls and coupling beams, as follows:

Post-Yield Stiffness as a Percentage of Initial Stiffness

Case	Walls	Coupling Beams
1	2%	3%
2	5%	6%
3	9%	10%
4	5%	10%

In all cases, the corresponding initial slopes for walls and
beams were kept constant. Results for these four cases are
shown in Figs. 51 and 52.

Response envelopes indicate that for the range of values
assumed, maximum wall displacements and forces are not signifi-
cantly affected by variations in post yield slope. In
contrast, maximum beam forces appear to be significantly
affected by changes in magnitude of the second slope. This can
be explained by high level of inelastic action and associated
ductilities in beams. Maximum beam moments and shears are
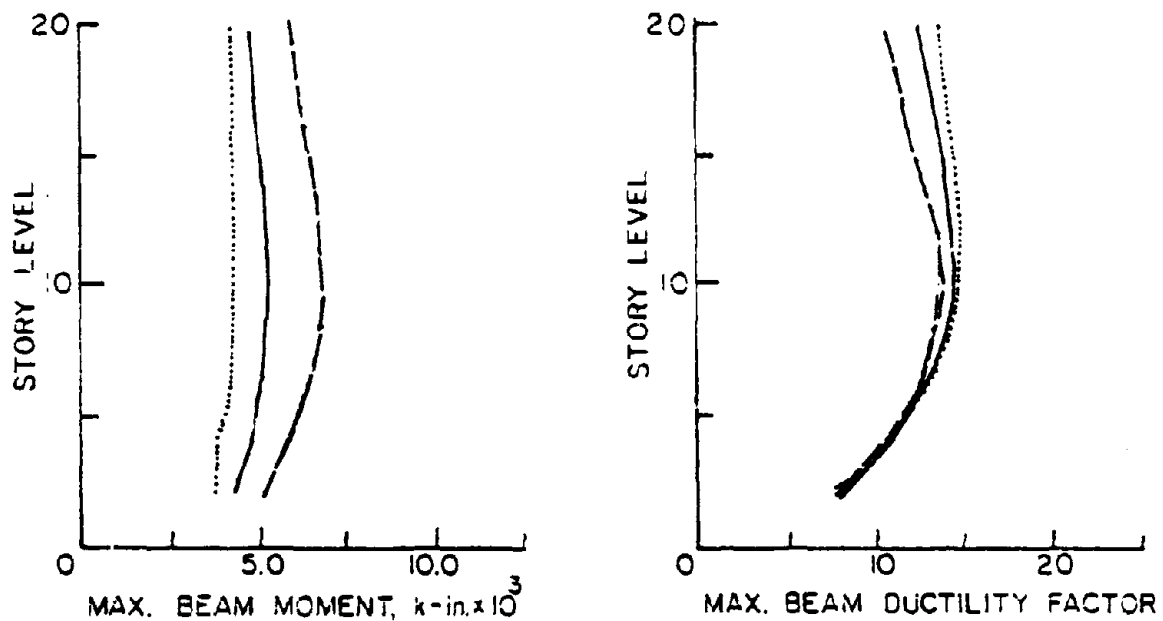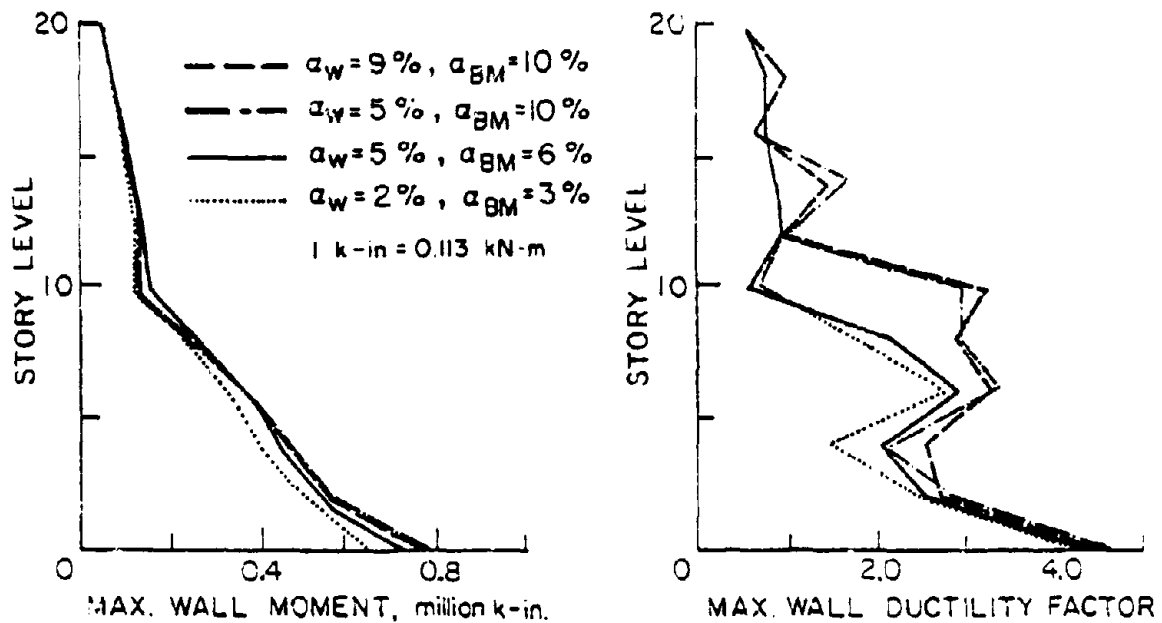
Fig. 51 Response Envelopes Showing the Effect of Inelastic Slope
of Primary Moment-Rotation Relationship as Percentage
of Elastic Slope
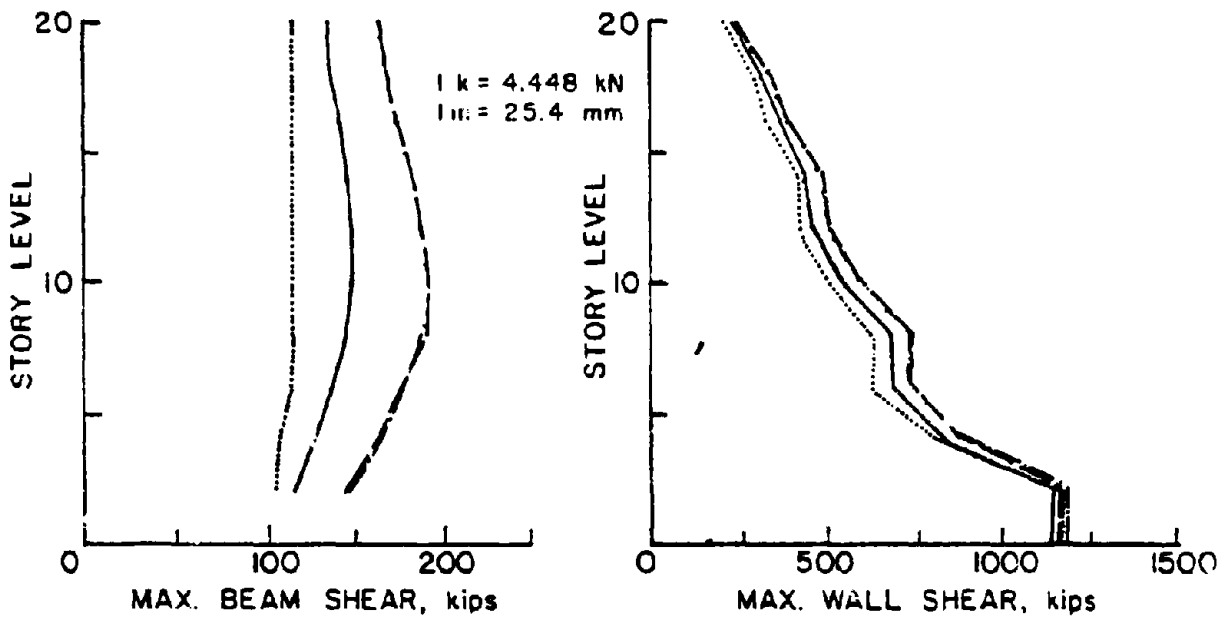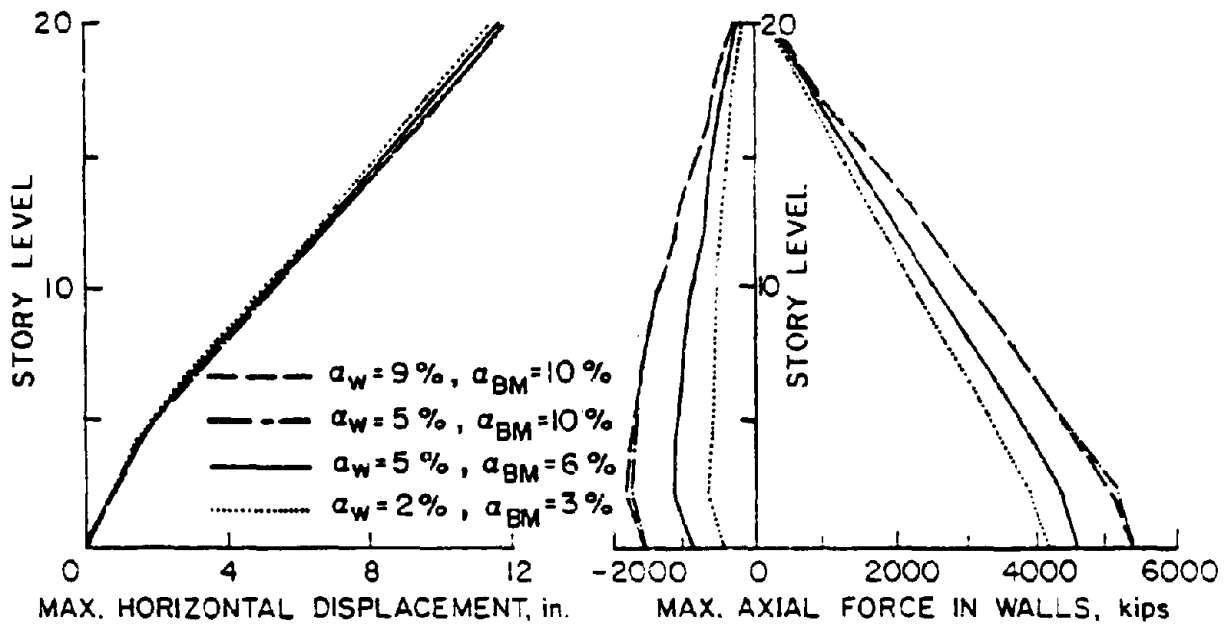
Fig. 52 Response Envelopes Showing the Effect of Inelastic Slope
of Primary Moment-Rotation Relationship as Percentage
of Elastic Slope
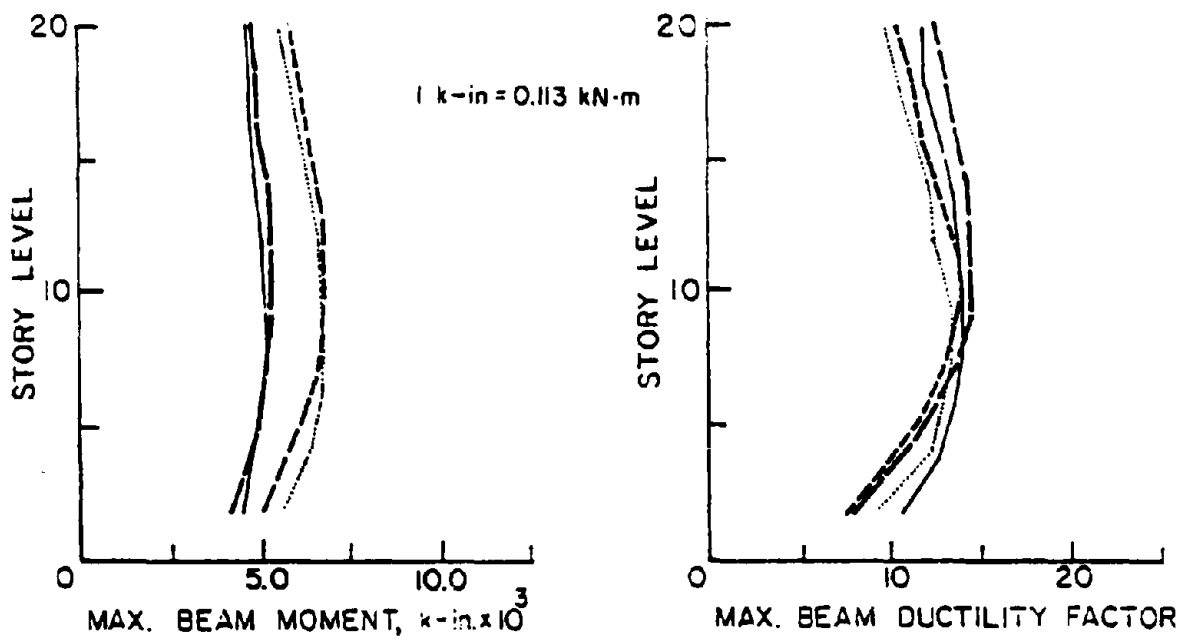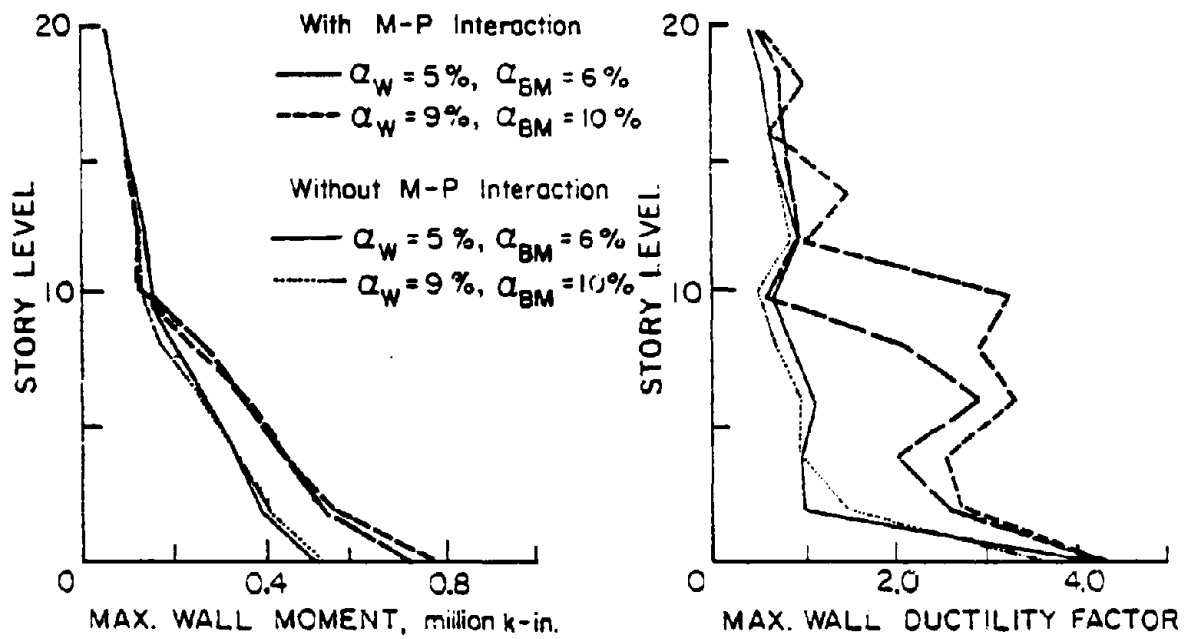
Fig. 53 Response Envelopes Showing the Effect of Inelastic Slope
of Primary Moment-Rotation Relationship as Percentage
of Elastic Slope

greater for structures with steeper second slopes, as expected. The increase in beam shears directly contributes to an increase in axial forces in walls. This increases tensile forces in walls and leads to a reduction in yield moment. As a result, walls yield even at upper floors (Fig. 51), and maximum wall ductilities show higher values for the case where net tension in walls was higher due to stronger coupling.

To further confirm this point, another set of analyses was carried out. In one case, axial force-moment interaction is permitted to examine the effect of a reduction in yield capacity of walls due to tensile forces. In the other case, this effect is neglected. Comparison of maximum response quantities are shown in Fig. 53. When the effect of axial force in walls is not considered, structures with low and high values of second slope show close agreement in terms of wall ductilities. However, when axial force-moment interaction is considered, the difference between the two wall ductility envelopes becomes significant (Fig. 53).

Unloading and Reloading Slopes of Hysteretic Loop

In Program DRAIN-2D, the character of hysteresis loops is governed by rules orginally proposed by Takeda[3]. A basic feature of this model is the decrease in reloading stiffness that occurs in load cycles subsequent to first yielding. The reloading stiffness is a function mainly of the maximum previous deformation. A decrease in unloading stiffness may also be
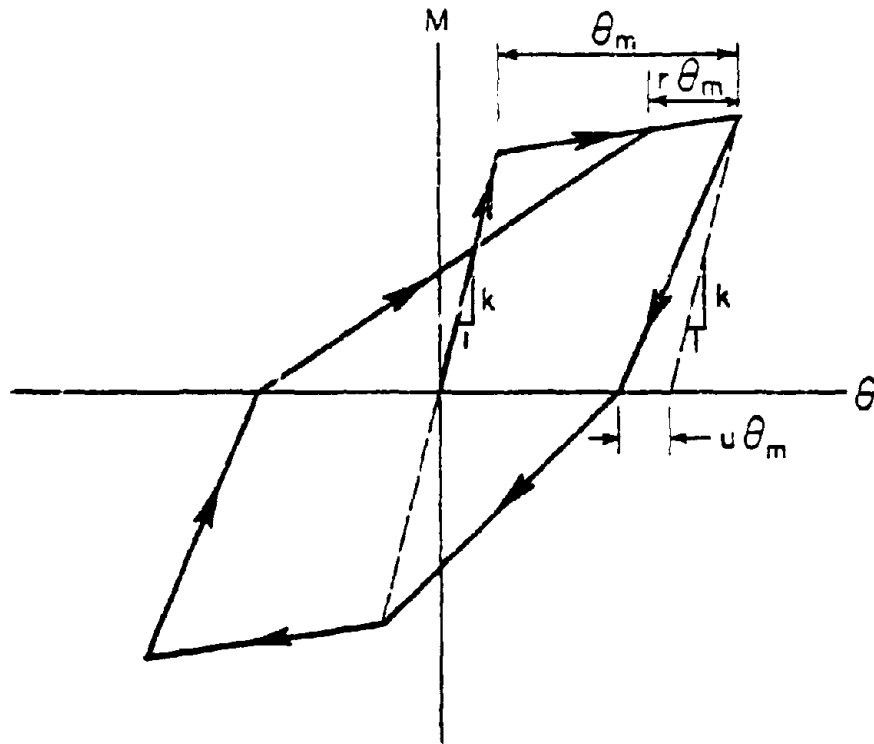
Fig. 54 Unloading and Reloading Parameters of Hysteretic Loop

specified. Input parameters "r" and "u" are used to specify reloading and unloading stiffness, respectively, as indicated in Fig. 54.

To investigate the effect of variations in values of unloading and reloading parameters "u" and "r" for coupling beams on dynamic response of coupled walls, a set of three analyses were carried out. The previously selected 20-story coupled wall structure, with properties listed in Table 1 was analyzed for this purpose. Parameters characterizing the moment-rotation hysteretic loop of coupling beams for the three cases considered were as follows (refer to Fig. 54):

Case	Unloading Parameter, u	Reloading Parameter, r
1	0.1	0
2	0.3	0
3	0.1	1.0

For the walls, "u" and "r", were kept constant at 0.1 and 0, respectively.

Comparison of these results indicate that maximum forces and displacements for the three cases do not differ by more than 5%. Thus, even for the fairly wide range of values represented by the three cases considered, effect of variations in reloading and unloading stiffnesses of coupling beams appear to have little effect on dynamic response of coupled walls. This observation confirms an earlier similar finding relative to isolated walls[8].

Decrease in Stiffness Due to Bond Slip

Tests of concrete members under slow load reversals show that loss of bond between reinforcement and concrete results in slip which is reflected in a stiffness decrease during laoding. This is in addition to the decrease in stiffness due to cracking. Although there is no separate mechanism in the analytical model used in DRAIN-2D for bond slip action, its effect can be accounted for by assigning appropriate slopes to loading branches. Contribution of bond slip to reduction in member stiffness can be determined through tests. Appropriate adjustments can then be made in both the effective elastic slope of the primary curve and reloading branches of the hysteretic loop.

Comparison with Test Results

As a check on validity of the analytical model employed in this investigation, a comparison was made between the results of a dynamic test of a particular structure and an analysis of the same structure. The experimental data were for a 10-story small-scale coupled wall structure tested on the University of Illinois earthquake simulator by Aristizabal-Ochoa[14]. Figure 55 shows overall dimensions of the test specimen. Cross sectional dimensions of walls and beams were 1.0 x 7.0 in. (25.4 x 177.8mm) and 1.0 x 1.5 in. (25.4 x 38.1mm), respectively. Structure weight was simulated by placing a 0.5 kip (2.22kN) weight at each floor. Structural properties used in the analysis are listed in Table 9.

TABLE 9 - PROPERTIES OF TEST SPECIMEN USED IN THE ANALYSIS

Fundamental Period	0.2 sec.
Number of Stories	10
Wall Stiffness Parameter (EI)	5.77×10^4 k-in.^{2}
Stiffness Taper	1.00 EI at base
	0.67 EI at 4th floor
Beam Stiffness Parameter (EI)	1.0×10^2 k-in.^{2}
Wall Yield Moment, M_y	39.0 k-in.
Strength Taper*	1.00 M_y at base
	0.51 M_y at 4th floor
Beam Yield Moment, M_y	1.56 k-in.
Damping	2.0% of critical
Post-Yield Stiffness on Primary Curve	2.0% of elastic
Weight	2.5 k/wall
Base Fixity Condition	fully fixed
Base Motion	El Centro 1940 N-S

*Yield moments are adjusted at every floor based on the weight of the structure.

1 k = 4.488 kN   1 k-in.^{2} 0.113 kN m
   1 k-in.^{2} = 0.00287 kN m^2
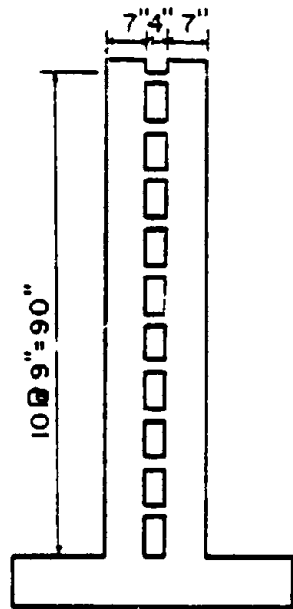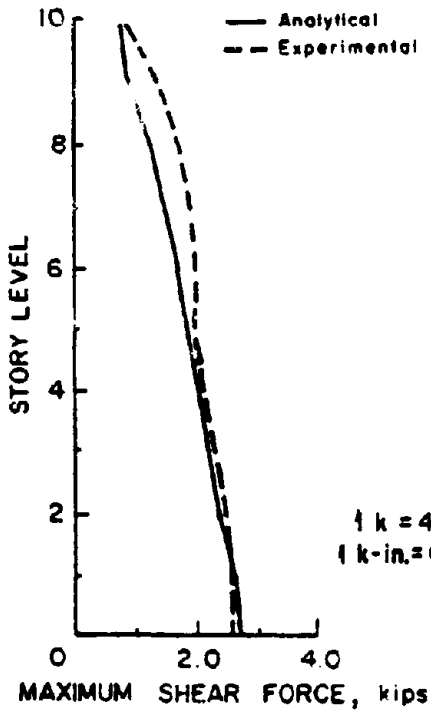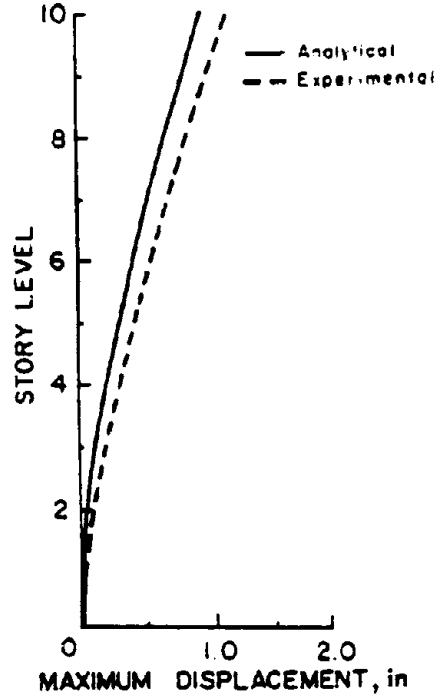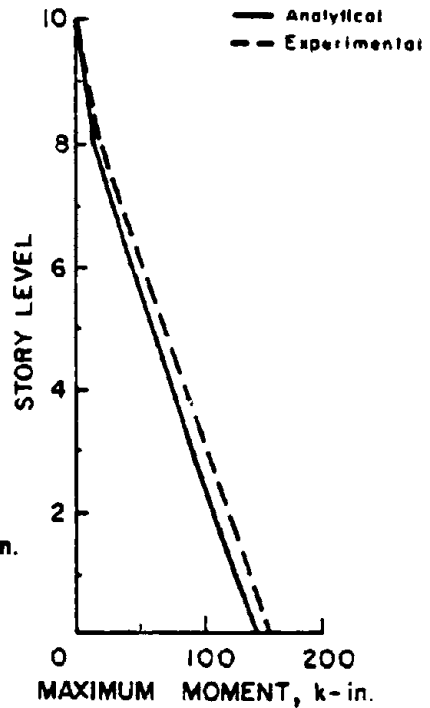
Fig. 55 Comparison of Displacement, Total Shear Force and
Overturning Moment Envelopes of the Analytical
and Simulater Test Results

Fig. 56 Comparison of Top Displacement, Base Overturning
Moment and Base Shear Force Time Histories of
the Analytical and Simulator Test Results

The input motion used was the N-S component of the 1940 El Centro record. The original time axis was compressed by a factor of 2.5, which implies that 3.0 seconds of analysis corresponds to 7.5 seconds of actual ground motion.

Effect of axial force-flexure interaction was considered in the analysis. Pinching of hysteresis loops, and strength loss under cycling loading were considered for coupling beams. The degree of pinching and strength loss used was determined from static tests of coupling beams used in the dynamic test. Elastic axial and shear rigidities were assumed.

The analytical and the test results are compared in Figs. 55 and 56. Response envelopes and time histories of horizontal displacement, total shear, and overturning moment appear to be in good agreement.

SUMMARY AND CONCLUSIONS

An examination of a number of variables affecting the modeling and dynamic inelastic response analysis of reinforced concrete coupled wall structures has been carried out. Principal among these is the effect of axial force-moment interaction on wall behavior. This factor assumes significance in coupled walls because of substantial axial forces that can be induced in walls of coupled wall structures as a result of lateral displacements due to ground shaking. The major effect of axial forces in walls, which arise from the coupling action of beams linking adjacent walls, is the reduction in yield moment and

stiffness accompanying a decrease in axial force, and vice versa. To our knowledge, this effect on dynamic inelastic response of coupled walls has not open investigated in detail before. A procedure for considering axial force-flexure interaction has been incorporated into the computer program DRAIN-2D.

Other factors considered are parameters defining the force-displacement hysteresis loop of the structure. Specifically, effective elastic stiffness, post-yield stiffness, strength decay, reloading and unloading stiffnesses, and pinching in the loop are considered. The effect of inelastic shear deformation is also investigated. A range of values of these parameters is covered to determine their relative importance with respect to selected response quantities.

Particular attention is placed on appropriate stiffness values to use in the analytical model. Results of tests on isolated structural walls were used as basis for estimating ranges of values of effective elastic stiffness and post-yield stiffness as percentages of the gross cross sectional properties of members. Other questions, such as lumping, integration time step, and stiffness and strength taper along the height of a structure, were also considered. The analyses were carried out using a reduced 10-story model of a 20-story prototype structure.

A comparison of experimental data for a small-scale coupled wall model tested on an earthquake simulator and results of an

analysis of the same structure using program DRAIN-2D, as modified for this investigation, is presented as a check on reliability of the analytical model and modeling techniques used in this investigation.

Based on the results of this investigation, the following conclusions can be made:

1. The computer program DRAIN-2D as modified for this investigation, can be used to predict dynamic inelastic behavior of coupled wall structures reasonably well. Results of an analysis using the program and those for a simulator test appear to be in good agreement.

2. Axial forces in walls due to coupling can have a significant effect on force-deformation characteristics of individual walls. Response envelopes of walls can be increased by as much as 50%, depending on the degree of coupling. The axial force-flexure interaction model for concrete hysteretic loop, introduced into DRAIN-2D by the authors, produces reasonable results for members under changing axial forces.

3. In general, maximum forces and displacements in a multistory coupled wall structure are not too sensitive to shear yielding. However, if decrease in shear stiffness under cyclic loading is very high, sizable effects in some response quantities can be observed. In the lower extreme of shear stiffnesses considered in this investigation, maximum shear force is reduced

by about 17% at the base of the wall due to shear yielding. Although ductility envelopes for walls do not show any appreciable change due to shear yielding, maximum rotational ductilities for beams are reduced by about 40%. This can be attributed to the increase in the shear component of total deformation which implies a corresponding decrease in flexural component. In the hinging region, at the base of walls, there have been instances during response in which horizontal displacement due to shear yielding formed more than 50% of total hinging region displacement. This is comparable to values observed in static tests of isolated walls for the same stiffness range[5, 6]. However, under dynamic loading conditions maximum shear deformations and maximum flexural deformations generally do not occur simultaneously. Therefore, displacement response envelopes do not necessarily reflect the same effect of shear yielding. Furthermore, any effect of shear yielding in the hinging region does not appear to influence overall dynamic response of a multistory coupled wall structure. In cases where reduction in shear stiffness due to cracking and yielding was moderate, very little effect was observed in response envelopes due to shear yielding.

4. Stiffness and strength taper of walls along the height of a structure can, under earthquake excitation, lead

to yielding at locations where changes in stiffness and strength occur. Although ductility demands at upper floors are usually less severe than at the base hinging region, inelastic deformations at upper floors can be substantial under critical earthquake motions. From this point of view, structures having uniform wall strength and stiffness along the height exhibit superior behavior under earthquake loading.

5. Coupling beams under cyclic loading show varying degrees of strength decay at different levels of ductility. Analysis indicates that dynamic inelastic response of coupled wall structures can be affected drastically by this parameter. If beams are designed such that they show early and rapid strength decay rotational ductility requirements two to four times of those associated with beams with no decay can be expected.

6. Tests of reinforced concrete members subjected to slow load reversals usually exhibit some pinching action in force versus deformation relationships[5, 6, 13]. This phonomena is most apparent in shear-shear distortion hysteresis loops. In general, the effect of pinching in force-displacement hysteresis loops on overall dynamic response is small. In certain cases, where pinching is severe and for certain frequency characteristics of input motion, a drift in the axis of oscillation of the structure can occur.

7. Moderate variations in inelastic loading, unloading, and reloading branches of the hysteretic loop of mem- bers do not affect dynamic response of coupled wall structures. This implies that any inaccuracy involved in estimating the slopes (stiffnesses) of inelastic branches need not be of concern to the analyst, par- ticularly in view of uncertainties associated with other aspects of earthquake engineering. For members that experience large inelastic deformation, as in the case of coupling beams, effect of variations in the post-yield slope of the primary curve becomes more pronounced.

8. The 20-story structure, considered in this investiga- tion, can be modeled as a reduced 10-story model for dynamic analysis.

9. An integration time increment of 0.01 sec. is suffi- ciently small to produce accurate results for the structure considered in this investigation.

ACKNOWLEDGMENTS

REFERENCES

1. Uniform Building Code. 1976 Edition, International Conference of Building Officials, 5360 South Workman Mill Road, Whittier, California 90601.

2. Kanaan, A.E. and Powell, G.H., "General Purpose Computer Program for Inelastic Dynamic Response of Plane Structures", Report No. EERC 73-6, Earthquake Engineering Research Center, University of California, Berkeley, April 1973.

3. Takeda, T., Sozen, M.A., and Nielsen, N.N., "Reinforced Concrete Response to Simulated Earthquakes", Journal of the Structural Division, ASCE, Vol. 96, No. ST-12, December 1970, pp. 2557-2573.

4. Takayanagi, T., Derecho, A.T., and Corley, W.G., "Analysis of Inelastic Shear Deformation Effects in Reinforced Concrete Structural Wall Systems", Proceeding of the CSCE-ASCE-ACI-CEB International Symposium on "Nonlinear Design of Concrete Structures", SM Study No. 14, University of Waterloo Press, Waterloo, Ontario, 1980.

5. Oesterle, R.G., Aristizabal-Ochoa, J.D., Fiorato, A.E., Russell, H.G., and Corley, W.G. "Earthquake Resistant Structural Walls - Tests of Isolated Walls - Phase II" Report to the National Science Foundation, Portland Cement Association, October 1979.

6. Oesterle, R.G., Fiorato, A.E., Johal, L.S., Carpenter, J.E., Russell, H.G., and Corley, W.G., "Earthquake Resistant Structural Walls - Tests of Isolated Walls," Report to the National Science Foundation, Portland Cement Association, November 1976.

7. Sozen, M.A. "Hysteresis in Structural Elements," Applied Mechanics in Earthquake Engineering, ASME AMD Vol. 8, Nov. 1974, pp. 63-98.

8. Derecho, A.T., Ghosh, S.K., Iqbal, M., Freskakis, G.N., and Fintel, M. "Structural Walls in Earthquake-Resistant Buildings, Dynamic Analysis of Isolated Structural Walls, Parametric Studies" Report to the National Science Foundation, Portland Cement Association, March 1978.

9. Saatcioglu, M. and Derecho, A.T., "Dynamic Inelastic Response of Coupled Walls as Affected by Axial Forces", Proceedings of the CSCE-ASCE-ACI-CEB International Symposium on "Nonlinear Design of Concrete Structures", SM Study No. 14, University of Waterloo Press, Waterloo, Ontario, 1980.

REFERENCES
(cont'd)

10. Vallenas, J.M., Bertero, V.V., and Popov, E.P., "Hyste-
retic Behavior of Reinforced Concrete Structural Walls,"
Report to the National Science Foundation, Earthquake
Engineering Research Center, University of California,
Berkeley, August 1979.

11. Wang, T.Y., Bertero, V.V., and Popov, E.P., "Hysteretic
Behavior of Reinforced Concrete Framed Walls," Report to
the National Science Foundation, Earthquake Engineering
Research Center, University of California, Berkeley,
December 1975.

12. Ma, S.M., Bertero, V.V., and Popov, E.P., "Experimental
and Analytical Studies on the Hysteretic Behavior of
Reinforced Concrete Rectangular and T-Beams," Report to
the National Science Foundation, Earthquake Engineering
Research Center, University of California, Berkeley, May
1976.

13. Barney, G.B., Shiu, K.N., Rabbatt, B.G., and Fiorato, A.E.,
"Earthquake Resistant Structural Walls--Tests of Coupling
Beams," Progress Report to the National Science Foundation,
Portland Cement Association, October 1976.

14. Aristizabal, J.D., "Behavior of Ten-Story Reinforced Con-
crete Walls Subjected to Earthquake Motions", Ph.D. Disser-
tation, Department of Civil Engineering, University of
Illinois at Urbana-Champaign, Urbana, Illinois, 1977.

15. Takayanagi, T. and Schnobrich, W.C., "Computed Behavior
of Reinforced Concrete Coupled Shear Walls", Civil En-
gineering Studies, Structural Research Series No. 434,
University of Illinois at Urbana-Champaign, Urbana,
Illinois, December 1976.

NOTATIONS

A	=	Cross sectional area.
E	=	Modulus elasticity of concrete.
EA	=	Axial rigidity.
EI	=	Felxural rigidity.
GA	=	Shear rigidity.
I	=	Moment of inertia of a section.
$I_{mod.}$	=	Moment of inertia of a section in a model structure.
$I_{prot.}$	=	Moment of inertia of a section in a prototype structure.
K_s	=	Stiffness of a point hinge in elastic range (= 1×10^8).
L	=	Length of a member.
M	=	Bending moment.
M_{max}^e	=	Maximum moment in elastic deformation range.
M_{max}^{ie}	=	Maximum moment in inelastic deformation range.
M_y	=	Bending moment at flexural yield.
P , P_1, P_2,	=	Axial forces.
q	=	Pinching factor which defines the reduction in the slope of reloading branches of hysteretic loops.
r	=	Reloading parameter for hysteretic loops.
r_1	=	(I_{mod}/I_{prot}) of a wall section.
r_2	=	(I_{mod}/I_{prot}) of a beam section.
S	=	Elastic stiffness

T	=	Fundamental period of vibration.
u	=	Unloading parameter for hysteretic loops.
V	=	Shear force.
V_{max}^e	=	Maximum shear force in elastic deformation range.
V_{max}^{ie}	=	Maximum shear force in inelastic deformation range.
V_y	=	Shear force yield level.
ΔM	=	Increment of bending moment.
ΔM_A , ΔM_B	=	Increments of bending moment at member ends A and B respectively.
ΔV	=	Increment of shear force.
ΔV_A , ΔV_B	=	Increments of shear force at member ends A and B respectively.
γ_A , γ_B	=	Increments of shear distortion at member ends A and B respectively.
γ_A^e , γ_B^e	=	Increments of elastic shear distortion at member ends A and B respectively.
γ_A^p , γ_B^p	=	Increments of plastic shear distortion at member ends A and B respectively.
θ_A , θ_B	=	Increments of chord rotation at member ends A and B respectively.
θ_A^e , θ_B^e	=	Increments of elastic chord rotation at member ends A and B respectively.
θ_A^p , θ_B^p	=	Increments of plastic chord rotation at member ends A and B respectively.

α = Ratio of the second slope to first slope of bilinear moment-chord rotation relationship.

α' = Input value for the ratio of second slope to first slope of bilinear moment-chord rotation relationship when default option of DRAIN-2D is used. Note that $\alpha' = \alpha$ if the member is a cantilever with zero moment at one end.

α_A, α_B = Ratio of the second slope to first slope of bilinear moment-chord rotation relationship of point hinges.

α_W = α for walls.

α_{BM} = α for beams.

α'_H = Ratio of the second slope to first slope of bilinear moment-rotation relationship of a point hinge at the restrained end of a cantilever member. Note that if $M_B = 0$; $\alpha'_H = \alpha_A$ and if $M_A = 0$; $\alpha'_H = \alpha_B$.

β = Ratio of the second slope to first slope of bilinear shear-shear distortion relationship.

β_A, β_B = Ratio of the second slope to first slope of bilinear shear-shear distortion relationship of point hinges at member ends A and B respectively.

-116-

θ	= Rotation.
θ^e	= Elastic rotation.
θ^P	= Plastic rotation.
θ_{max}	= Maximum rotation.
θ_y	= Rotation at yield.
μ_r	= Rotational ductility factor
	$(\mu_r = \theta_{max}/\theta_y)$
ξ	= Ratio of moment at end B to moment at end A $(\xi = M_B/M_A)$

APPENDIX A

AXIAL FORCE-FLEXURE INTERACTION MODEL

Nature of the Problem

Nonlinear analysis of reinforced concrete members has been a major concern in investigating response of structures under earthquake forces. Dynamic inelastic analysis requires an analytical model that accurately represents behavior under flexure, shear, and axial forces. A reinforced concrete beam model was developed by Takeda[3] for constant level of axial force. This model has been implemented into program DRAIN-2D in a slightly modified form as Element No. 6.

Coupled walls usually exhibit substantial changes in axial forces during their response to earthquake motions as illustrated in Fig. A1. A force couple is formed by the axial forces in the coupled walls that resists overturning. These forces either increase or decrease compressive forces due to gravity loads. In some cases, axial force due to coupling may far exceed gravity load, creating net tension. This results in a reduction in member flexural capacity. On the other hand, compressive forces tend to increase flexural stiffness and strength of walls. This makes the compression wall attract more forces. Continuous change in level of axial force during response affects yield level due to interaction between axial force and flexure. This effect not only alters initial flexural yield level, but also affects behavior of the structure in the post-yield range. Therefore, the original decreas-

ing stiffness" beam model was modified to include axial force-moment interaction.

Axial Force-Moment Interaction

A typical axial force-moment interaction diagram is shown in Fig. A2. Yielding of a section is associated with yielding of reinforcement. This condition corresponds to points on the interaction diagram below the balanced point marked "B" (or "B'") in Fig. A2. During response, axial forces are expected to have values below that corresponding to the balanced point. In this region, the relationship between axial force and moment is assumed to be bilinear. If the axial force increases beyond the balanced point, then the program prints a warning message indicating possible crushing of concrete prior to yielding of reinforcement. This case may also indicate unrealistic input data.

During analysis, the yield moment of a section is determined for each time increment, corresponding to the axial force calculated at the end of the immediately preceding interval. These yield moments are used both for checking against yielding and establishing post yield rules of the hysteretic loop. Points B, B', C, C', and D in Fig. A2 are specified as input to the computer program.

Moment-Rotation Relationship

In simulating behavior of a reinforced concrete member, realistic representation of moment-rotation relationship is important. For members under uniform moment, the moment-rotation
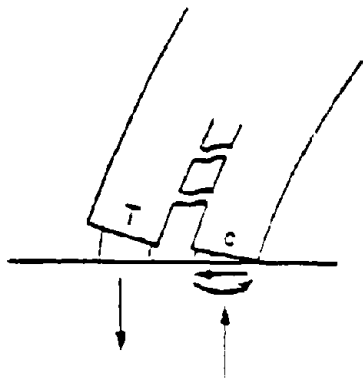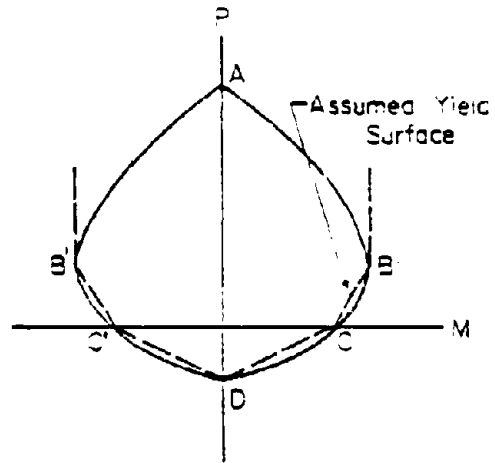
Fig. A1   Axial Forces Due
to Coupling

Fig. A2   Axial Force-Moment
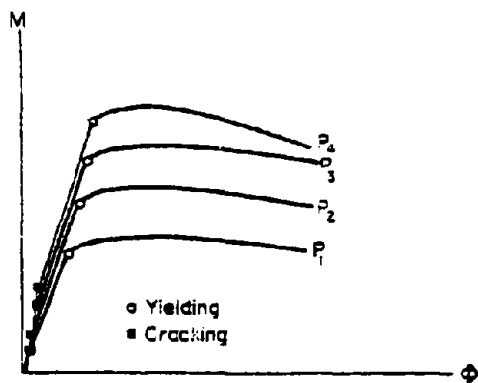Interaction Diagram

Fig. A3   Moment-Rotation Relation-
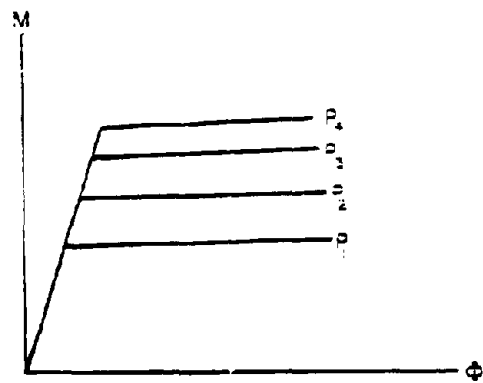ship Under Different
Levels of Axial Forces

Fig. A4   Bilinear Idealization of
Moment-Rotation
Relationship

A-3

relationship for a specific level of axial force has the same shape as the corresponding sectional moment-curvature relationship. This relationship can be idealized as a bilinear curve as shown in Fig. A4. This indicates identical slope for curves corresponding to different magnitudes of axial force. Inelastic slope remains constant only if the axial load remains constant. During response of a structure, there will be smooth shifts between curves of different axial forces, reflecting either hardening or softening of the structure due to increase or decrease in the axial force, respectively. For purposes of this development, bilinear moment-rotation relationship is used.

Hysteretic Loop

The hysteretic loop under consideration consists of 11 post-yield branches, 6 of which are loading, and the remainder unloading as shown in Fig. A5. Beginning and end points of each branch are found by following rules proposed by Takeda[3] and are modified as affected by changing axial forces. A set of loops, corresponding to different levels of axial force, is used as a guide in predicting change in stiffness due to axial force effects. This is shown in Fig. A6. The basic concept in introducing the effect of changing axial forces is to update stiffness for the subsequent time increment, based on axial force calculated for the current time increment.
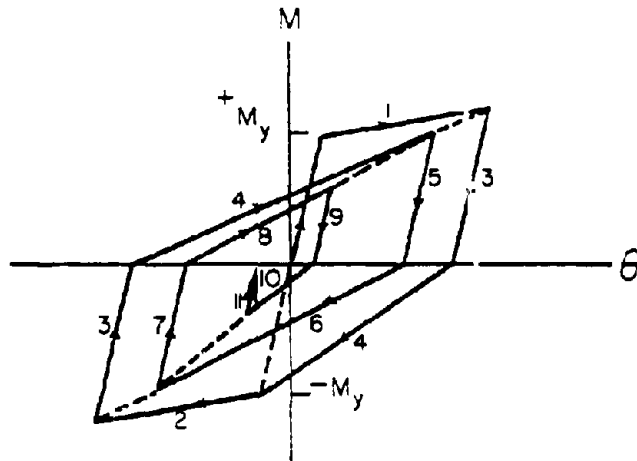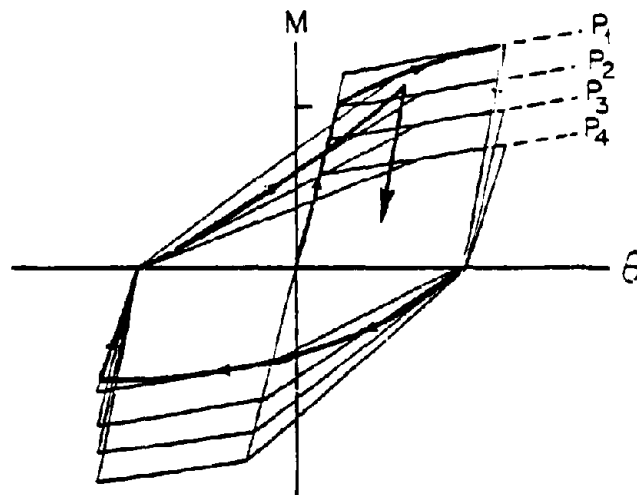
A-4

Fig. A5   Takeda's Hysteretic Loop

Fig. A6   Hysteretic Loop Under Changing
Axial Forces

Loading in Elastic Branch

Loading in the elastic branch follows the same stiffness, irrespective of level of axial force. At the end of each time increment, a new level of axial force is computed. The corresponding yield moment is found from moment-axial force interaction diagram. This value is compared with the current moment to check if yielding has occurred at a given section. Loading along the elastic branch continues until yielding is detected at the appropriate yield level.

Loading in Inelastic Branches

Upon exceeding the current yield moment, loading continues along inelastic branches. During the first time increment after yielding, the element is assumed to have a stiffness corresponding to the second slope of the primary moment-rotation relationship. At the end of the first time increment, a new level of axial force is obtained. The difference between axial forces at beginning and end of the current time increment causes either softening or hardening of the element. This new stiffness given by the slope of the moment-rotation diagram is followed during the subsequent time increment.

The procedure described is illustrated in Fig. A7 for a case of decreasing axial force. At the end of the first time increment i.e. the current time increment, point C is obtained. At point C, the section has a specific value of moment, M_2, and axial force, P_2. However, any point on line AC corresponds to an axial load of P_1. Therefore, to be able to develop M_2 and

P_2, the section should be loaded with reduced stiffness (slope) of BC'. This reduction in slope reflects the decrease in member stiffness due to the reduction in axial force from P_1 to P_2. In this model, correction to stiffness due to change in axial force during current time increment is applied to the member during the subsequent time increment. If the integration time step is sufficiently small, this delay of one time increment in making the correction is believed to have no significance as far as accuracy of the results are concerned.

If there is an increase in compression or decrease in tension, then stiffness is increased during response. Figure A8 shows an example of increasing axial force. If there is too much increase in force within one time increment, then a very steep slope or a negative slope can be encountered by this procedure. Since neither case is physically possible, the program enforces a maximum stiffness equal to the elastic stiffness. Figure A9 illustrates the possibility of a negative slope.

Unloading Branches

Unloading in the elastic range follows the same stiffness as loading. The behavior up to yielding is straightforward.

Unloading in the inelastic range can occur from a loading branch (after yielding) or a reloading branch. The beginning point of an unloading branch is determined by the last point of loading or reloading branch. Similarly, the final point of unloading, which is the plastic residual rotation, is governed by
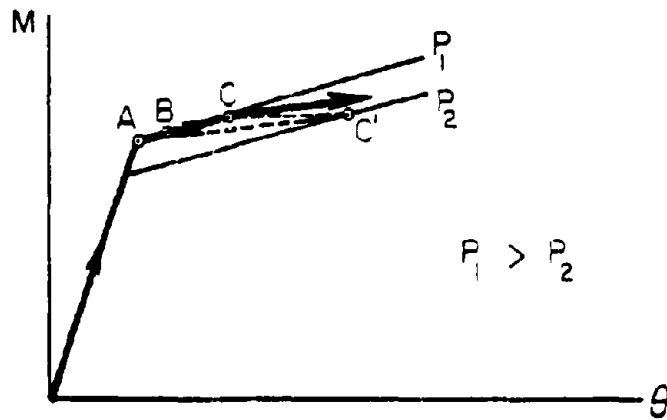
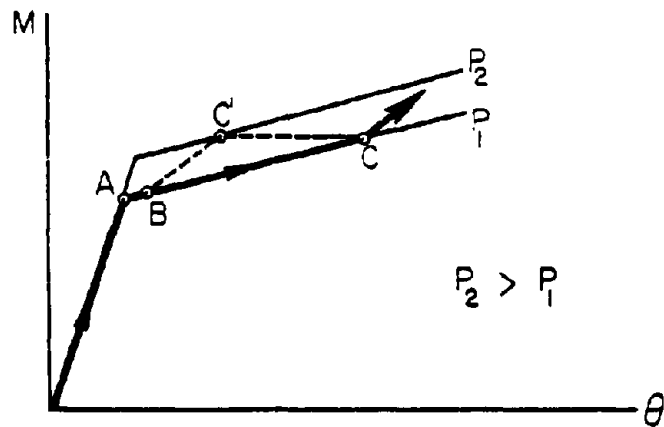Fig. A7   Loading on Primary Curve Under
Decreasing Axial Forces

Fig. A8   Loading on Primary Curve Under
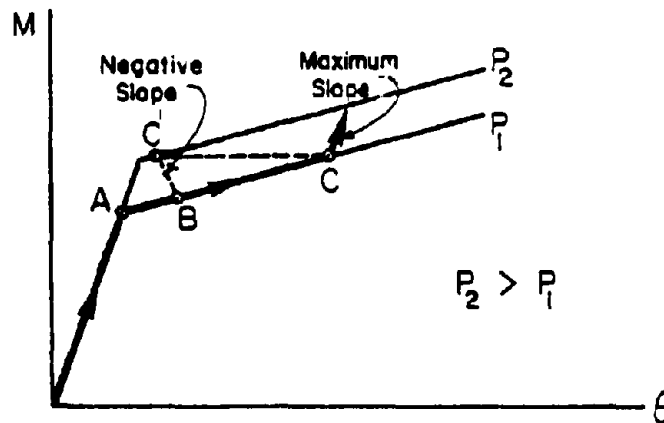Increasing Axial Forces

Fig. A9   Possibility of Negative Slope and
Limit to Increase in Slope

the previous maximum rotation and is assumed to be unaffected by the change in axial forces during unloading. Therefore, in Fig. A10, no matter what the axial force during unloading, the response starts at point "D" and ends at point "E". Any correction to slope due to axial force effects will eventually be directed to point E. Therefore, the effect of variation in axial force during unloading is believed to be small and assumed to have no significant contribution on the overall behavior of a member. For this reason, a constant stiffness is assumed during unloading. This stiffness corresponds to the level of axial force present during the last time increment of loading or reloading branch prior to unloading.

Reloading Branches

The same procedure employed for inelastic loading branches applies to reloading branches. An increase or decrease in axial force is reflected by updating stiffness at the end of each time increment. This is illustrated in Fig. A11.

Discussion of the Model

The moment-axial force interaction model was developed by modifying the original "decreasing stiffness" beam element of program DRAIN-2D. The original model was based on rules suggested by Takeda, that were developed for a constant axial force level. An effort was made to assess reliability of the modifications introduced to the original model.

One way to verify the analytical model is to compare results of analysis with experimental results. Since the computer
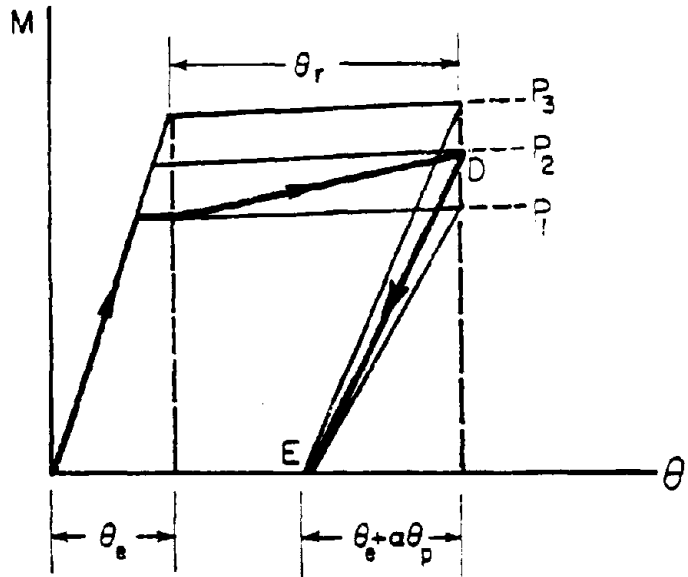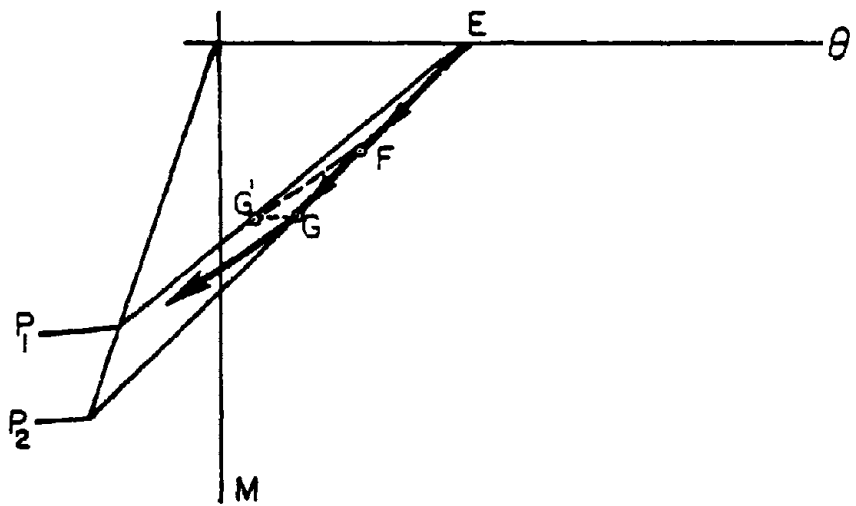
Fig. A10   Unloading Branch

Fig. A11   Reloading Branch

program DRAIN-2D produces results for dynamic analysis, any comparison with experimental data will have to be made with dynamic test results. Therefore, a comparison was made by using the analytical model developed here to analyze response of a small-scale 10-story coupled wall specimen . The model structure was tested on the University of Illinois earthquake simulator by Aristizabal-Ochoa.[14] The comparison is discussed under "Dynamic Analyses" in the main body of this report. Comparison of response histories and envelopes shows good agreement between analytical and experimental results. The test data, however, provide information only on overall structural behavior such as displacements and total forces developed in the system. No data are available on response quantities for individual members.

In a coupled wall system, shear and bending moment continuously shift from "weak" (tension) wall to "strong" (compression) wall and may subject individual walls to critically high forces and/or high deformation demands. Examination of this behavior was the primary purpose of developing the axial force-interaction model. It is unfortunate that this type of information is not available from the dynamic test reported in Ref. 14 for comparison. In the simulator test, the strong wall tends to cancel the negative effect of the weak wall and produces an overall "average" behavior that masks behavior of individual walls. Although the test does not provide enough data to verify the analytical model, this should not be taken to suggest that the effect of axial force-flexure interaction can be ignored

A-11

in the analysis. The comparison of gross behavior does provide some verification of the analytical model.

In lieu of available test data, some form of verification of the accuracy of the analytical model can be done by using well established engineering principles, or by comparison with results obtained using other analysis programs. Dynamic analysis of the previously described test specimen was also carried out by Takayanagi at the University of Illinois, using a trilinear moment-rotation relationship.[15] Comparison between the analysis of this study and that at the University of Illinois shows excellent agreement. The sequence and pattern of yielding among members of the structure is the same for both analyses.

Another interesting observation of this comparison is that both analytical results of this investigation and analytical results of the University of Illinois do not show yielding in walls when the moment-axial force interaction is ignored. This indicates the importance of the effect of axial force on wall capacity. A wall that may have behaved elastically under gravity loads may experience significant yielding under tensile axial force due to coupling. The two analyses produce identical results when moment-axial force interaction is considered.

To provide further description of the model, two examples are discussed with reference to Figs. A12 and A13. These figures show computer plots of moment-rotation hysteretic loops for point hinges. As previously discussed, inelastic action is

accounted for by allowing formation of point hinges at member ends. There are three points that deserve attention when studying these plots. First, the yield moment level; second, the maximum plastic rotation; and third, the stiffness (slope of each line segment). These three points are interrelated and vary with the level of axial force. In Fig. A12, elastic action is traced by a vertical line along the vertical axis. When the member is in compression, the actual yield moment is indicated by point "B", which exceeds the yield moment corresponding to gravity load of 400,000 in-kips (point A). This is mainly because of the increase in yield moment from "A" to "B" due to compressive axial force. When the same wall is under tension, yielding occurs at point "D" prior to reaching "C", which is the prescribed yield level under gravity load. Variation of yield moment with axial force is based on well known moment-axial force interaction relationships.

Yielding is followed by inelastic loading along line $\overline{DE}$, as shown in Fig. A12. During the first time increment following yielding, the input stiffness for the second branch of bilinear moment-rotation relationship is used. Depending on level of axial force, input stiffness is updated to allow for softening of the element since the element is under increasing tension (or decreasing compression) force. A question may arise about the exact location of point "E". If the axial force is reduced from P_1 to P_2, then "E" is located such that plastic rotation is less than that associated with loading under constant
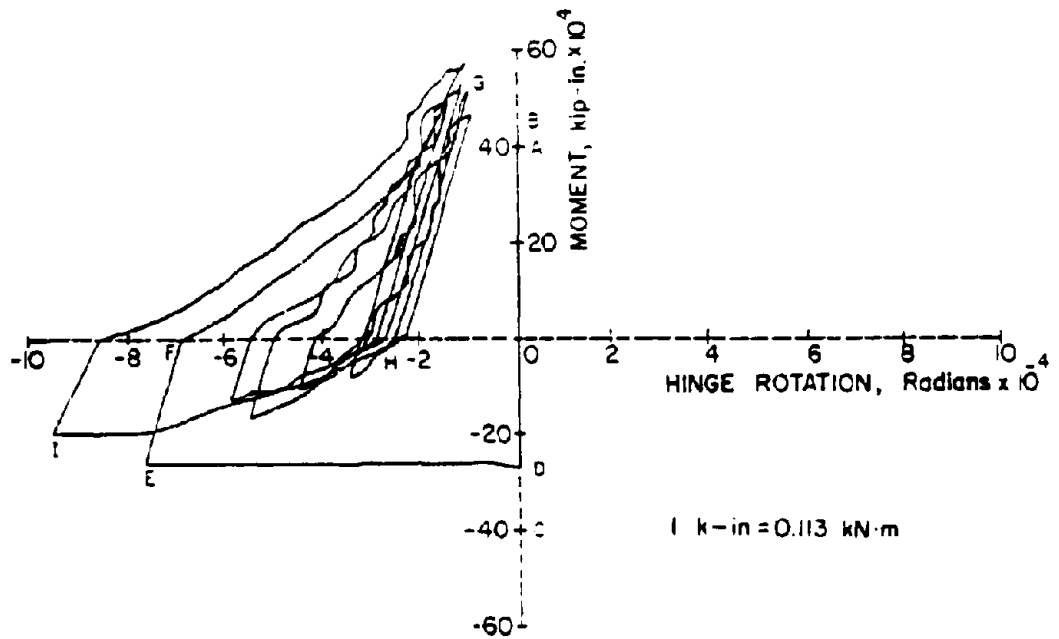
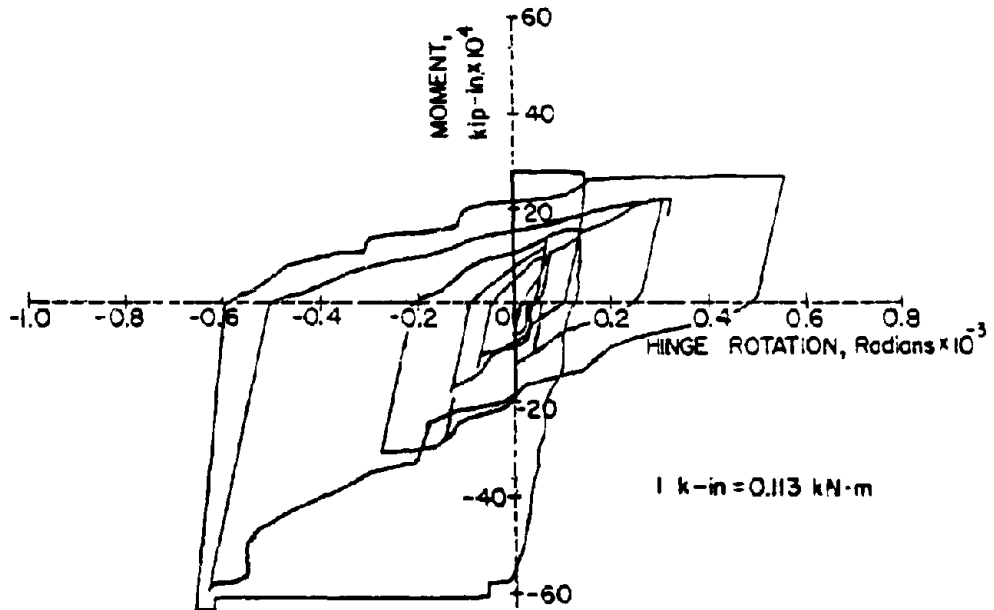**Fig. A12 Moment-Hinge Rotation Relationship Under Changing Axial Forces**

Fig. A13 Moment-Hinge Rotation Relationship Under Changing Axial Forces

P_2 and greater than that for constant P_1. This is mainly because of the history of loading. If the structure is initially stiff and becomes flexible during loading, then rotation is less than that for the case where it is originally flexible. This concept is modeled by updating stiffness and allowing the structure to respond with this new stiffness rather than adjusting moment or rotation to match the current level of axial force. The amount of change in stiffness is related to the amount of change in axial force in an approximate way. It is observed that the structure is not sensitive to small variation in the stiffness of one member for a small time increment. Therefore, the location of "E" is found to be reasonably accurate.

The other important point is the change of stiffness during reloading. Lines between "F" and "G" in Fig. A12 are curving upward, indicating an increase in stiffness due to increasing compression. The reverse can be observed between "H" and "I" when the compressive force on the wall is decreasing. The amount of increase or decrease in reloading slopes depends on the current level of yield moment which is used to determine the end points of reloading branches. Since computation of current yield moment involves nothing more than moment-axial force interaction, yield moments and thus slopes of reloading curves are found to be reasonably accurate.

Figure A13 shows another example of moment-inelastic rotation hysteretic loop. The behavior of the reloading curves in

the "tension" (above the x-axis) and "compression" (below the x-axis) zones indicate typical axial force-flexure interaction effects.

A plot of base moment-versus-hinging region rotation (which includes elastic rotation) of individual walls of a coupled wall system is shown in Fig. A14. Difference in behavior between the "tension" and "compression" walls can be seen in this figure. Also shown in the figure for comparison are the primary moment-rotation curves under constant dead load.
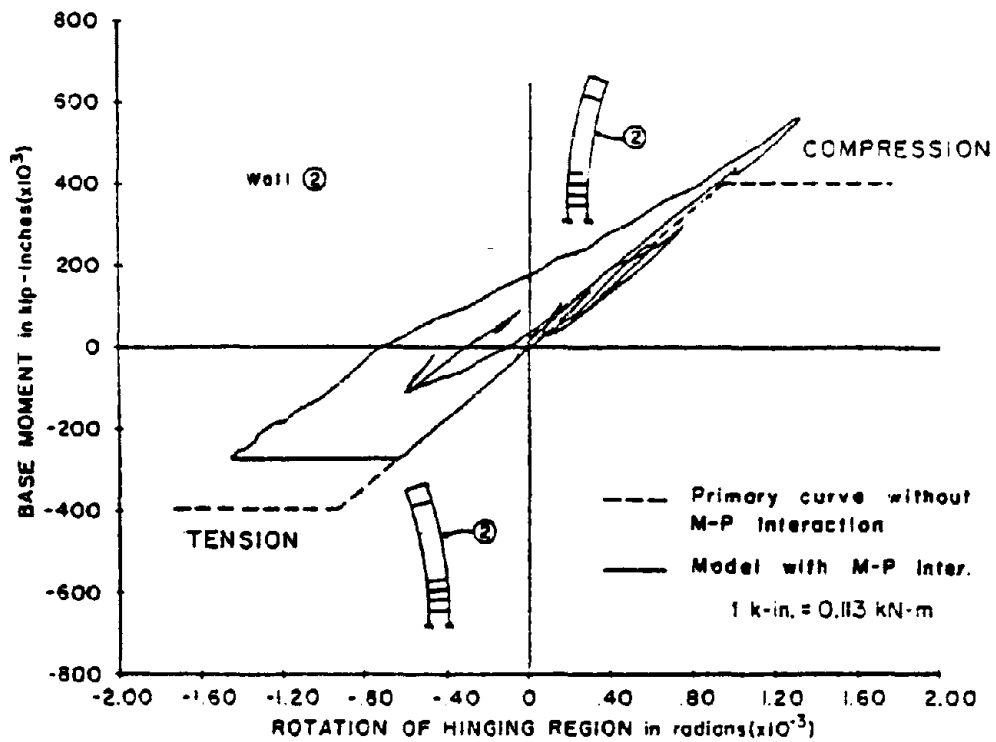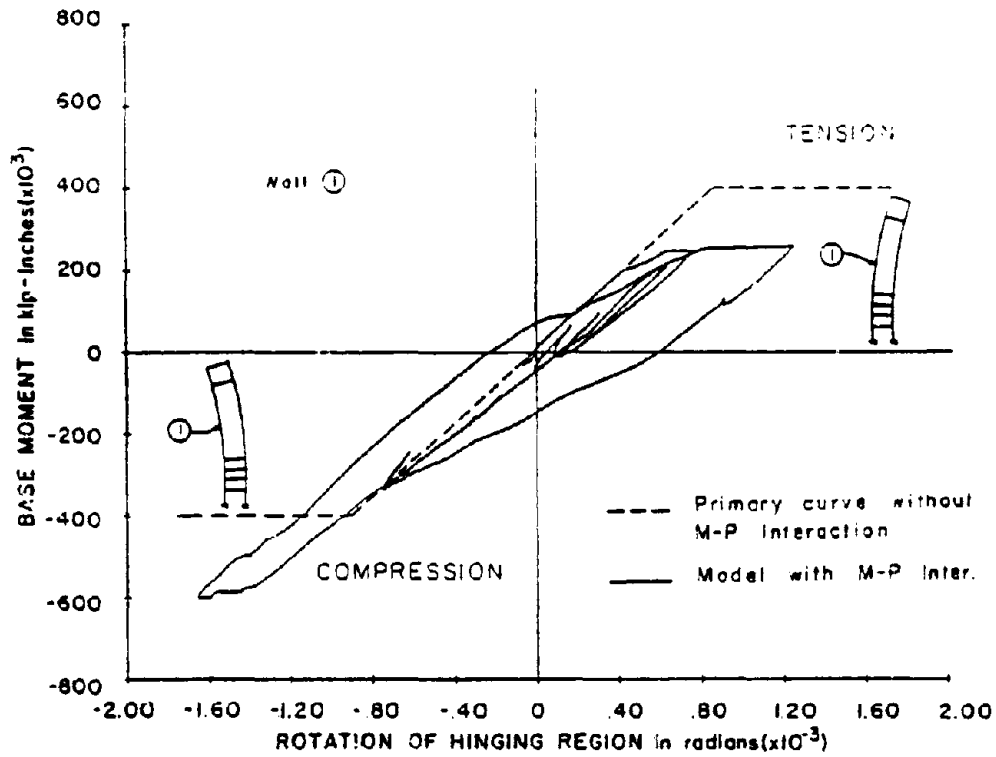
Fig. A14 Hysteretic Loops of Tension and Compression Walls

APPENDIX B

DETERMINATION OF INPUT PARAMETERS

FOR INELASTIC HINGES IN DRAIN-2D

Program DRAIN-2D allows for inelastic action in a member through formation of point hinges at both ends of an elastic line element. The elastic line element together with point hinges simulate both elastic and inelastic behavior of a real member. This section describes the procedure used in determining input parameter values defining properties of the analytical model as used in DRAIN-2D, when using the default option.*

Elastic stiffness parameter "EI" is necessary to define the stiffness of the elastic beam element. When using the default option, the program multiplies this input "EI" by a large number (i.e., 10^8) and assigns it to point hinges. This means that in the elastic range, point hinges do not rotate (or rotate negligibly) due to their very high stiffness, while the elastic beam element alone simulates the actual member behavior.

Beyond the elastic range, stiffnesses assigned to point hinges are determined on the basis of rules for the hysteretic loop. However, the second slope of the primary curve is required to establish rules for the hysteretic loop. This information is specified by inputing the ratio of the second

---

* In DRAIN-2D the so-called "default" option governs when the elastic stiffness parameter EI for point hinges are left unspecified where called for. Users of DRAIN-2D must be familiar with this input option.

slope to the first slope of the moment-chord rotation relationship of a member (α'). The program then computes stiffness ratio for <u>point hinge</u> (α'_H), based on a linearly varying moment distribution with zero magnitude at one end. The relationship between α' and α'_H is derived below.

ACTUAL MEMBER

MOMENT DIAGRAM

COMPUTER MODEL
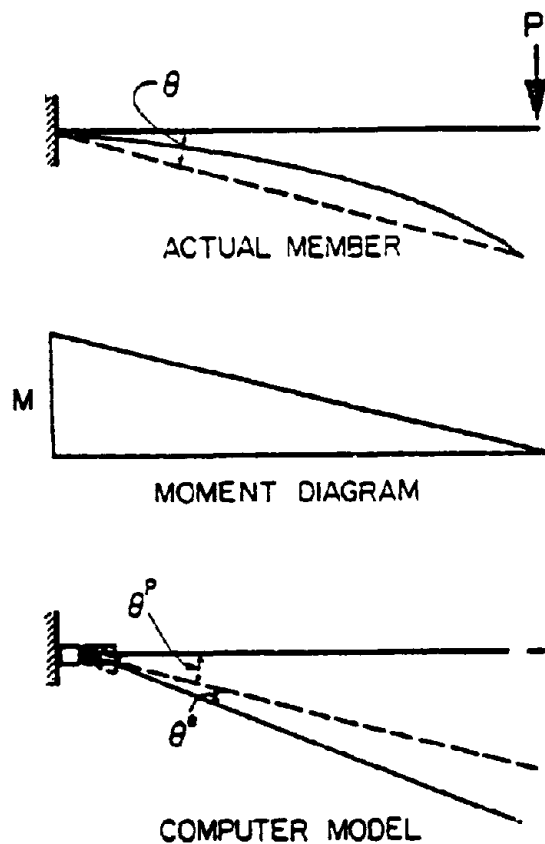
$$\theta = \theta^e + \theta^P$$

$$\frac{L}{3\,\alpha'EI}\,M = \frac{L}{3EI}\,M + \frac{1}{\alpha'_H\,K_S}\,M$$

$$\alpha_H' = \frac{3EI}{L} \frac{\alpha'}{(1 - \alpha') K_S} \qquad \text{(B1)}$$

where α' = Input stiffness ratio of real member.

α_H' = Computed stiffness ratio of a point hinge.

K_S = A very large member stiffness ($= 10^8$ in DRAIN-2D).

This expression is used in program DRAIN-2D to internally compute the point hinge property "α_H'" based on an input value "α'". However, this derivation holds true only if the moment diagram is linear and zero at one end. In reality, different types of structures are exposed to different moment distributions. In a coupled wall structure, wall elements have almost uniform moment between any two floors and coupling beams have linearly varying moment with double curvature. Therefore, when using the default option of DRAIN-2D, the input item "α'" should be modified such that, when Eq. (B1) is used, "α_H'" for point hinge will be the correct value. This can be done by substituting the correct value of α_H' (as given by Eqs. 9 or 10 in the text of this report) into Eq. (B1) and solving for input item α'.

It should be noted that Eq. (B1) is a special case of Eq. (9) that was developed in the main body of this report. Equation (9) applies to any kind of moment distribution, whereas Eq. (B1) holds true only for a cantilever with concentrated

force at the tip, producing a linear moment distribution with zero moment at free end. Similarly, α' and α'_H are special cases of α and α_A (or α_B) respectively. In Eq. (9), if $\xi = 0$ implying zero moment at free end then Eq. (B1) is obtained. An example of specifying input for the point hinge of a wall element at end "A" is given below:

$$\alpha = 0.05$$

$$\xi = -0.8 \text{ (minus sign comes from sign convention)}$$

$$\alpha_A = 0.1128 \frac{EI}{LK_S}$$

Substitute α_A into Eq. (B1) as α'_H and solve for α'.

$$0.1128 \frac{EI}{LK_S} = \frac{3EI}{L} \frac{\alpha'}{(1 - \alpha') K_S}$$

$$\alpha' = 0.03623$$